Charles University in Prague
Faculty of Mathematics and Physics

DOCTORAL THESIS

Anna Fučíková

Bioapplications of novel nanostructured materials

Department of Chemical Physics and Optics, Faculty of Mathematics and Physics, Charles University in Prague

Supervisor of the doctoral thesis: Doc. RNDr. Jan Valenta, Ph.D.,

Study programme: Biophycics, Chemical and Macromolecular Physics

Specialization: Biophycics (F4)

Prague 2011

Chtěla bych poděkovat svému vedoucímu disertační práce J. Valentovi za trpělivost a pomocnou ruku kdykoli byla potřeba. Dále svému konzultantovi I. Pelantovi za velice užitečné rady a pomoc s přípravou křemíkových nanokrystalů. I. Březinovi za uvedení do biologie a péče o buněčné kultury. M. Kalbáčové a A. Brožovi za pomoc s konfokální mikroskopií. Dále svým kolegům K. Kůsové za rady a pomoc s články, J. Alsterovi za trpělivost a pomoc s korekcemi prací, K. Dohnalové a K. Žídkovi za dobré rady a mnoha dalším, kteří přispěli k vytvoření této práce a jsou uvedeni v Apendixu této práce.

V neposlední řadě chci poděkovat rodičům za péči, lásku a podporu, kterou poskytují nezištně po mnohá léta a příteli T. Staňkovi za jeho oporu.

Dále by jsem ráda poděkovala za podporu těmto grantům:

- Centrum LC510, MŠMT.
- projekt č. 202/07/0818 GAČR
- Výzkumný záměr MSM0021620835
- Výzkumný záměr AV0Z 10100521
- KAN400100701 (GAAV CR)
- GAUK 101008
- 202/09/H041
- SVV-2010-261304

Declaration

I declare that I carried out this doctoral thesis independently, and only with the cited sources, literature and other professional sources.

I understand that my work relates to the rights and obligations under the Act No. 121/2000 Coll., the Copyright Act, as amended, in particular the fact that the Charles University in Prague has the right to conclude a license agreement on the use of this work as a school work pursuant to Section 60 paragraph 1 of the Copyright Act.

In Prague date 12. 12. 2011 Anna Fučíková

Název práce: **Bioaplikace nových nanostrukturních materiálů**

Autor: Anna Fučíková

Katedra: Katedra chemické fyziky a optiky, Matematicko-fyzikální fakulta Univerzity Karlovy v Praze

Vedoucí doktorské práce: Doc. RNDr. Jan Valenta, Ph.D. Katedra chemické fyziky a optiky, Matematicko-fyzikální fakulta Univerzity Karlovy v Praze

Abstrakt: Tato práce se zabývá vývojem nových fluorescenčních značek na bázi křemíkových nanokrystalů. Pro srovnání jsou zkoumány také nanodiamanty a komerční kvantové tečky na bázi CdSe. Křemíkové nanokrystaly jsou malé (1-4 nm) ve srovnání s ostatními testovanými nanočasticemi; připravujeme je pomocí elektro-chemického leptání v roztoku HF. Povrch Si nanokrystalů lze aktivovat různými molekulami a tím modifikovat jejich luminiscenční vlastnosti. Luminiscence má kvantovou účinnost až 30 % a je relativně fotostabilní (na rozdíl od ostatních fluorescenčních značek, které vybělují) Si nanočástice jsou poměrně stabilní v biologickém prostředí, z dlouhodobého hlediska ovšem biodegradabilní a netoxické. Pomocí mikro-spektroskopie jsme schopni pozorovat jednotlivé luminiskující Si nanokrystaly a to i uvnitř živých buněk. Studované nanodiamanty vykazují pouze slabou luminiscenci, jsou velmi stabilní v biologickém prostředí, ale neodbouratelné a při větších koncentracích značně toxické. Komerční CdSe kvantové tečky prokázaly vysokou míru toxicity a jejich luminiscence nevratně degradovala při větších intenzitách excitace. Křemíkové nanokrystaly se tedy ukázaly jako výborný materiál pro fluorescenční značení a to i pro in vivo aplikace v biologii a medicíně.

Klíčová slova: luminiscence, nanočástice, křemíkové nanokrystaly, nanodiamanty, fluorescenční značka, bioaplikace.

Title: **Bioapplications of novel nanostructured materials**

Author: Anna Fučíková

Department / Institute: Department of Chemical Physics and Optics, Faculty of Mathematics and Physics, Charles University in Prague

Supervisor of the doctoral thesis: Doc. RNDr. Jan Valenta, Ph.D., Department of Chemical Physics and Optics, Faculty of Mathematics and Physics, Charles University in Prague

Abstract: This work is aimed at development of new fluorescent labels based on silicon nanocrystals. Nanodiamonds and commercial CdSe quantum dots have been used as comparative materials. Silicon nanocrystals are relatively small (1-4 nm) compared to other studied nanomaterials. They are prepared by electro-chemical etching and their surface can be activated by various molecules which strongly influences luminescence properties. Luminescence quantum efficiency can be as high as 30 % and perfectly photostable even in biological environment. Si nanocrystals are biodegradable in a living organism within reasonable time scale and non-toxic. We are able to detect luminescence of single nanocrystals, even inside living cells, with use of our micro-spectroscopy apparatus. Nanodiamonds have weak luminescence; they are toxic at higher dosages and very stable in living bodies (without available technique how to remove them). Studied CdSe commercial quantum dots are strongly cytotoxic and their luminescence bleaches out under stronger excitation. In conclusion, Si nanocrystals are outstanding in all relevant parameters and they are suitable as novel fluorescent labels for application in biology, even for single molecule tracking in living cells.

Keywords: luminescence, nanoparticles, silicon nanocrystals, nanodiamonds, fluorescent labels, bio-applications.

Contents

List of abbreviations

A-ND	aggregates of nanodiamonds
AFM	atomic force microscopy
ATR	attenuated total reflection mode
CQD	commercial quantum dots
DLS	dynamic light scattering
DAPI	4',6-diamidino-2-phenylindole
F-band	fast (UV-blue) PL band in Si-NC
FTIR	Fourier-transform infrared spectroscopy
FWHM	full width at half-maximum
G-R	Giemsa-Romanowski
HeLa	human cervical carcinoma cells
HOPG	highly oriented pyrolytic graphite
HRTEM	high-resolution transmission electron microscopy
IR-band	infrared PL band in Si-NC
L929	mouse fibroblast cell line
M-Si	ball milled micro-sized silicon crystals
NC	nanocrystal
ND	nanodiamonds
NMR	nuclear magnetic resonance
OD	optical density
PBS	Phosphate Buffered Saline
PL	photoluminescence
Por-Si	porous silicon
QE	quantum efficiency
ROS	reactive oxygen species
S-band	slow (red) PL band in Si-NC
SAOS-2	human osteoblast-like cell line
SEM	scanning electron microscopy
Si-NC	silicon nanocrystals
TIR	total-internal-reflection

1. Introduction

Silicon nanocrystals (Si-NC) and nanodiamonds (ND) are in the main focus of many researchers due to their very promising attributes for biological applications. These, as any other materials, have advantages and disadvantages. But when we compare all relevant properties of our materials with other available nanomaterials, the conclusion is that silicon nanocrystals show the best parameters for in-vivo and nanodiamonds for in-vitro applications. Both these nanomaterials exhibit better biocompatibility than those based on Cd-chalcogenides, and silicon nanocrystals are even biodegradable.

During the last two decades Si-NCs have been extensively studied in many research fields like photonics (e.g. solid-state light emitting devices [1]), quantum computing, solar cells, chemical sensing [2] and other industrial areas, but silicon nanocrystals can also be used in biology [1A, 3] as novel florescent marks. Indeed, the efficient room-temperature photoluminescence of Si-NCs (it can reach values of about 23% [4] for Si-NCs studied here, which is more than enough for biological experiments) is the most remarkable property of this material. The precise mechanism of Si-NC luminescence is still not known today, but both quantum confinement and surface effects are supposed to play crucial role. The electronic bandgap of Si-NCs is broadened significantly due to quantum size effect for crystals smaller than the bulk exciton Bohr radius (~ 4.9 nm). For such small crystals we observe an enhancement of the spontaneous emission rate, a blue-shift and broadening of the luminescence band, which then covers also the whole visible spectrum. A bit unexpected feature of Si-NC is an ability to generate reactive oxygen species (ROS), which are most probably produced by transferring excitonic energy to the O_2 molecule [5]. The properties of Si-NCs are also strongly depending on their doping, size, shape and surface termination.

The enhancement of radiative decay of e-h pairs in Si-NC is due to a larger overlap of electron and hole wave functions caused by confinement and the fact that the carriers transport is restricted due to potential barriers between nanocrystals [6]. The decay of Si-NC luminescence can be generally described by a stretched exponential curve which reflects significant distribution of relaxation rates [7].

In this study, we are investigating silicon nanocrystals with size between 1-3 nm and emission peak around 600 nm for 1.5-3 nm particles and 420 nm for smaller particles. If we presume that a silicon particle with diameter of 2 nm has icosahedral shape, then the particle is assembled from about 280 Si atoms, from which 43 % (120 atoms) are on the surface [8]. This is in agreement with observed fact that photoluminescence is sensitive to changes of surface; it is logical – more than 1/3 atoms of the whole particle are surface atoms.

The first report on photoluminescence from porous silicon emerged in 1990 [9] in the paper by Canham. However, this material had been known even before - it was produced as a side product of electropolishing studied by A. Uhlir in 1956 in Bell laboratories [10].

Silicon nanocrystals have markedly different properties than bulk silicon, which has indirect band gap and only weak infrared luminescence at cryogenic temperatures. On the other hand, silicon in nanocrystalline form (when the size is reduced to 1-6 nm) has very bright photoluminescence in the visible region at room temperature [11, 12, 13, and 14]. The origin of Si-NC luminescence involves more than one physical phenomenon. Namely, the surface-related radiative recombination and effect of quantum confinement are mainly presumed in the literature [15], but other models are still explored [10, 16].

For our samples we generally observe emission band in blue and/or red-orange region(s) of spectrum. A green band is only observed for surface-hydrogenated Si-NC before oxidation in peroxide or on air. The green band vanishes when the surface is oxidized. Although Si-H termination is relatively stable for bulk silicon, it is highly unstable on a nanocrystalline particle. This is probably due to the different curvature of surfaces, which for nanoparticles results in exposition of the Si-H bonds to attack by oxygen and formation of stable Si-O bonds (*Fig. 1*). The blue band is generally connected to the presence of oxide related defects and an infrared band is connected with dangling bonds or bandgap luminescence in large crystallites.

Figure 1: Si-H bonds on a) Si-NC and b) bulk material.

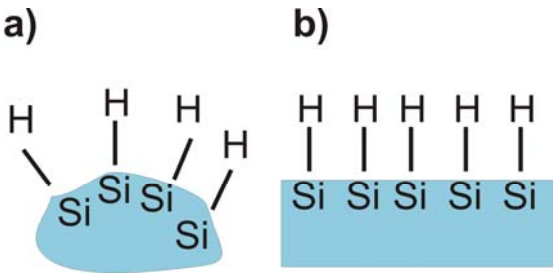

Oxidation introduces energy states in the Si-NCs bandgap, which pin the transition energy [14]. Wolkin et al. [14] claim that Si=O double-bond is present on Si-NCs, but it is also possible that one atom of oxygen is bonded to two silicon atoms (Si-O-Si bridge bond). We can see from calculations that Si-O is the most probable and energetically more stable than other studied bonds. This kind of bond creates localized states within the bandgap that are not affected by quantum confinement as was previously predicted [17].

In this study, we are concentrating on properties of silicon nanocrystals and their application in biological experiments. For comparison we use nanodiamonds and commercial quantum dots; these are competitive nanomaterials for application in biological studies. Nanodiamonds (NDs) are known for more than 15 years. First note about NDs was in a paper by Vul, but they had been known before as a side product from preparation of diamonds [18]. They already found wide use in industry (e.g. polishing, additives to engine oils and galvanic electrolytes etc.). ND can be functionalized and used in a wide spectrum of biological studies, but there is no known pathway for them to be removed from a living body [19, 20].

The other comparison material used in this study are commercially available quantum dots based on Cd-chalcogenides (mainly CdS and CdSe), emitting at around 600 nm. About 10 years ago the particles have been considered safe. But when more detailed biological studies had been performed, it was found that Cd atoms are released into the biological environment, even if the particles are covered by thick shells. It is commonly accepted fact that cadmium is toxic [21, 22]; therefore the particles are not well suited for biological experiments.

In this work, we study complex properties of nanomaterials, from a process of manufacture through various optical studies to biological studies.

The investigated fabrication processes of silicon nanocrystals include traditional preparation method of electro-chemical etching, but also novel methods based on the ball milling of Si crystal and further disintegration by either chemical means or laser fragmentation. Obtained

particles were characterized by dynamic light scattering, atomic force and electron microscopy.

Optical properties of nanomaterials were studied with fluorescence spectroscopy, luminescence micro-spectroscopy and, in case of Si-NCs, also with PL lifetime and quantum efficiency measurements. Silicon nanocrystals were also studied in different solutions simulating biological environment to test the possible degradation of luminescence over a period of more than 80 days.

Biological interactions between nanomaterials and cells were studied on HeLa (human carcinoma), L929 (mouse fibroblast), and SAOS-2 (Human osteosarcoma) cell lines. The growth of cells in presence of nanomaterial was measured by time-lapse microscopy. The nanomaterial-cell interactions were observed with use of confocal florescence microscopy and micro-spectroscopy. The changes in structure and functionality of cells were visualized by optical microscopy (with and without staining of inner cell structures) and scanning electron microscopy. The toxicity was determined using growth curves and lactase dehydrogenase test.

2. Preparation of samples

2.1 Preparation of silicon nanocrystals

2.1.1 Electrochemical etching

The most studied method of preparation of Si-NC is electrochemical etching with use of hydrofluoric acid. This technique allows sufficient control of the size of silicon nanocrystals and resulting nanocrystals are chemically pure. The silicon nanocrystals (Si-NC) are in our case prepared from porous silicon. Porous silicon is a pillar structure rising from a silicon wafer (*Fig. 2*).

Figure 2: Porous silicon structure: light blue – SiO_2, dark blue - Si.

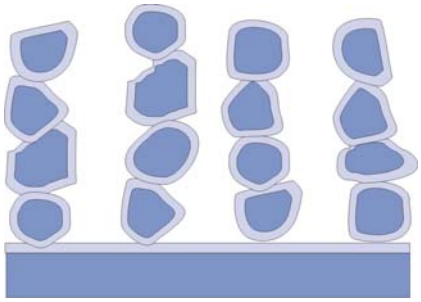

The pillar consists of Si-NC grains, the core of a grain is from Si and a SiO_2 layer forms the surface. The average size of Si-NCs is between 1 nm to 3 nm depending on parameters of the preparation.

The etching solutions were based on hydrofluoric acid (with hydrophobic character); ethanol 1and H_2O_2 were added for better wettability.

The concentrations of chemicals in the etching solution for our experiment were:
- 25 % of HF (50 % aqueous solution)
- 4 % of H_2O_2 (30 % aqueous solution)
- 71 % of pure ethanol (99,6 % aqueous solution of ethanol)

The p-type [1,0,0] Si wafer (resistivity of 0.075-0.100 Ω cm, doped with boron) was processed in the etching chamber displayed on *Fig. 3*.

Figure 3: The cross section of the etching container (half of the cylindrical form) with wafer and etching solution.

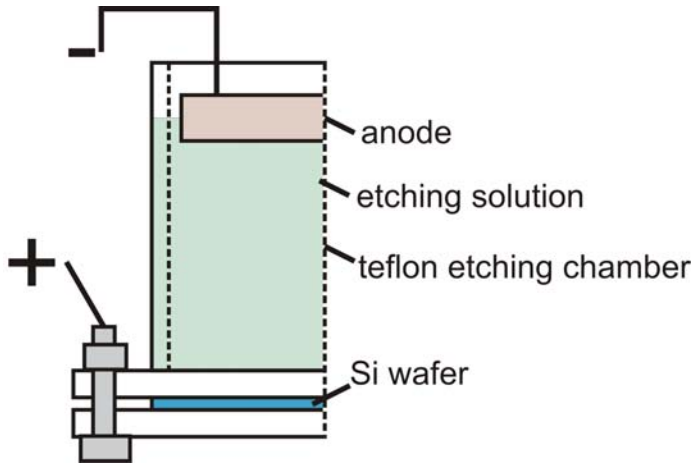

The etching current density was set to 2.6 mA/cm^2. The wafers were etched for 2 hours and the etching solution was mixed continuously for exclusion of bubbles and homogenization of the etching solution.

After the etching a wafer was dipped into hydrogen peroxide for 5-20 minutes and then thoroughly washed with ethanol. This treatment with hydrogen peroxide increased the porosity of surface and decreased size of Si-NCs. The etched wafer with Si-NC layer on its surface was left to age for 12-48 hours in a chamber with controlled temperature and air humidity. Etched wafers with Si-NCs on the

surface are displayed on *Fig. 4*, taken from [2A], where we also discussed preparation parameters influencing resulting photoluminescence of Si-NCs.

Figure 4: Photographs of etched wafers with Si-NCs on surface, excitation is done by an ultraviolet lamp. A – green photoluminescence (PL) of Si-NCs (immediately after etching), B – red PL of Si-NCs, C – orange PL of Si-NCs, D – blue PL of Si-NCs, E – yellow-orange PL of Si-NCs. Taken from [2A].

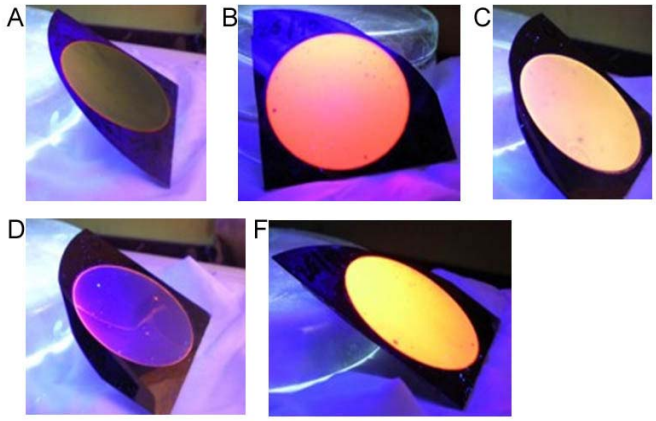

The Si-NC powder was obtained by mechanical pulverization of the etched wafer surface.

The surface of a freshly etched wafer is covered with hydrogen atoms; when exposed to air the surface is rapidly oxidized [2]. Although flat silicon surfaces terminated with hydrogen tend to be long time (up to a few days) stable and chemically inert in time. They get also oxidized but not as fast as the nanocrystals (e. g. prepared by electrochemical etching and also by non-thermal plasma synthesis); this is most probably due to the curvature of the surface of the nanocrystals.

2.1.2 Overview of methods used for preparation of silicon nanocrystals

In general, nanocrystal can be prepared by two approaches; one is top-down (disintegration of a massive crystal into nanocrystals) and the other is bottom-up (build up nanocrystals from molecular precursors). Both approaches have advantages and disadvantages. The main disadvantages of top-down approach are a low yield and a wide distribution of sizes of the particles. The main advantage is that the particles are chemically pure. On the other hand, the bottom-up approaches usually offer high production yield, but obtained nanoparticles are not chemically clean [3A].

The porous materials are usually sorted by a pore size into three groups: microporous $\leq$ 2 nm, mesoporous 2-50 nm and macroporous >50 nm silicon [23]. Not all of those materials are photoluminescent; some of them are used as scaffolds, or carriers of drugs. We concentrate mainly on microporous materials or materials which are on the lower limit of mesoporous (porous silicon, see 2.1.1), from which we prepare Si-NCs with size of generally less than 10 nm.

One group of nanomaterials representing a top-down approach is mesoporous silicon, consisting of the particles with usually 100 nm – 1000 nm size, and having pores with diameter of about 2-50 nm. Another material produced by a top-down approach are micro-crystalline Si particles prepared by ball milling of Si crystals [24]. The material is formed by particles sized from 100 nm to 50 μm which are not usually photoluminescent. Both of these types of particles are mainly used for biosensing, e.g. of triglycerides with capacitance-voltage characteristics [25]; mesoporous silicon is also used for enhancing sensitivity of analytical methods due to a high surface/volume ratio (e.g. DNA sensing [26]).

Bottom-up preparation of nanomaterials can produce big volume of material, but the products are not chemically pure and have non-uniform surface containing various chemical species which are usually toxic and, therefore, dangerous for biological environment. If some purification method exists, it is usually connected with big loses of nanomaterials. The bottom-up methods are represented by various colloidal syntheses, e.g. octane-capped crystalline silicon synthesis, which consists of decomposition of phenylsilane in supercritical octane/hexane and exclusion chromatography to separate the right size of nanocrystals [27]. This last material possess efficient luminescence, but its safe application in living organism is disputable due to residual presence of hexane.

In 2001, Holmes et al. prepared sterically stabilized silicon nanocrystals by thermally decomposing diphenyl silane in supercritical octanol. The resulting particles had diameter from 1.5 nm up to 4 nm, and FT-IR analysis confirmed that a surface organic layer was bonded through an alkoxide linkage (Si-O-C) [28]. They did not show any separation method or improvement of fabrication aimed to decrease the large range of sizes.

Another category of preparation of silicon nanomaterials, which is on the border between bottom-up and top-down, is based on an explosion technique similar to preparation of ND. It is done via simultaneous heterogeneous reduction of silicon tetrachloride and alkyl trichlorsilane in a high-pressure bomb reactor [29]. The reaction is described by a scheme given below

$$SiCl_4 + RSiCl_3 + Na \rightarrow Si \text{ (diamond lattice)} + NaCl \qquad (2.1)$$

An enormous quantity of nanomaterial can be obtained using this technique, but the product is chemically unclean and, most importantly, not homogeneous in size and shape. Separation of particles by size is impractical due to big losses or due to time consumption of the process (ultra centrifugation allows only a rough selection).

Another method how to prepare Si nanomaterials is the low-pressure non-thermal plasma synthesis [30]. This technique enable to add various chemical compounds to the source materials in the non-thermal plasma chamber and in that way prepare functionalized particles with quite high quantum yield of luminescence (up to 60 %) [31]. The most usual surface groups achievable by non-thermal plasma synthesis on Si-H surfaces are alkenes $–CH=CH_2$, alkynes $–C\equiv CH$, and amines $–NH_2$; the resulting bonding sequences are Si-C, Si-N-C, and Si-O-C [32]. Again, the obtained particles are non-uniform in size, but their chemical composition is quite uniform. The main disadvantage of non-thermal plasma synthesized particles is that they tend to have broad photoluminescence spectra (FWHM around 100 nm) due to a fairly broad nanoparticle size distribution [33].

2.1.3 Preparation of milled Si

Milled Si (M-Si) is used in this work mainly for biological experiments, but also as a source material for a new method of preparation of Si particles as small as 50 nm. M-Si is prepared by wet milling of small pieces of p-type Si [100] boron doped wafers (resistivity 0.075-0.100 Ω cm) in a ball mill (Analysette 3 – SPARTAN, Fritsch). The wafers are milled until a light grey suspension is formed and big grains - visible with unaided eye - are not observed. The suspension is then removed from ball mill and centrifuged for 3 minutes at 1500 RPM

(Centrifuge 5804R, Eppendorf). We use only the supernatant, which is composed of M-Si with size mainly around 450 nm (measured with SEM) in pure water. Crystals with size of 1000 nm and higher remain in the precipitate. Materials in various steps of this process are displayed in *Fig. 5*. Solution with M-Si can be dried in order to obtain a powder or used directly depending on the experiment.

Figure 5: Phases of preparation of milled Si: a) small pieces of silicon wafers, b) ball milled Si wafers, c) centrifuged water solution with M-Si.

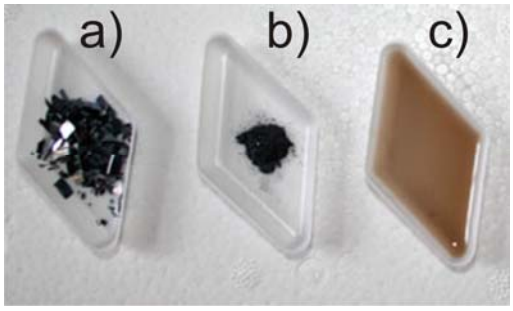

2.1.4 Alternative Si-NC fabrication method

a) Fojtik´s method

The M-Si seems to be as a good source material for further preparation of Si-NCs. We tried the method developed by Fojtik et al. [34] for obtaining small luminescent Si-NCs. In this method a silicon powder (originally formed by the thermal pyrolysis of silane SiH_4) is mixed with cyclohexane, 2- propanol and hydrofluoric acid. The solution forms two separate phases with cyclohexane in one and HF and 2-propanol in the other (see *Fig. 7* taken from [35]). The silicon grains cycles between the two phases and their size is gradually decreased by many steps of oxidation and oxide removal by etching. The phases in our experiment are displayed in *Fig. 6*.

Figure 6: Etching of silicon powder by Fojtik□s method. a) solution with two phases intermediately when mixed (it bubbles how the particles are jumping from one phase to another), b) solution after 5 hours (there is observed no jumping of particles).

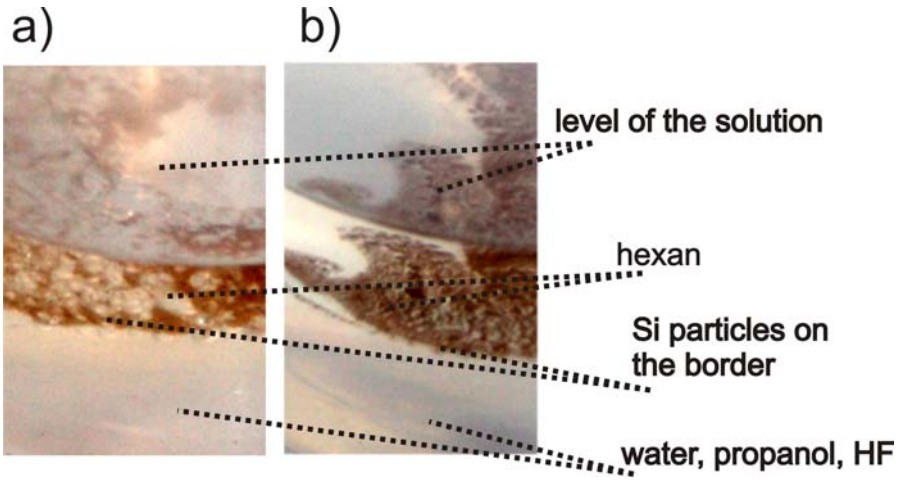

Figure 7: Preparation of Si-NCs by Fojtik´s method. a) The composition and configuration of etching solutions in cuvettes, b) PL spectra of Si-NC suspensions after annealing in different concentration of HF for various time. The PL peak is shifted with prolonged etching from near-IR to orange spectral region and eventually switches to blue-green for Si-NC below ~ 2 nm (taken from [35]).

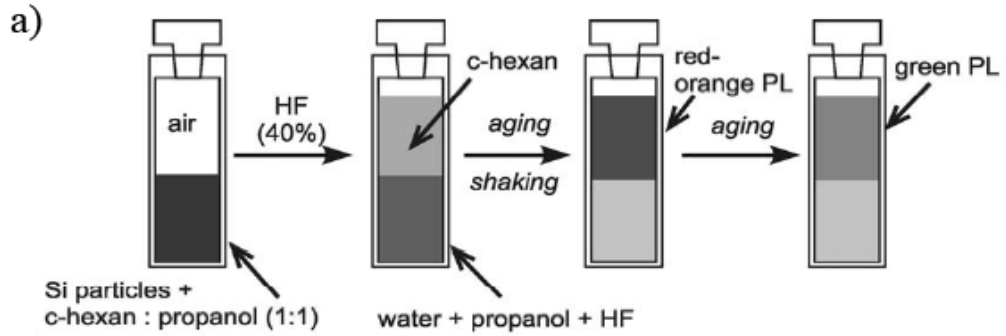

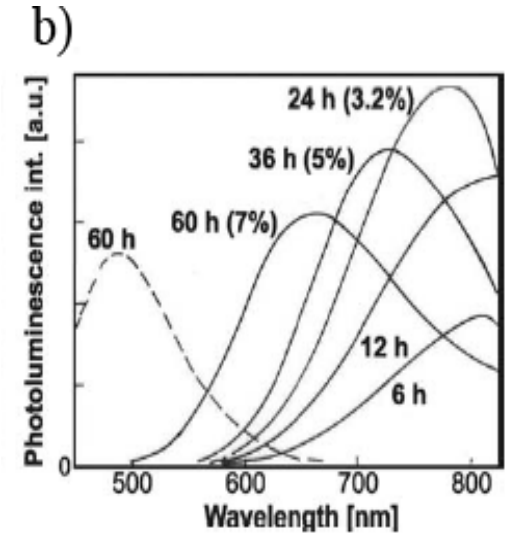

In the articles [34, 35] the reaction stopped after 2 days, but the Si grains continued to degrade slowly – authors only observed different structures and photoluminescence during the degradation (see *Fig. 7*). In our case the reaction stopped after 5 hours (the particles did not move from one phase to another). We have not been able to separate the silicon particles from solution without chemical impurities (mainly residual hydrofluoric acid, which etched all glass surfaces we put the nanomaterials on, so we have not been able to measure their optical properties). As the particles have not been luminescent (most probably due to big size of Si particles), this method was abandoned.

b) Laser-induced fragmentation method

Si grains of sizes ranging from 130 nm to 5 000 nm (*Tab. 1,* 0 min) prepared by ball milling (see Chapter 2.1.3) were ablated in water using XeCl eximer laser with 30 ns pulses with wavelength 308 nm and peak power of around 84 mJ, repetition rate of 20 Hz. The excitation pulses were focused approximately 1 cm below the surface of a cuvette with solution containing milled Si under constant stirring.

The crystals tend to break possibly due to a thermal gradient in the crystal or due to Columbian explosion. We obtain a clear solution without visible crystals after 8 minutes long ablation. We also ablated germanium as a comparison material (the starting water suspension was also prepared by ball milling).

The sizes of particles obtained by the laser-induced fragmentation of Si and Ge crystals are summarized in *Tables 1* and *2*, respectively. The parameters were measured using dynamic light scattering in the Zetasizer Nano S (Malvern) apparatus (its application range is from 0.3

nm to 10 microns). The measurement is not precise for mixtures of 10 nm and bigger than 200 nm particles; the colloidal sample had to be filtered to observe also the smaller particles. We used 650 nm and 100 nm centrifugation filters from Millipore (Ultrafree-MC Centrifugal Filter Units with Microporous Durapore PVDF Membrane). The samples were centrifuged for 3 minutes with 1200 rpm (MiniSpin, Eppendorf).

Table 1: Sizes of laser-processed Si crystals in water with number and volume percentage measured by dynamic light scattering.

Duration of processing [min]	particle size [nm] / number percentage [%]		particle size [nm] / volume [%]	
0 min	130	60	130	20
	> 130	40	400	30
			5000	50
1 min	130	20	130	20
	200-300	40	200-600	40
	> 300	60	5000	40
2 min	130	20	100-200	20
	200	60	200-400	40
	> 200	20	400-1000	20
			5000	20
4 min	130	20	100-400	70
	200	60	400-1000	10
	> 200	20	5000	20
8 min	100-200	25	100-200	20
	200-400	70	200-400	60
	> 400	< 5	400-800	20
16 min	< 200	20	< 200	20
	200-600	80	200-600	80
16 min *	60	90	60	60
	> 60	10	440	40

* Suspension filtered using the membrane with 650 nm pores.

The smallest size of particles (60 nm in diameter) is obtained after 16 minutes long treatment. The largest crystals of 5 μm disappeared after 4 minutes and shift to diameters around 800 nm after 8 minutes and around 600 nm after 16 minutes of treatment. The suspension becomes visibly clear after about 8 minutes; that is in agreement with the dynamic light scattering experiments (scattering by particles smaller than wavelength of light, in general smaller than 400 nm, is very low).

Si nanocrystals start to emit visible photoluminescence at sizes smaller than 10 nm. We were far from this border (our smallest particles are ~60 nm big). Efficiency of the laser-induced fragmentation decreases with volume of a particle. To obtain a few nm big particles, we have to apply chemical methods (oxidation and/or etching).

Table 2: Sizes of laser-processed Ge crystals in water with number and volume percentage measured with dynamic light scattering.

Duration of processing [min]	particle size [nm] / number percentage [%]		particle size [nm] / volume [%]	
0 min	130	60	60-150	30
	> 300	< 5	300-800	40
			5000	10
1 min	60-150	80	60-150	30
	150-300	15	150-300	60
	300-600	5	> 300	10
2 min	60-150	80	60-150	20
	150-300	15	150-300	70
	> 300	5	> 300	10
4 min	30-60	60	30-100	50
	60-100	30	100-400	40
	> 100	10	> 400	10
8 min	30-60	40	30-100	50
	60-100	55	100-400	40
	> 100	5	> 400	10
16 min	30-100	10	30-100	10
	100-250	70	100-200	80
	250-350	15	200-600	10

From comparisons of the data in *Tab. 1* and *2*, it is clear that we obtained smaller particles for ablation of germanium. The 5 μm particles disappeared after 1 minute of ablation; the smallest particle is 30 nm big and it is observed after 4 minutes. This is probably due to different thermal conductivity and expansion of Si and Ge (Si and Ge have the same diamond crystal structure). The relevant parameters are summarized in *Tab. 3*.

Table 3: Selected physical parameters of Si and Ge crystals

Material	Thermal conductivity [$W \cdot m^{-1} \cdot K^{-1}$]	Thermal expansion (25 °C) [$\mu m \cdot m^{-1} \cdot K^{-1}$]	Crystal structure
Si	149	2.6	Diamond cubic
Ge	60.2	6	Diamond cubic

The comparison of the above given parameters suggest that the Si and Ge crystals are breaking due to thermal gradient rather than due to Columbian forces.

2.2 Preparation of nanodiamonds

Nanodiamonds are prepared by combustion of oxygen-deficient explosive mixture of TNT/T4 in a closed chamber and then purified with various acids [19]. Samples in this study are fabricated by NanoCarbon UDD-TAH, Diamond Centre, St. Petersburg, Russia. This product is a mixture of ND, aggregates of nanodiaomonds (A-ND), and various chemical solvents. The product is purified in Institute of Physics AVCR v. v. i.. After the purification treatment we obtain a mixture of ND around 10 nm in diameter (56.6 vol. %) and A-ND around 460 nm in diameter (43.4 vol. %) in deionized water. The size was measured by DLS. These two sizes can be separated by simple sedimentation. After three days of sedimentation, an upper transparent part is formed. Only nanodiamonds with sizes of 10 nm are left in this supernatant, so they can be easily separated from the precipitate consisting of A-ND [1A]. The ND surface is covered by various carboxy-, keto-, hydroxyl-, and oxygen groups [36].

The termination of nanodiamonds plays crucial role, for example O-terminated surfaces are hydrophilic while H-terminated surfaces are hydrophobic [37]. There are various chemical functionalizations for layers of nanodiamonds deposited on surfaces, which makes them bio-passivated or having bio-active properties [38].

2.3 Commercial quantum dots

Commercial quantum dots (CQD) are represented in our work by Cd-chalcogenides based quantum dots eFlour^{TM} 605 NC from the company eBioscience. The Cd-chalcogenides nanoparticles can by prepared by various methods (e.g. high temperature pyrolysis, sonochemical and radiolytic methods, arrested precipitation in solution, and others [39, 40]), but the supplier does not give the information which method was used for preparation of the nanoparticles. The core of the nanoparticles is composed from cadmium selenide, the surface is covered with various carboxyl-like groups. The size of the nanoparticles is around 8 nm and they have maximum of luminescence at around 605 nm. A particle is composed from 50 atoms of Cd or Se and its structure can be seen in *Fig. 8a*. Emission and absorption spectra are displayed in *Fig. 9*.

Figure 8: Cadmium selenide eFlour quantum dots from company Biosience. a) Pure CdSe core is in blue, carboxyl groups on the surface are yellow. b) CQD covered by conjugated bio-layer c) AFM picture of CQDs. (Taken from [41])

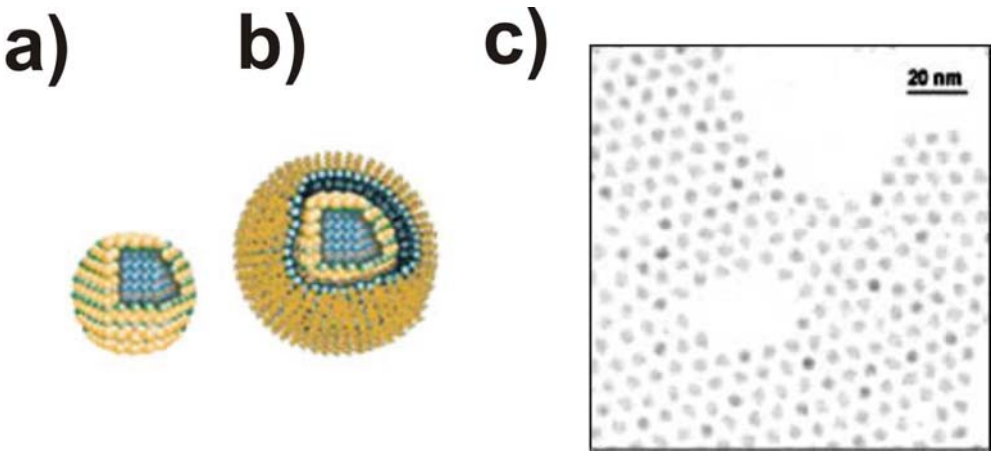

Figure 9: Emission and absorption spectra of CQD with various sizes. (Taken from [41])

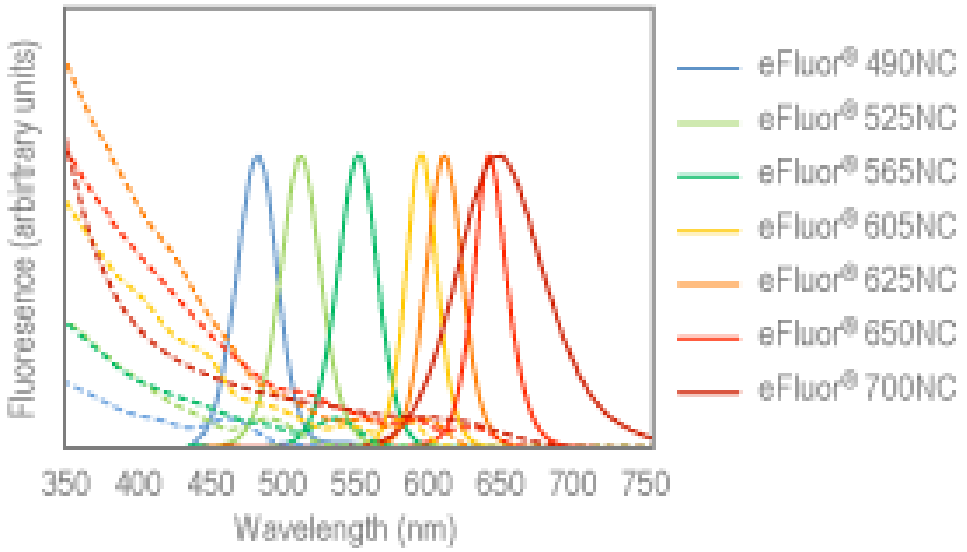

Luminescence is adjusted by the diameter of a particle; the luminescence peak is shifted to the red part of the spectra for bigger particles. The absorption spectra of nanocrystals consist of a series of overlapping peaks due to excitonic transitions and a broad absorption tail due to band to band transitions (in case of the weak quantum confinement regime) increasing toward the UV/violet range (see *Fig. 9*). The emission band is of Gaussian shape with a big Stokes shift (larger than those typical for organic dyes). Although the particles have quite narrow size distribution, they tend to aggregate strongly if not covered with a bio-layer.

2.4 Characterization of silicon nanocrystals and nanodiamonds

The nanomaterials were studied with atomic force microscopy (AFM) and DLS. The AFM images were obtained by the Agilent Technologies 5500 Atomic Force Microscope with multipurpose small scanner (9 µm xy) in AAC mode (air). The Si-NC/ethanol colloids were dropped onto a HOPG and dried. A 0.75-µm scan revealing Si-NCs of 1.5-2 nm height is shown in *Fig. 10*. A larger 3 µm scan of many particles is shown in Fig. *11*. There is quite uniform distribution of particles about 1-2nm in height and terraces of about 1 nm in height, which are probably formed by a surfactant, and from time to time an aggregate of Si-NCs. This method cannot answer the question how thick is the oxide layer. The results were independently proved by measuring the same samples by the high-resolution transmission electron microscopy (HR-TEM) by our colleagues Pelant et al. in [42].

The nanodiamonds displayed in *Fig. 12* are a bit blurry due to the charging of nanoparticles, therefore, it was not possible to measure the size of particles by AFM. Instead, DLS was successfully applied. Clusters of A-ND can be also observed by scanning electron microscopy (SEM).

Figure 10: 0.75 × 0.75 µm AFM scan of Si-NCs on HOPG. a) overview of Si-NCs, b) the topography profile (along the line shown in panel a) revealing two Si-NCs with height of about 2 nm.

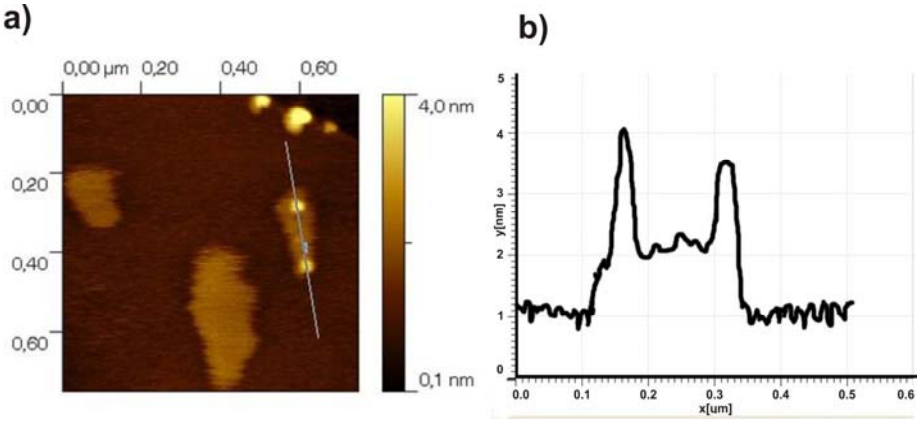

Figure 11: Larger 3 × 3 µm AFM scan of Si-NCs on HOPG. Top view of many small Si-NCs with a few aggregates.

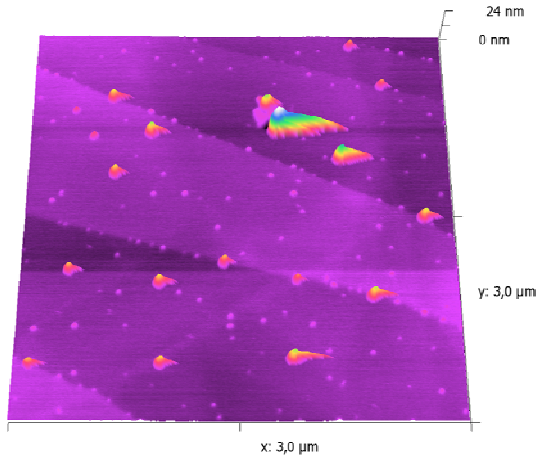

Figure 12: 3 × 3 µm AFM scan of nanodiamonds on HOPG. a) A blurry image caused by ND charging by the AFM tip, b) a detail of ND from the panel a.

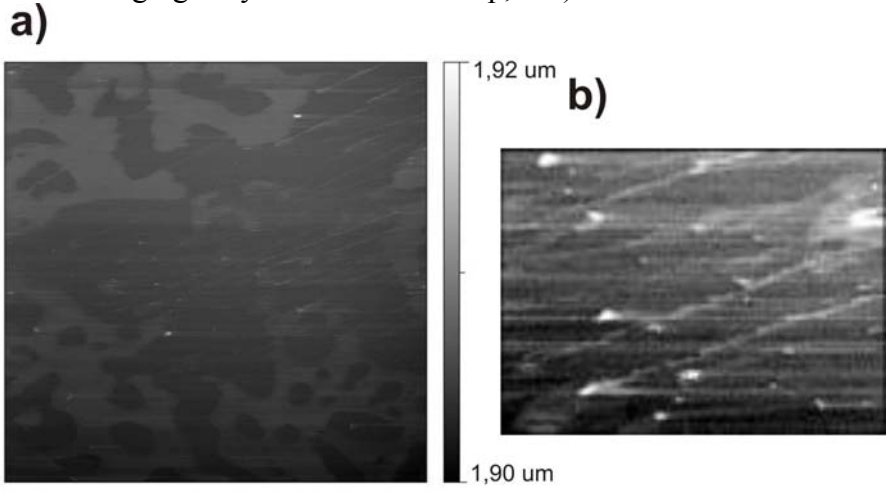

2.5 Chemical activation of silicon nanocrystals

Liquid-phase techniques for chemical activation of flat hydrogenated Si surfaces are known for a long time, but applying them to freestanding particles is quite difficult. Main problems concern separation of activated particles from the solution, their purification and, obviously, production losses. Liquid phase techniques are easily applicable to Si-NCs attached to the wafer (like porous Si layers), but the surface of particles obtained in that way is not entirely covered by the desired coating. Liquid-phase treated, organically caped porous silicon surfaces or silicon nanoparticles attached to a surface show efficient visible photoluminescence and are fairly resistant to oxidation [43], but they cannot be fully rinsed off the treating solution.

One example of liquid phase activation is alkyl attachment to Si-NCs surface [44, 45]. Si-NCs, freshly prepared by non-thermal plasma synthesis, are transferred from the reaction chamber directly to a solution of 1-dodecene and mesitylene, and heated up to 80 °C. This procedure takes long time (several hours) and it needs to be done in protective atmosphere without oxygen. Variously sized grains of Si-NCs (the process started with already non-uniformly sized Si-NCs, and the activation promotes further aggregation) with 1-dodecene and 1-octadecene on the surface are obtained. Activated Si-NCs have luminescence above 800 nm, with quantum efficiency of around 70 %. This technique is not adaptable to activation of our samples due to small amount of available material and inherent big losses which are connected with this procedure.

The special properties of the surface of our Si-NCs have to be taken into account, when the surface activation is planned. It is presumed that after preparation we have Si=O double bonds [46] or Si-O-Si bonds on surface of Si-NCs. The bond energies have been calculated e.g. by a theoretical work [32] and are summarized in *Tab. 4*. From the table it is clear that Si-O has higher bond energy than Si-H and both are significantly higher than Si-Si in bulk crystals. Therefore, Si-O bond is preferred, especially if we take in account the curvature of surface of nanoparticles, as has been discussed in Chapter 1. In some chemical activations, which we will discus later, Si-NCs have Si-C bonds on the surface after activation, which is in the middle energies between Si-O and Si-H bonds. The highest bond energy is for Si-Cl which is found on some specially activated Si-NCs.

Table 4: Overwiew of bond energies.

Type of bond	bond energies (kJ mol^{-1})
Si-H	323
Si-C	369 (usual polar covalent bond)
Si-Cl	391
Si-O	368
Si-Si (bulk)	210-250
Si-Si (disilane)	310-340
Si-Si (disilene)	105-126

Another method of chemical activation is hydrosilylation, which is the most widely studied method for modifying the surface bonds of Si-NCs. The process leads to replacement of unsaturated bonds by Si-H bonds; it is activated by UV light at room temperature, or at 120-200 °C, under moisture and oxygen-free conditions.

Jurbergs et al. [31] prepared Si-NCs via non-thermal plasma synthesis and passivated their surfaces by hydrosilylation (forming Si-H bonds) followed by activation with alkenes or alkynes via free-radical mechanism (at 165 °C in a solvent mainly formed by mesitylene under nitrogen atmosphere) in order to obtain Si-C bonds on the surface. The highest luminescence quantum yield of Si-NC known to date (up to 60 %) was measured for these Si-NCs with Si-C surface bonds [31].

Experiments on silicon nanocrystals with different doping with Si-Cl or Si-alkoxy surface activation showed that their luminescence is quenched after 15 days. On the other hand, siloxane activation of Si-NCs (Si-NCs with hydrogen on the surface have been treated with octadecene or undecylenic acid octadecyltrimethoxysilane) seems to be stable and resistant to photobleachning in ambient conditions for at least 60 days [47].

These methods are useful when more than a few grams of source Si-NCs are available, but our production of Si-NCs is more or less in mg range. Therefore we need to explore other methods of preparation of activated particles. One successful example of our new surface activation technique is described in the next chapter.

2.5.1 Organic capping of silicon nanocrystals at room temperature

We have developed a new technique for organic passivation of oxidized Si-NCs using xylen treatment at room temperature and ambient pressure [4A, 5A, Patent No. PV2008-246], (for details of our patent see Chapter 6 section *Ap1*). With this technique the core of nanocrystals stays unchanged; we are only modifying the surface, which allows us a unique comparison to other, more severe capping techniques.

The mean diameter of initial Si-NCs is about 2.7 nm (naturally oxide passivated) which are dispersed in a mixture of xylene isomers (ethylbenzene and isopropylbenzene with trace amounts ~0.1% of di-trimethylcyclohexane). This colloid is constantly stirred and irradiated twice a week for 30 minutes with UV laser (at 325 nm, i.e. 3.81 eV, with 367 kJ mol^{-1} per session).

This mechano-optical treatment leads to slow quenching of the red luminescence band (600-650 nm) where a new yellow band emerges (precise process is described in [5A]). The suspension is filtered (with either the 220 nm Millipore Millex-GV syringe filter or Millipore Ultrafree centrifugal filters with pore sizes of 650 nm and 100 nm) in order to obtain a clear supernatant colloid with organically capped Si-NCs. This filtering does not diminish the photoluminescence intensity of the yellow band of the optical spectrum. The final suspension is long term stable (in the order of years).

The size distribution of Si-NCs is measured with dynamic light scattering and the crystalline Si core is observed with high-resolution transmission-electron microscopy (HR-TEM) as shown in *Fig. 13*, for details see [4A].

As a control experiment we dispersed Si-NCs in ethanol and treated it in the same way as the xylene sample; after a few weeks the luminescence intensity of the ethanol sample decreased to 1/3 of the original value, but the PL maximum shifted only by about 8 nm to longer wavelengths (from 642 to 650 nm) [5A] and the colloid was not clear.

Figure 13: a) DLS measurements of the mass-weighted distribution function of particle diameters of the colloidal suspension (the peak at d~300 nm is due to presence of Si-NC clusters), b) HR-TEM measurement of small 2-3 nm Si-NCs (Si cores are indicated by circles for easier orientation), c) The detail of the HR-TEM image with the electron-diffraction pattern (in the inset) taken from the indicated square area reveals the characteristic silicon crystal structure. (Figure was reproduced with permission from [4A]).

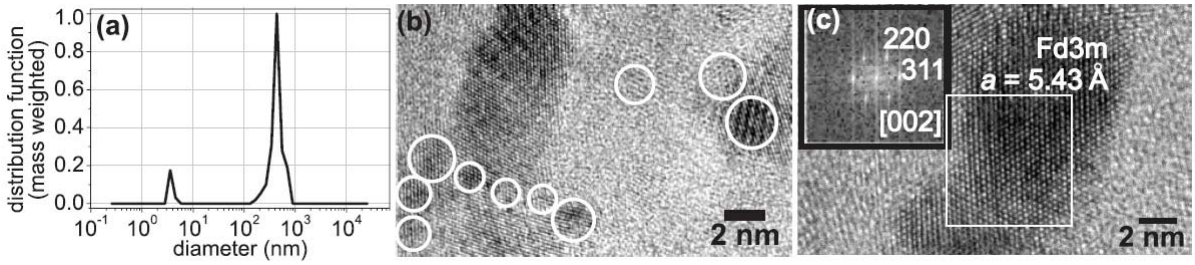

The chemical reactions leading to capping are not fully understood at present time. The surface of capped and uncapped Si-NCs was studied with Fourier-transform infrared absorption measurements in the attenuated total reflection mode (FTIR-ATR) [4A]. It is clear from this measurement that Si-CH_3 groups are present on the surface; in addition, a weak signal suggests presence of Si-C_x groups on the surface. This observation suggests that a Si-O-C linkage is involved in the capping process. We know that methyl group is involved in formation of this linkage, we presume that carbon is on Si-NCs surface in quaternary form (without any hydrogen groups) or other forms (e.g. Si-O-aromatic, Si-O-(C=O)-R' etc). The signal attributed to Si=O and Si-O-Si bonds (major bonds in non-capped oxidized Si-NC) is lower for capped Si-NCs, which suggests that these bonds have been replaced with new, carbon based ones. Studies by nuclear magnetic resonance have been performed in order to obtain the independent proof of the above mentioned conclusions [4A]. The possible processes of attacking Si-O-Si bridge with methyl group are illustrated in *Fig. 14*.

Figure 14: Proposed mechanisms of breaking the Si-O-Si bridge bonds (the figure was reproduced with permission from [4A]).

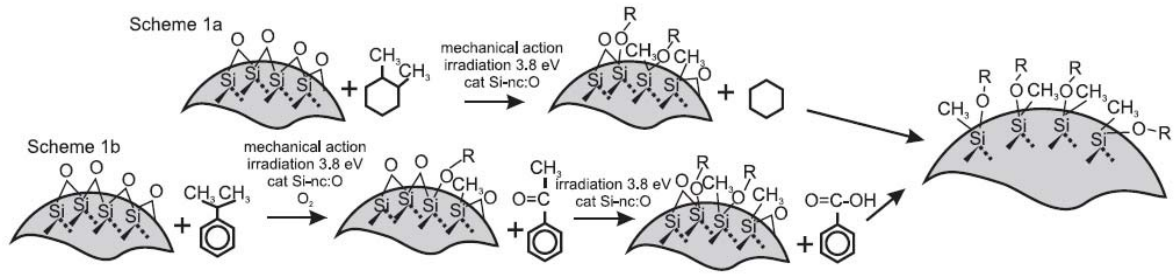

The mechanism of generating methyl radicals via photodissociation of alkyl-substituted cyclohexane is displayed in *Fig. 14(1a)*. One of the radicals can attack Si-O-Si bridge bonds, leading to a free dangling bond left on Si-NCs, which can induce further photodissociation (in agreement with [48]). Another way how to create methyl radicals could be initiated by creation of dangling bonds via the addition of hydrogen from the oxidized surface hydride groups –O_x-SiH_y in presence of UV irradiation. In Process *Fig. 14(1b)* we presume that

autooxidation of isopropylbenzene to acetophenone consumes atmospheric oxygen and transforms finally to the benzoic acid and produces methyl radicals for capping of Si-NCs [4A, 49].

Even though the cores of Si-NCs remain unchanged, the optical properties change dramatically. We can summarize the main properties as follows: the peak of luminescence shifts from 640 nm to 570 nm and photoluminescence decay is shortened by about four orders of magnitude (23μs to 2 ns) with quantum efficiency increasing up to 20 %.

3. Photoluminescence studies

3.1 Theoretical background

3.1.1 Silicon nanocrystals

The precise mechanism of luminescence of Si-NCs is not known at the present, but new tools have been developed that provide new insight in it. Results of *ab initio* calculations are approaching the size and composition of real Si-NCs measured experimentally and experimental techniques allows studies of single nanocrystals.

Si-NCs exhibit several luminescence bands, depending on size, surface termination and other properties. Parameters of the bands are described in *Tab. 5*, taken from [9].

Table 5: Optical characterization and average lifetimes of excited state of Si-NCs.

Spectral region	PL peak [nm]	PL peak [eV]	PL decay time	Name
UV	350	3.54	1 ns	UV-band
Blue-green	470	2.64	1 ns	F-band
Green-red	470-800	2.64-1.55	100 μs	S-band
Near infrared	1100-1500	1.12-0.83	100 μs -1ms	IR-band

We are mostly investigating the S-band, which is spectrally tunable through a wide range of the optical spectrum. This band is the most often encountered and widely studied [6A, 33, 50, 51]. Its label is abbreviation of "slow band" characterizing its slow decay on the order of μs to ms.

The so-called "fast band", abbreviated as F-band, is characteristic by luminescence decay time in the ns range [52, 53]. F-band is observed predominantly in hydrogenized Si-NCs. Its properties are summarized in principal works [54, 55]. The F-band has been interpreted with two distinct mechanisms, (a) intrinsic optical recombinations in ultra-small Si nanoparticles (with large bandgap opening and strong quantum-confinement) [56, 57], or (b) recombinations on defects in silicon oxide surface layer of oxidized particles [53]. Precise models of luminescence for F-band do not exist, although applications and studies are in progress.

In general, the width of bandgap gets larger with shrinking of the size of nanocrystal due to quantum confinement effect. Wavelengths of emitted light are then shifted to lower wavelengths (red-yellow) compared to bulk Si. The shortest attainable wavelength for oxidized Si-NCs is around 590 nm [58]. Green emission of Si-NCs is sometimes observable for a very limited time directly after etching procedure, when the surface of Si-NCs is still hydrogenated. It indicates that luminescence in the red part of spectrum can be strongly related to the oxydized surface states. Beside the size and surface passivation there are many other parameters that influence Si-NC PL wavelength: nanocrystal shape (spherical or elongated), stress between the core and shell material, possible presence of amorphous Si phase or collective effects in densely packed nanocrystals etc.

The single particle spectroscopy of Si-NCs at room-teperature reveals relatively broad PL band (100-150 meV) compared to other quantum dots. This broadening is due to an indirect bandgap structure of Si which is preserved in nanocrystals with diameters down to 2 nm.

Radiative processes are coupled to phonon vibrations (both phonon related and zero-phonon bands can be observed by the single nanocrystal spectroscopy at low temperatures). On the other hand, the large Stokes shift between absorption and emission of Si-NCs and vibronic structures in single Si-NC spectra in some samples suggest that emission could be due to interfacial radiative centers [59, 60].

The intensity of luminescence from Si-NCs is limited by non-radiative recombinations. Main representative of non-radiative recombinations for Si-NCs is the Auger process. Beside the "classical" Auger process involving interaction of three carriers (eeh or ehh) also the so called bimolecular Auger recombination (kind of inelastic exciton-exciton scattering) is discussed in literature. Delerue et al. [61] suggested that the observed Auger processes is very fast (faster than 1 ns), and from this observation deduced that if more than one exciton is present in Si-NCs, the other present exciton will decay non-radiatively. The possible exciton reactions in Si-NCs in our experiments are discussed in Chapter 3.7 and displayed in *Fig. 65*. Another effect occurs when the Auger recombination gives enough energy to an electron (or hole), which consequently escapes from the nanocrystal or is trapped on the interface. In this way a Si-NC becomes charged. Such mechanism is supposed to be behind the effect of PL intermittence (ON-OFF blinking) observed in single NCs.

Another loss in luminescence comes from presence of defect centers formed by non-passivated surface bonds (so called dangling bonds), which act as efficient non-radiative traps. When the surface is passivated with e.g. oxygen molecules, then energy levels are hybridized. They split into bound and unbound states, that lie outside of the forbidden band and this leads to suppression of non-radiative recombination [62].

When we presume that Si-NC has icosahedral shape and is 2 nm in diameter, then the crystal consists of around 280 Si atoms. About 120 of them are on the surface, which means that nanocrystals really have a big surface to volume ratio. It also means that if anything is attached to the surface of Si-NC, it will have strong influence on optical and physical properties of the nanocrystal. For example, it is known from theoretical calculation that, when a carbon-carbon multiple bonds are in close bonding proximity to the Si-NCs surface, the photoluminescence intensity of Si-NCs is diminished. If this double bond is in conjugation with an aromatic structure, the characteristic emission is completely quenched [63].

The optical properties are a bit different for nanocrystals embedded in films. The quantum confinement picture and the interfacial state model have been in accordance by demonstrating that a Si=O double bond introduces size-independent levels (both for electrons and for holes) within the gap. According to this picture, the radiative recombination of an electron-hole pair trapped at the Si=O double bond or of a trapped electron and a free hole (depending on the Si-NC size) is the process responsible for the observed emission. This emission, however, is still size dependent (within limited range) due to quantum confinement effects, thus explaining the experimentally observed blue shift [64].

The influence of energy states in forbidden band related to impurities can be neglected for our samples. The probability to have an impurity atom (we use boron doped wafers as a source material for Si-NCs preparation) in a Si-NCs is very small, so having negligible influence on the ensemble PL properties.

3.1.2 Commercial quantum dots based on cadmium chalcogenides

CdSe and CdS (II-VI semiconductors) based quantum dots have a direct bandgap and are extensively studied. Their optical properties and energy levels can be well approximated by the effective mass approximation calculations [65]. Luminescence of these particles is tunable through a wide part of the visible optical spectrum and they have quite narrow emission peaks. The narrow PL band is due to direct recombination of e-h pairs in the core of nanocrystals.

These particles need to be properly surface passivated or covered with appropriate shell in order to achieve high quantum efficiency of luminescence, which could by as high as 70-85 % [66]. This covering also protects the CQD from quenching by metal ions, which could induce non-radiative recombination of excitons or electron-hole pairs [67].

3.1.3 Nanodiamonds

Although the precise mechanism of luminescence in nanodiamonds (ND) is not known, the visible and near-UV PL must be related to the presence of intrinsic defects (e.g. intersticial carbon atoms displaced from crystal lattice) or impurities in nanosized diamond crystal. (Diamond has very wide indirect band gap of ~5.5 eV, so the excitonic emission is around 230 nm in the far UV region.) The most discussed and studied emission center in ND is the nitrogen-vacancy point defect (N-V center) with absorption around 400-500 nm, which result in a specific PL bands at 500-800 nm [68]. This impurity can be introduced into ND by annealing. Chapman et al. [69] excited a nitrogen centre in ND with a 532 nm laser from its ground triplet state to the phonon band of their first electronically excited triplet state. This excitation was followed by the fast phonon-assisted relaxation to the bottom of the excited state and by broadband luminescence centered at around 680 nm. Other impurities, which are common in ND, is silicon (isoelectronic impurity) and also adsorbents from air.

Specific features which are different in ND compared to bulk diamond are: (i) A bending of valence and conduction bands due to violation of grain boundaries, (ii) Another band emerges in the bandgap due to distortion of sp3 bonds and dangling bonds, (iii) In some cases new bands, which have origin in sp2 bonds, are also observed. For example, incorporation of nitrogen leads to a strong absorption in the whole energy spectrum, as a result of increased number of sp2 carbon atoms [70]. The quantum yield has not been specified up to today, the estimated values in literature range from 10 % up to 90 %.

3.2 Macroscopic luminescence spectroscopy

The colloidal suspensions of nanomaterials were studied using fluorescence spectrometer FluoroMax®-3 (Horiba Jobin Yvon). The samples were excited with a 150 W ozone-free xenon lamp. All data were corrected for spectral sensitivity of the apparatus and spectral dependence of excitation power. A clear solvent was measured separately in order to correct data for signals caused by Raman-scattering of solvent. Measured data have been processed with Origin8.

The emission spectra of a freshly prepared Si-NCs ethanol suspension (one week old) are displayed in *Fig. 15*, the excitation spectra are displayed in *Fig. 16*. The maximum of photoluminescence was around 600 nm for this sample. The emission intensity decreased with increasing excitation wavelength.

Figure 15: Emission spectra of Si-NCs in ethanol for various excitation wavelengths.

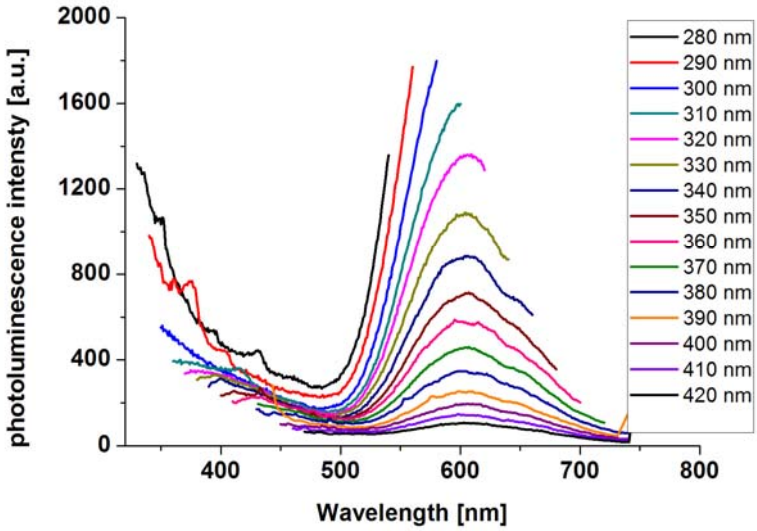

Figure 16: Excitation spectra of Si-NCs in ethanol for various emission wavelengths.

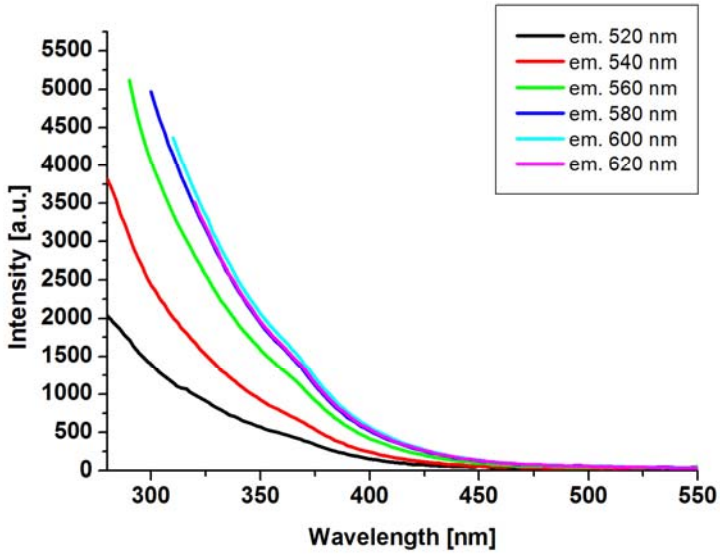

Figure 17: Emission spectra of CQDs in ethanol for various excitation wavelengths.

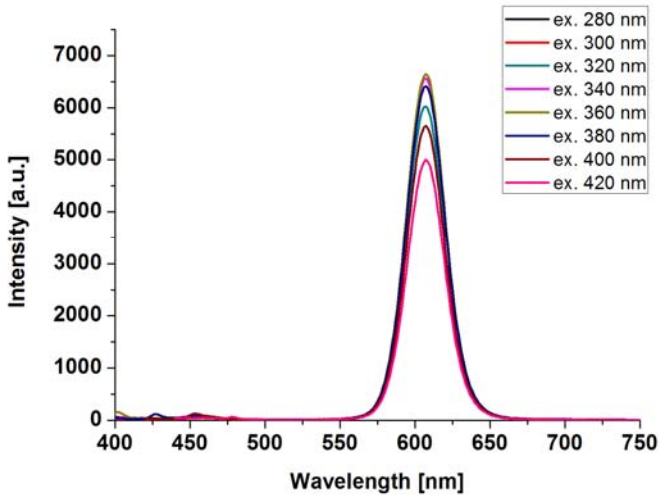

Ethanol colloid of CQD was measured in disposable cuvettes, because we can not effectively clean out the CQDs from the fused silica (expensive) cuvettes. CQD had luminescence peak centered at around 605 nm. Emission spectra of CQD in ethanol are shown in *Fig. 17* and excitation spectra in *Fig. 18*.

Figure 18: Excitation spectra of CQDs in ethanol for various emission wavelengths (The PL peak is around 605 nm).

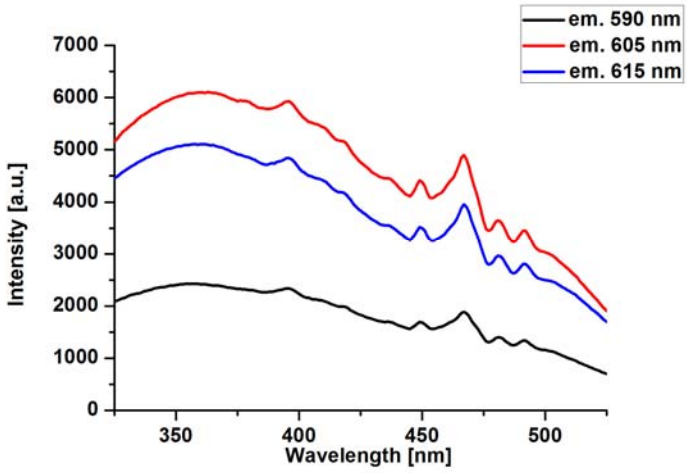

Figure 19: Emission spectra of ND in water for various excitation wavelengths.

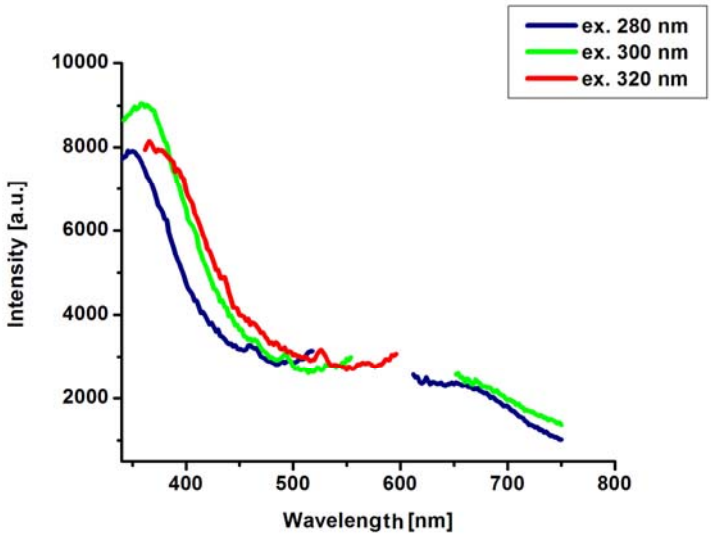

The nanodiamonds used in this study nanodiamonds emitted in the blue region of optical spectrum. The emission was very weak for excitation wavelengths longer than 320 nm. Emission spectra of NDs in water are displayed in *Fig.19*. The photoluminescence maximum was around 360 nm.

The PL of ND was weak in the visible part of optical spectrum and efficiently excitable only by photons below 340 nm. If we introduce a nitrogen vacancy into ND, the luminescence peak is red-shifted, while the surface of ND and other physical properties stay the same. The excitation spectra were not measured because the apparatus was not able to measure below 280 nm and excitation spectra detected at the emission wavelength of 360 nm will be very noisy.

A comparison of luminescence spectra of all studied nanomaterials is shown in *Fig. 20*. We can see that the spectrum of CQDs is relatively narrow compared to Si-NCs, whose spectrum is broadened due to the broad size distribution. Both of them had quite efficient luminescence (even on a single nanocrystal level) more than sufficient for biological experiments. Luminescence of ND without any specific luminescence centre (like N-V center) has a monotonously descending shape without any narrow band in the observed spectral region. Although this luminescence was weak, we have been able to observe NDs in a cell using a confocal microscope (Chapter 4.8).

Figure 20: Emission spectra of the three studied nanomaterials: ND – nanodiamonds, Si-NCs – silicon nanocrystals, CQD – commercial quantum dots, excited at 320 nm.

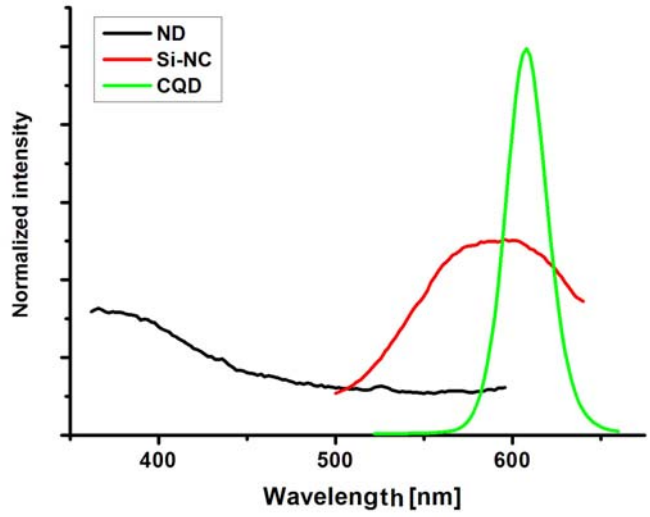

Figure 21: Emission spectrum of a small Si-NC agglomerate taken with confocal microscope (artifacts caused by the dichroic and edge filters are visible at 480nm and 550nm).

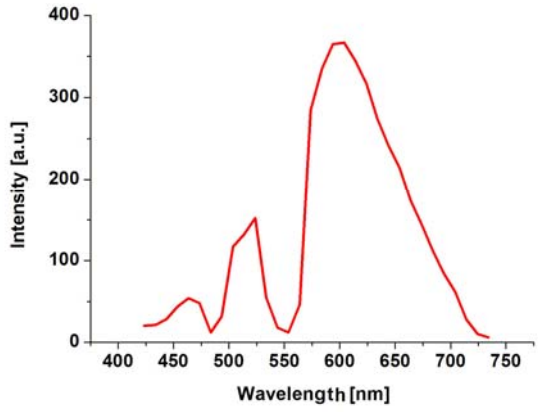

The confocal microscope is described in Chapter 4.8. It enables also detection of a full spectral shape of an emitting spot but we used this spectral detection only for separation of different emitting species in PL images (cell autofluorescence, labelled organels, and nanomaterials). Moreover the filters in a fluorescence cube were not adapted for very broad PL spectra of some of our materials and caused significant distortion in detected spectra (see *Fig. 21*).

3.2.1 F-band spectroscopy of Si-NCs

When the used colloidal suspension of Si-NCs in ethanol was having two PL emission bands (peaking at around 400 and 600 nm and labeled as F- and S-band, respectively) was filtered (using Millex millipore filter with 100 nm diameter pores), only the 400-nm PL band remained. The PL of the filtered Si-NCs suspension is shown in *Fig. 22*.

Figure 22: a) Photoluminescence spectra of filtered Si-NCs in ethanol (excited with wavelengths from 270 to 420 with 10 nm steps). b) Differential photoluminescence spectra calculated as a difference between neighboring spectra from the upper panel. (Taken from [6A]).

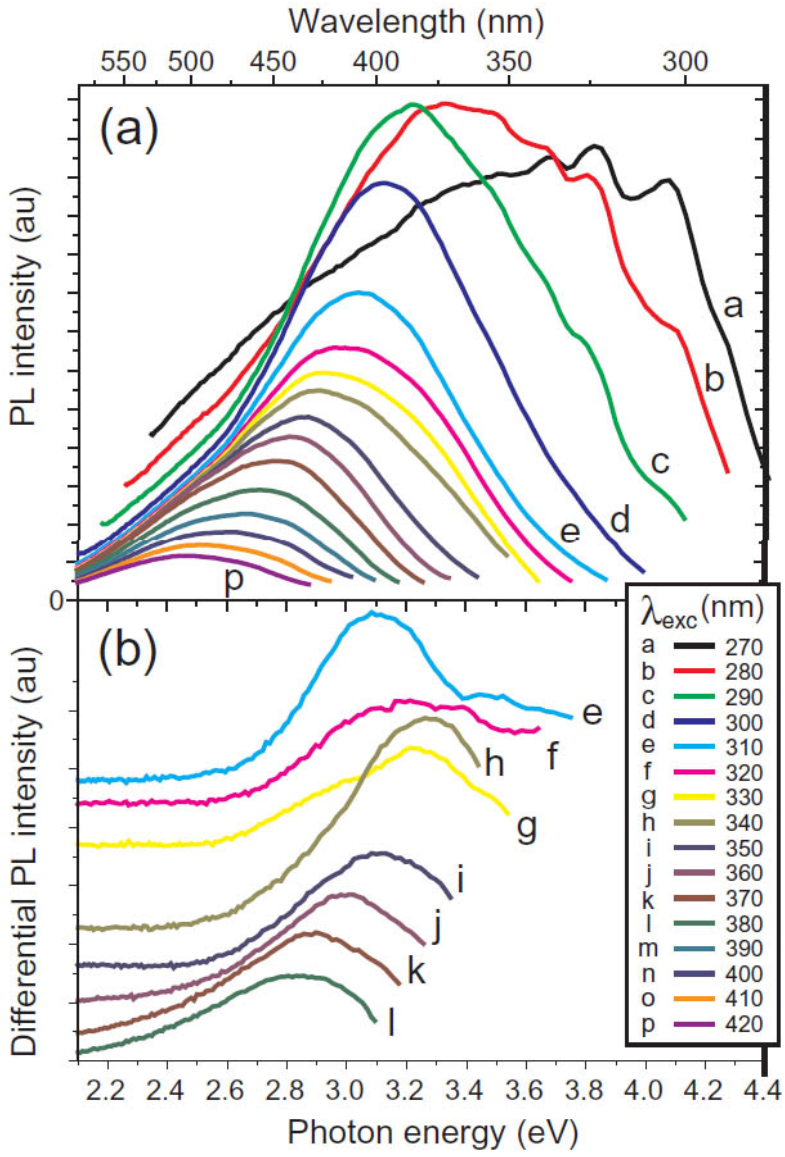

The PL spectra in *Fig. 22b)* were recalculated from nm to eV, i.e. measured PL was multiplied by λ^2 in order to transform the wavelength scale correctly [71]. The PL maximum shifts with change of the excitation wavelength. Such behavior was not observed for any of our Si-NCs samples emitting at around 600 nm (the S-band emission).

The Stokes shift of the differential PL band increased from 0.2 eV at 2.5 eV to 0.4 eV at 3.5 eV. At excitation around 3.7 eV the PL peak moved back to lower energies (the Stokes shift got even higher). Those results are in agreement with theoretical calculations of small Si clusters, where the anomalous Stokes shift in clusters diameter smaller than about 1.4 nm is explained to be due to enhanced structure relaxation [71] However, for excitation energies above 4 eV the experimental PL spectra reveal several peaks and cannot be easily compared with the theoretical model. This experiment also promote the idea that the origin of luminescence lies in the Si nanocrystal rather than in the SiO_2 surface layer [6A].

3.3 Luminescence micro-spectroscopy

This technique allows us to measure weak luminescence signals with spatial resolution of about 400 nm (when adopting the Rayleigh criterion for diffraction-limited spots, the distance of two emitting spots to be resolved must be at least $(1.22 \cdot \lambda)/(2 \cdot NA)$, which gives 400 nm for numerical aperture of 0.9 and wavelength of 600 nm). Spectra of single objects smaller than diffraction limit can be detected if their distance is bigger than resolution limit and all background signals (like substrate fluorescence, inelastic (mainly Raman) scattering etc.) are practically eliminated. Our apparatus enable measurement at room temperatures and also at lower temperatures, when equipped with a special cryostat head. A liquid helium (cooling down to 5 K) or liquid nitrogen ($T \geq 78$ K) can be used.

Our apparatus was designed and built especially for samples emitting low photon rate, like Si nanocrystals. In contrast to most of micro-spectroscopy set-ups our system is not based on the confocal imaging but the wide field imaging. The illumination optics is designed so that the laser excitation spot is of about 40 mm in diameter (with the 100x magnification objective lens). Consequently, multiple emitters can be observed simultaneously and long detection time (up to ~1 hour) can be used, while the confocal system detects only one diffraction at once and sample must be scanned in order to observe an image.

In this thesis we measured PL of our nanomaterials (possibly single grains). We measured spectra of Si-NCs not only in ethanol, but also in other solvents. Single spectra of our xylene treated Si-NCs are discussed in Chapter 3.3.3. The change of PL of Si-NCs in various solvents is discussed in Chapter 3.4. Micro-spectra of all our nanomaterials were also observed in a living cell, the results are discussed in Chapter 4.9. We were not able to measure the influence of aging and various solvents on CQD due to the fast degradation of PL of those particles. In case of ND, the PL of single ND was too low to be measurable on our apparatus with clear data interpretation.

3.3.1 Micro-spectroscopy setup

The experimental apparatus is shown in *Fig. 23*. It is based on an inverted optical microscope (IX-71, Olympus). Sample is excited by a laser beam either in the total-internal-reflection (TIR) or the "epifluoresecence" configuration.

For the TIR experiments we used the 458-nm line of an Argon-ion laser (type Sabre INNOVA SBRC-R-DBW-25/7, Coherent). The laser beam was reflected by several mirrors into a dove prism and totally reflected on its lower surface. In this way the sample deposited on this surface was excited with an evanescent wave. The main advantages of the TIR configuration are a strong reduction of excitation light penetrating to the detection system and a reduction of excited sample volume as the evanescent wave penetrates only several hundreds of nm below the prism surface. Data measured with this configuration have been published in two our papers [1A] and [4A].

Most of the later experiments were done in the epifluorescence configuration, which is much simpler for adjustment. The laser beam is sent to the microscope through the back port to the fluorescence filter cube (passing the excitation filter and reflected from the dichroic filter) and then the objective lens which is also used for collection of signal. The special feature of our illumination system is a diverging (fused silica) lens at the input port which is designed so

that the excitation spot is enlarged. Its diameter depends on the objective lens used; in case of 100x/0.8 lens it is about 40μm. The excitation laser was 405 nm continuous wave diode laser (type Bluephoton® CWA 405 nm Serie, Omicron). The output power of the laser was kept constant (24 V, 0.88 A). The intensity of the laser beam was regulated by neutral optical density (OD) filters in the range from 0 to 3. We used mainly OD 0.5 filter resulting in excitation power of around 608 μW in the sample area; and 173 μW for OD 1.0 filter. For majority of samples in the second set of experiments an OD 1.5 filter was used, with excitation power in the sample area reaching approximately 88 μW (with this excitation power the samples were not over-excited and the emission of nanoparticles was sufficient to complete the measurement in reasonable time - less than 20 minutes per spectral image).
For non-biological samples (i.e. all except cell samples) a 100x magnifying objective with 0.8 numerical aperture (type LMPlan FLN, Olympus) was used. For biological samples we needed to use the oil-immersion objective (Olympus UPlan FLN 100x/1.35NA,) as cells have to be kept either in cultivation media or in a fixative medium.

The emission signal from the sample was collected with the microscope objective and transmitted through the dichroic mirror and edge filters (see *Fig. 24*), where the scattered excitation light was removed from the signal. From here the emission was imaged to the entrance slit plane of an imaging spectrometer (ACTON SP-2300i, Princeton instruments). Both images and spectra can be detected by rotating a diffraction grating in the spectrometer into the zero- or first-order position, respectively. (Detailed description of the measurement procedure is given in the next paragraph). The signal was collected by a back illuminated CCD camera (type Spec-10:400, Princeton Instruments). The camera was cooled by liquid nitrogen to working temperature of -102 °C. All parameters of measurement, as well as setup of spectrometer and data acquisition were controlled in WinSpec program.

Figure 23: The principal scheme of the imaging micro-spectroscopy apparatus built at Department of Chemical Physics & Optics MFF UK (the near-infrared spectroscope and camera on the right-hand side of the microscope is not shown here): IX-71– Olympus inverted microscope, diode laser – 405 nm Omicron diode laser, F – optical density filter carousels, M – mirror, PCR – polarization and frequency cleaning element, El – entrance lens, O – objective, Slit – adjustable entrance slit of spectrometer, G – diffraction gratings, CCD – back-illuminated liquid nitrogen cooled CCD camera, COL – nitrogen cooling reservoir for CCD, Spectrograph- 30-cm imaging spectrograph (ACTON SP 2300).

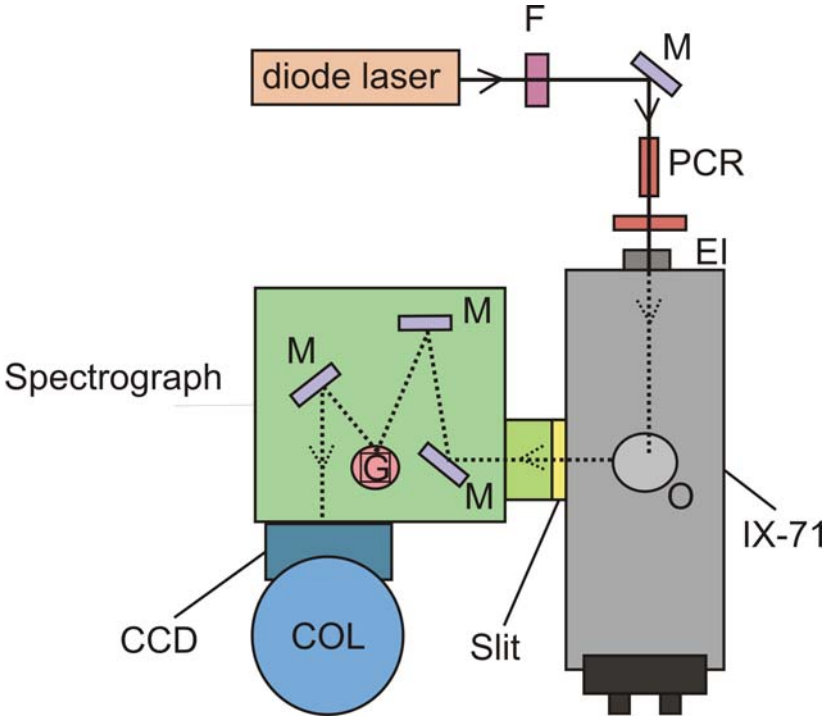

Figure 24: Transmittance of filter cube designed for the work with 405 nm excitation: Excitation filter FF01_406 (dark blue line), dichroic mirror Di01_R405 (red line), Long-pass edge filter BLP01_405R (cyan line). The LP03_532rs25 (green line) edge filter was sometimes added for ellimination of the blue-green spectral region below 532 nm (e.g. cell autoflorescence).

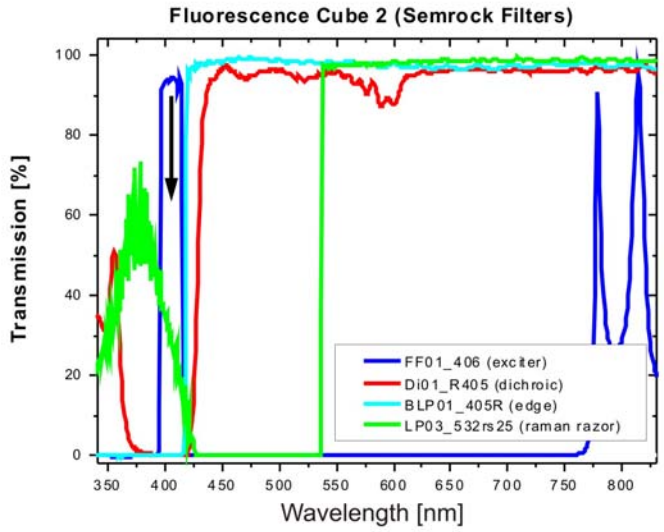

3.3.2 Micro-spectroscopy experiments

The micro-spectroscopy measurement procedure is illustrated in *Fig. 25*.

Figure 25: Micro-spectroscopy measurement procedure. a) observed sample b) section of region of interest (slit – dotted line), c – observed spectra from spots in sample. In the right corner are positions of grating.

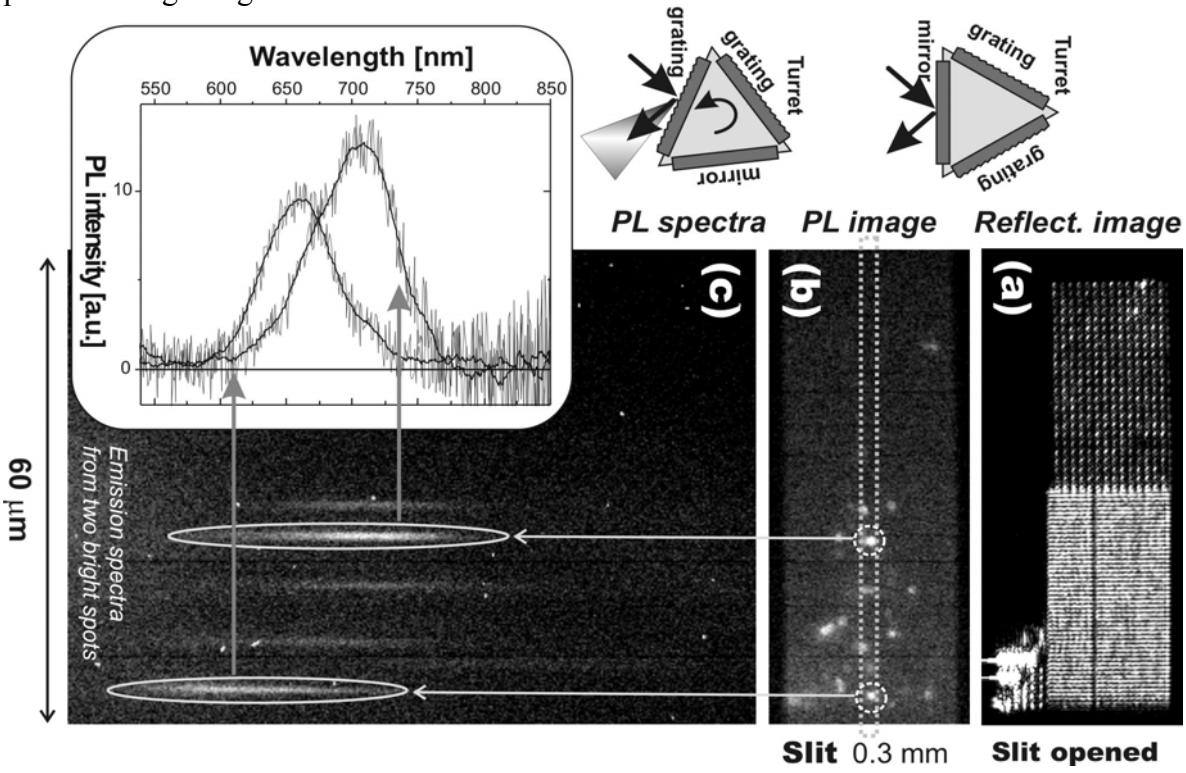

After the samples were fixed in the microscope sample area, the focus of the microscope and the selection of the region of interest was adjusted using the grating in zero-order position and the fast CCD data-reading frequency (1 MHz) with sample illuminated by halogen lamp in a transmission

or reflection configuration (the entrance slit is opened to maximum, i.e. 12 mm). Then a luminescence image is detected and sample position adjusted to have the studied emitting spots placed close to the vertical central axis of image. When closing the slit (typical width is 10-20 μm), only this central area of the image remains. Then the grating is rotated to the first diffraction order by setting a central wavelength (detected range is about 350 nm) and the spectra of emitting spots are dispersed along the horizontal axis. In order to reduce read-out noise of the CCD the data-reading frequency is reduced to 100 kHz. Typical acquisition time of micro-spectral images of single Si-NCs is several minutes up to 1 hour. The data were processed in Origin8, where we subtracted a background from the signal. We integrated signals typically from 3 pixel wide line (this corresponds to the size of diffraction limited spot); the background was preferably taken from lines near to the signal one.

In order to observe single nanocrystals, we had to ensure that emitting nanocrystals are spaced more than the optical resolution limit. For this reason we diluted samples, usually with ethanol or source solution in 1:100 ratios, until the optimal concentration is found. For measuring spectra of Si-NCs colloids, a droplet of colloid was deposited on a 1-mm thick quartz slide and dried in air for about 2 minutes; after this procedure it was placed in the sample area of the microscope and measured.

In case of living cell samples we were forced to work fast and measure within a 30 minutes time window, as our setup is not equipped with a protective chamber allowing to control CO_2 atmosphere and temperature. Under normal ambient conditions cells survive without significant damage only about 30 minutes. We also had to use excitation OD filters higher than 1.5, because higher excitation intensity causes damage to cells. There are no special precautions for fixed (i.e. non-living) cell samples.

Results of our micro-spectroscopy experiments are described in Chapters 3.3.3 (xylene treated Si-NCs), 3.4 (Si-NC samples in various solutions), and 4.9 (micro-spectra of nanomaterials in living cells).

3.3.3 Xylene treated Si-NCs

The as-prepared sample of organically capped Si-NCs was diluted 100 times by source xylene solution and then a 2-μl droplet was placed on the measuring quartz dove prism. The sample was dried out for about 2 minutes and a glossy film was formed. Excitation was performed by an evanescent wave of 458-nm line of Argon-ion laser (Sabre INNOVA SBRC-R-DBW-25/7, Coherent) totally reflected inside the prism.

We observed some aggregates in the sample (probably formed during drying of the sample), but mainly single isolated luminescent crystals. The spectra from single crystals are shown in *Fig. 26*, they have been corrected for the spectral response of the experimental setup and also background was subtracted.

The typical photoluminescence spectrum of organically caped Si-NCs had a double peak structure with 70 ± 10 nm (150 meV) distance between the peaks. The FWHM was 25 nm for the first peak and the peak was positioned between 525-575 nm. The FWHM for the second peak was not determined because of its overlap with the first peak and also its variable shape. The second peak was positioned between 560-620 nm.

Figure 26: Smoothed micro-spectra of single organically capped Si-NCs with one raw spectrum shown in the inset (Taken from [4A]).

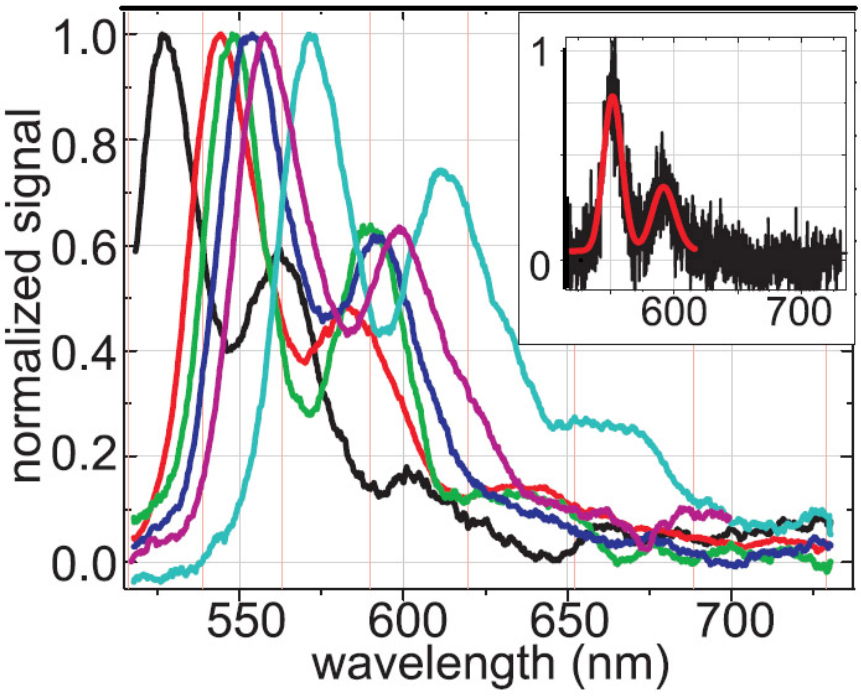

This double peak structure was also observed by other groups for different organically capped as well as oxidized Si-NCs [73, 74]. The origin of the PL double peak structure was explained in literature as Si-O-Si vibration related [73, 74], but these bonds seem to be rare in our sample. Observation of such multiple-peak spectra with very similar spacing in Si-NCs with various surface passivation as well as in completely different qunatum dots (ZnCdSe [75]) suggest that there is a deeper physical origin of this emission. One explanation could be the recombination of charged excitons (called trions) in a "parabolic-like" potential well giving rise to quantum.harmonic-oscillator-like levels [75].

3.4 Aging of Si-NC samples

The aim of this experiment was to simulate evolution of Si-NCs properties during a long time spend inside a cell, more precisely the luminescence spectral changes emerging during 3-month study. It is commonly accepted that Si-NCs are biodegradable in living body within several months [76]. As it is practically impossible to do such kind of long lasting experiment with living cells - i.e. measuring the micro-spectra of Si-NCs in the same living cells in 14 days intervals for several moths, we prepared several colloidal suspensions based on solutions which can be found in living cell and studied PL properties of Si-NCs in those solutions for about 80 days.

Another strong motivation for Si-NCs aging experiment was our observation of a significant blue-shift of Si-NCs PL maximum of Si-NCs inside cells (Si-NCs were incubated with cells for about 48 hours) compared to Si-NCs in ethanol. Micro-spectra of Si-NCs in a cell and in ethanol are shown in *Fig. 27*.

Figure 27: Luminescence from Si-NCs measured in L929 cell (black line) and in ethanol (in red); spectra were measured with micro-spectroscopy apparatus.

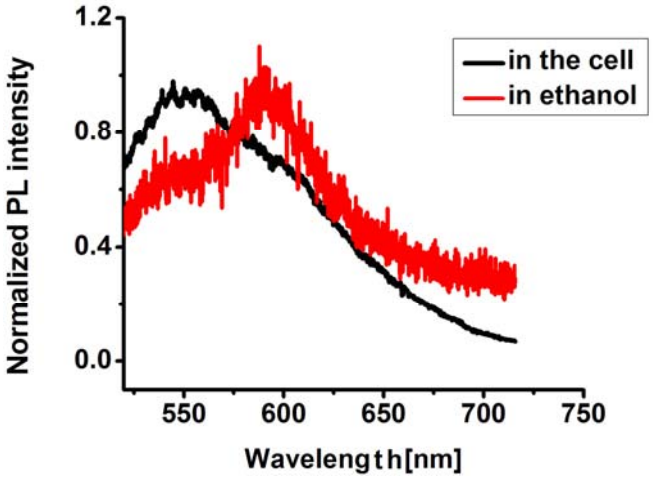

We wanted to find out if this shift in luminescence was caused by presence of various chemical groups in the cell or by the variable pH in cell organelles and regions. To test this, we prepared several solutions which can be found in the cell and solutions with various pH.

Last but not least reason for this experiment was observation of another change in PL after chemical activation of Si-NCs - organically (CH_3) capped Si-NC have very different emission spectrum compared to other Si-NCs samples. The luminescence peak is shifted from 640 nm (for oxidized Si-NCs) to 570 nm [4A] (more about preparation of these particles could be found in Chapter 2.5.1 and their optical studies in Chapter 3.3.3).

3.4.1 First aging study

Colloids prepared from Si-NCs in ethanol have been studied in our laboratory for more than 5 years; therefore, we chose Si-NCs in ethanol (99.8 % ethanol for UV spectroscopy) as a standard sample.

Other samples in this first study were Si-NCs in distilled water, Si-NCs in distilled water with D-glucose (concentration 0.12 g in 1 ml of water), and Si-NCs in distilled water with NaCl (concentration 0.05 g in 1 ml water). Both D-glucose and NaCl can be found inside cells and play crucial role in cell life and functionality. The same amount of Si-NCs (0.5 mg) was used for preparation of each sample and mixed with 1.2 ml of solution in the same type of cuvette. The molecular structures of chemical compounds used in our solutions are shown in *Fig. 52*. The influence of these structures on Si-NCs PL will be discussed below.

Si-NCs colloids in cuvettes were stirred continuously by rotation of a small teflon-coated magnet with speed of 220 rpm by a magnetic stirrer (Hei-Tec, Heidolph) at room temperature (22 °C) in ambient light for maximally 80-120 days. The Si-NCs samples were measured every 2-3 weeks in a fluorescence spectrometer and micro-spectroscopy apparatus. We also measured PL quantum efficiency for some samples after 80 days (see Chapter 3.5).

For each Si-NC sample, a corresponding control sample without Si-NC was measured as well to determine a background (including strong Raman scattering from the solvent). The background was subsequently subtracted from the signal.

The measured emission spectra are displayed in for Si-NCs in ethanol, water with D-glucose, pure water, and water with NaCl in *Fig. 28*, *29*, *30*, and *31*, respectively. The PL of samples was excited by various wavelengths from 280 to 420 nm at 10 nm intervals; only PL spectra

for 280 nm and 360 nm excitations are shown for clarity. The evolution of PL peak intensities with time for different solutions are summarized in *Tab. 6*.

Samples for micro-spectroscopy were prepared by the following procedure: One 2 µl droplet of Si-NCs colloid was placed on a fused-silica (often called quartz) slide and let to dry on air for about 3 minutes; then it was placed into the micro-spectroscopy apparatus (described in Chapter 3.3.1). The slide with sample was oriented in such a way that the sample side was facing the 100x magnifying objective (LMPlan FLN, 0.8 numerical aperture) and excited through the same objective (epifluorescence configuration). The intensity of excitation laser (405 nm, diode laser) was reduced by 1.0 OD filter. The excitation energy in sample area was approximately 173 µW. The samples were measured for 110 days. The emission spectra originating possibly from single Si-NCs in ethanol, water with D-glucose, pure water, and water with NaCl are shown in *Fig. 32*, *33*, *34*, and *35*, respectively.

Figure 28: Emission spectra of Si-NCs in ethanol measured after various duration of incubation (shown in legend in days) with a) excitation wavelength 280 nm, b) excitation wavelength 360 nm.

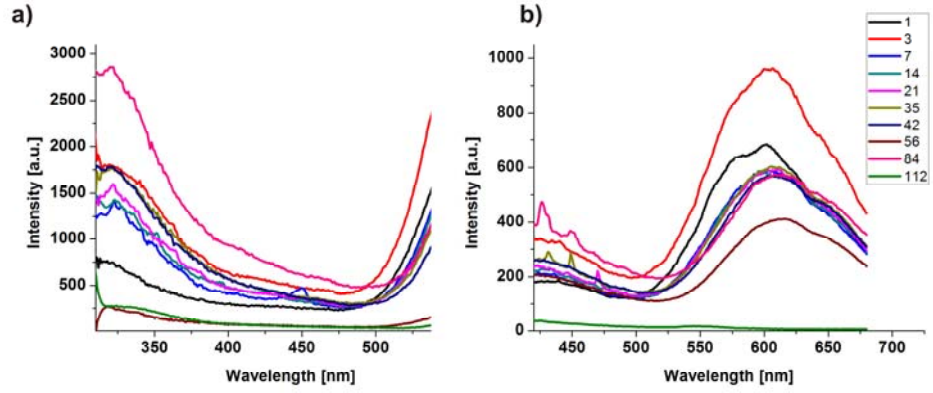

Comment: The increase in emission intensity at 3rd day of stirring was probably due to breaking down of small Si-NCs agglomerates, effectively increasing concentration of isolated Si-NCs and also due to further oxidation of Si-NCs from the incompletely oxidized during preparation. The intensity was stabilized after about 7-40 days and then started to degrade. After 100 days the emission intensity was very low compared to the starting one.

Figure 29: Emission spectra of Si-NCs in water and D-glucose with various duration of incubation (shown in legend in days) with a) excitation wavelength 280 nm, b) excitation wavelength 360 nm.

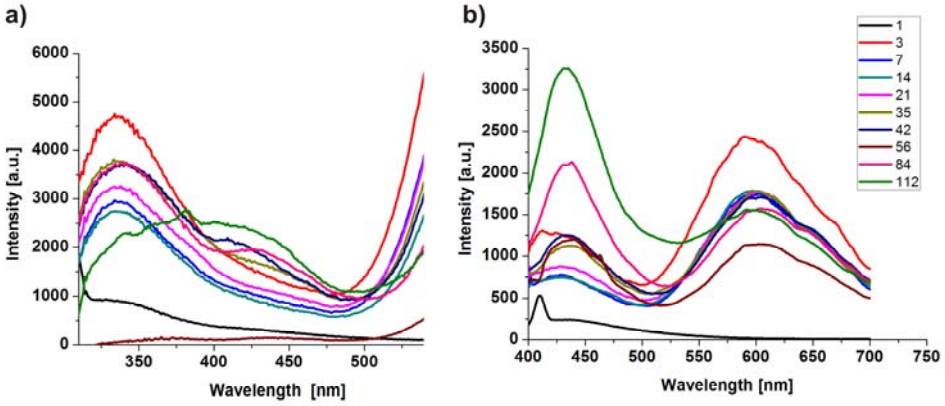

Comment: Similarly to Si-NCs in ethanol we observed slight increase in emission intensity on the 3rd day. Explanation of this effect

is the same as for the previous sample. We observed strong emission band around 350 nm under excitation at 280 nm (*Fig. 29a*) and around 420 nm for excitation at 360 nm (*Fig. 29b*). This luminescence band was actually coming from increasing concentration of D-glucose in solvent due to slow evaporation of water from the solution. The intensity of the PL peak around 600 nm was decreasing with time more slowly than for the Si-NCs in ethanol.

Figure 30: Emission spectra of Si-NCs in water with various lengths of incubation (indicated in the legend in days) with a) excitation wavelength 280 nm, b) excitation wavelength 360 nm.

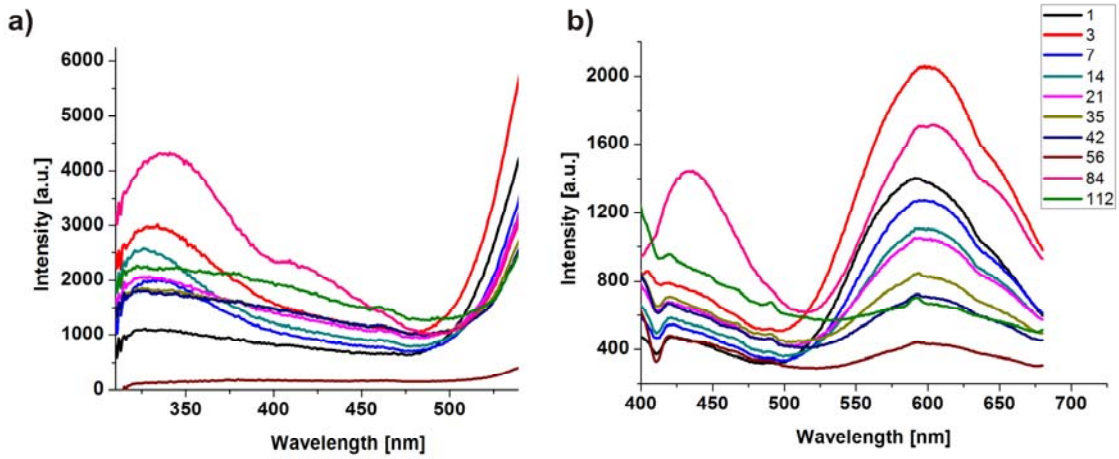

Comment: As for the previous two samples, PL intensity increased slightly after 3rd day also for Si-NCs in water. The reason for the increase was again further oxidation of particles and splitting of grains due to mechanical stirring. The PL intensity of the band around 600 nm decreased more slowly than in previous two cases.

Figure 31: Emission spectra of Si-NCs in water with NaCl detected after various duration of incubation (shown in legend in days) with a) excitation wavelength 280 nm, b) excitation wavelength 360 nm.

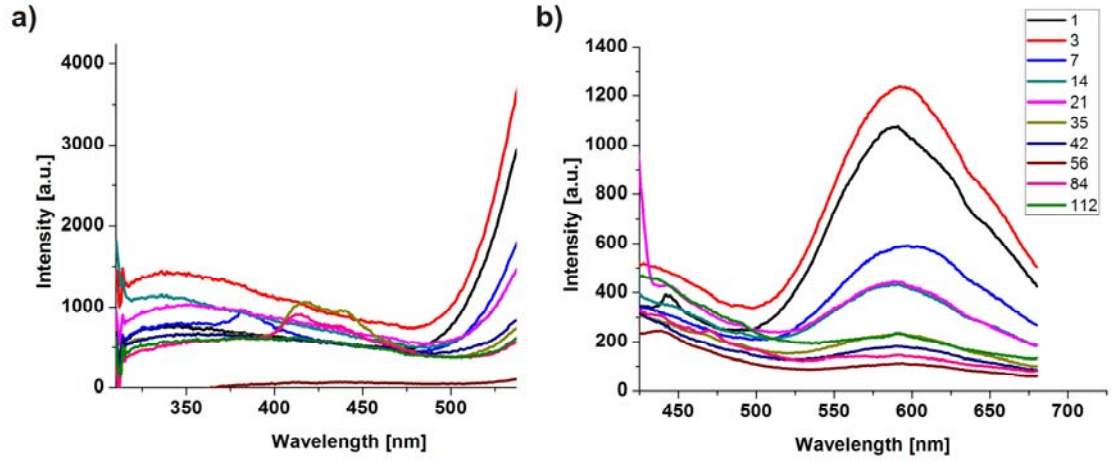

Comment: As in the previous sample, PL intensity of the 600 nm band increased the 3rd day. Then PL started to decrease steadily, showing no period in which the PL would be considered stable (as was the case for Si-NCs in ethanol and in water with D-glucose). The PL intensity decreased to the low levels in quite short time compared to previous samples. We observed slight salting around the cuvette bottle-neck after three weeks, the concentration of NaCl then shifted slightly.

Figure 32: Emission spectra of single Si-NC grains in ethanol measured using the micro-spectroscopy apparatus (sample was excited with 405 nm diode laser) after several days of incubation: a) 4 days, b) 9 days, c) 16 days, d) 36 days, e) 80 days - all spectra, f) 80 days - selection of spectra.

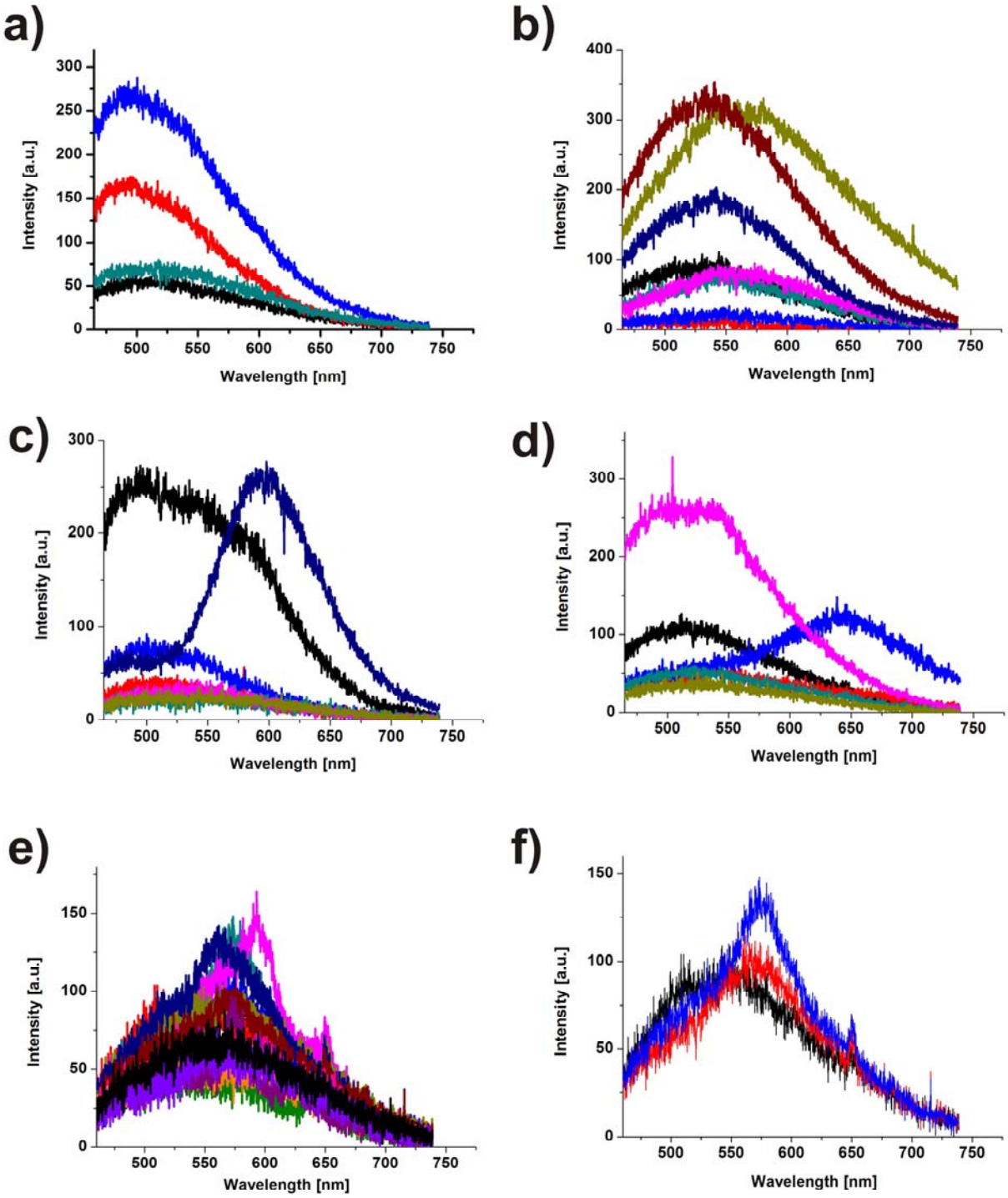

Comment: We observed grains of Si-NCs for the first 10 days. After 10-40 days we succeeded also in measuring smaller Si-NCs agglomerates. After 40 days luminescence intensity started to decrease and the signal coming from single Si-NCs grains was more noisy (*Fig. 32e,f*).

Figure 33: Emission spectra of single Si-NC grains in water with D-glucose measured using the micro-spectroscopy apparatus (sample was excited with 405 nm diode laser). The aging lasted for (in days): a) 4, b) 9, c) 16, d) 36, e) 80 days - all spectra, f) 80 days - selection of spectra.

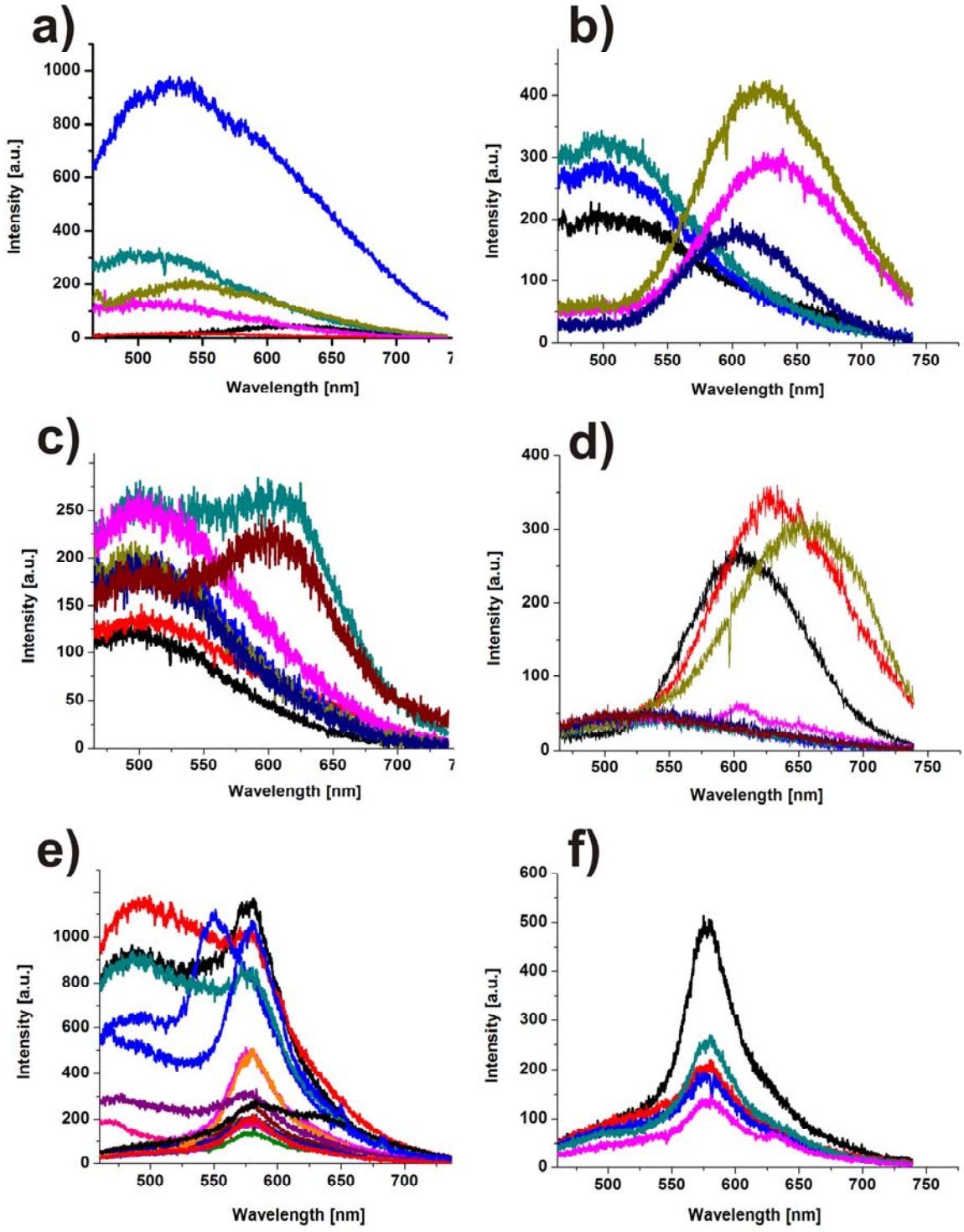

Comment: In the first measurement (4th day) we observed mainly big aggregates of Si-NCs. For longer delays, numbers of small PL objects (possibly single Si-NCs) were observed. After two weeks we observed spectra with two PL peaks having maxima at around 500 and 620 nm. After 80 days a new PL maximum emerged at around 560 nm.

Figure 34: Emission spectra from single PL spots of Si-NCs in water measured using the micro-spectroscopy apparatus (sample was excited with 405 nm diode laser). The duration of aging was (in days): a) 4, b) 9, c) 16, d) 36, e) 80 days - all spectra, f) 80 days - selection of spectra.

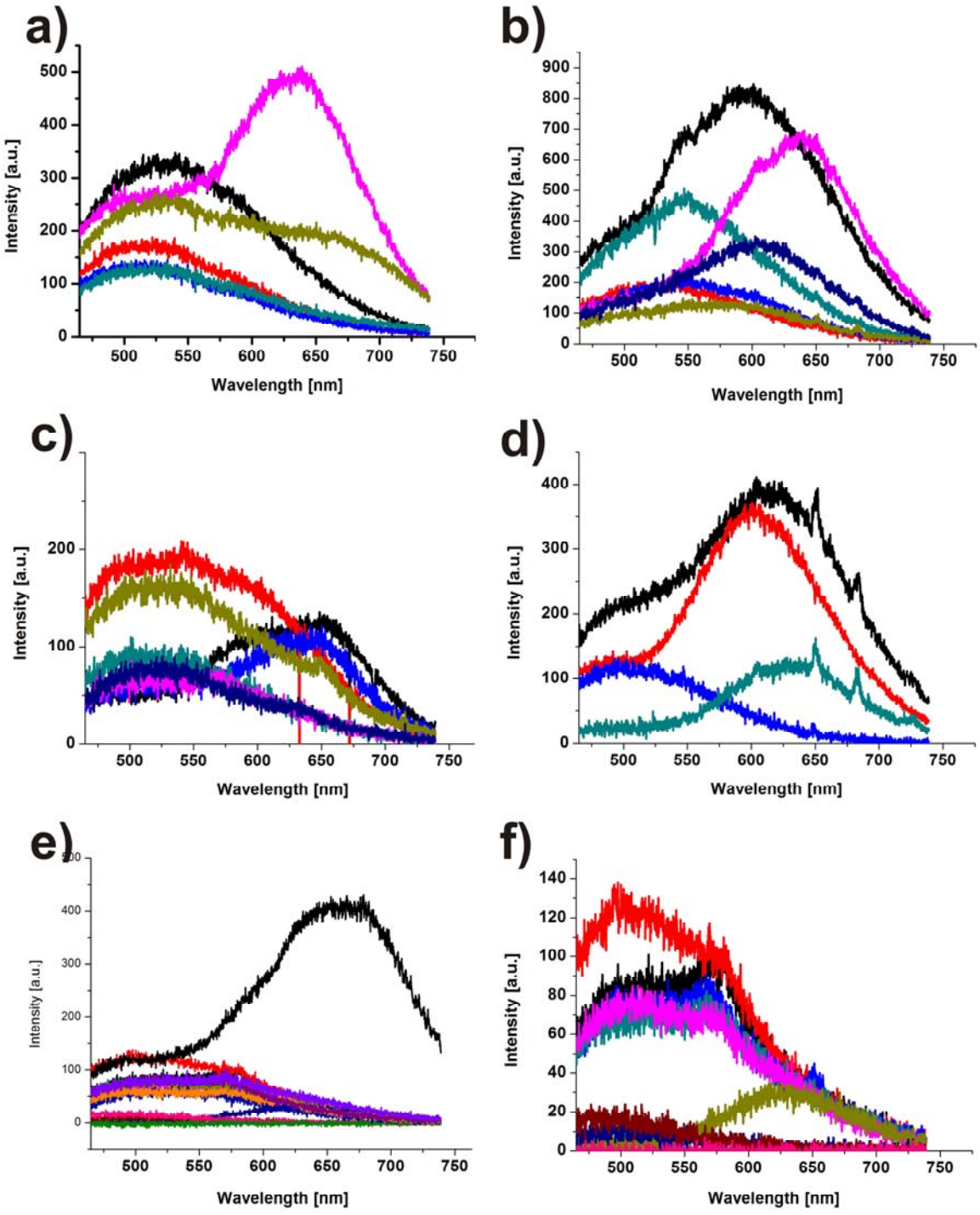

Comment: This sample had PL properties quite similar to that one containing Si-NCs in ethanol. The only difference was that in the first two weeks we observed shifts of PL band. This effect was probably caused by progressing oxidation of Si-NCs.

Figure 35: Emission spectra of Si-NCs in water with NaCl measured using the micro-spectroscopy apparatus (sample is excited with 405 nm diode laser). The incubation time was (in days): a) 4, b) 9, c) 16, d) 36, e) 80 days - all spectra, f) 80 days - selection of spectra.

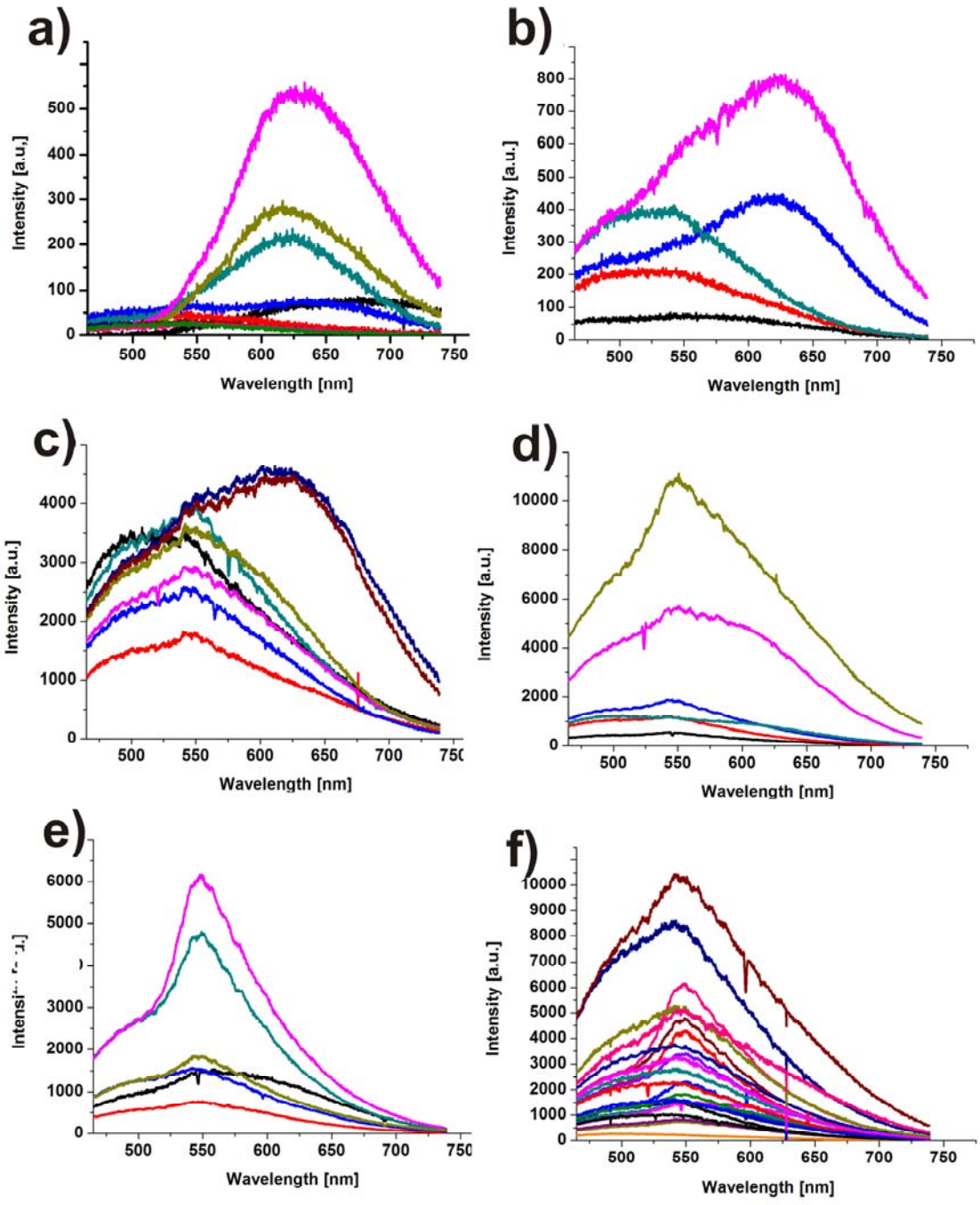

Comment: We have not been able to see PL from single Si-NCs for this sample. This was probably caused by the crystallization of NaCl on quartz slide immediately after the drop was placed on it. Therefore only PL from grains was measured.

All the samples showed slight increase of PL intensity of 600 nm peak the 3rd day of experiment. This effect was presumably caused by further oxidation of surface of Si-NCs,

which may had been incomplete from the process of preparation. Another reason may be an increased concentration of single standing Si-NCs in the colloid, caused by breakdown of bigger Si-NCs agglomerates due to the mechanical stirring. Likely, both of those effects were responsible for the observed increase of PL intensity.

The luminescence intensity of Si-NCs decreased with time. The fastest and strongest decrease was observed for Si-NCs in water with NaCl. The slowest decrease of PL intensity was observed for Si-NCs in pure water and in water with D-glucose. The time evolution of PL intensity at 600 nm in all studied samples are summarized in *Tab. 6*.

Table 6: Time-evolution of photoluminescence intensity of the 600-nm peak of Si-NCs incubated in various solutions. The samples in cuvettes were excited at 360 nm and the measurement was done using the fluorescence spectrometer. The initial PL intensity (first day of aging) was normalized to 100 % and the other values are related to this value.

	PL intensity at 600 nm [%]						
Sample name	1st day	3rd day	14 day	35 day	56 day	84 day	112 day
Si-NCs in ethanol	100	140	85	86	58	8	2
Si-NCs in water	100	149	80	60	31	12	5
Si-NCs in water and NaCl	100	119	40	22	10	13	2
Si-NCs in water and D-G*	100	106	108	108	82	94	94

D-G*: D-glucose

The micro-spectroscopy study of the samples showed that, in case of Si-NCs in water with D-glucose, we were able to observe several "single-like" Si-NCs within the studied droplet for long time. In addition a new PL peak emerged after 80 days and for 112 days old sample we only observed Si-NCs with PL peaks at around 570 nm. The number of luminescing Si-NC agglomerates was very low compared to other samples. This sample also showed the longest PL stability compared to other three Si-NC samples (see *Tab. 6*).

We had problems to observe single emitting nanocrystals in ethanol or in water after 50 days of aging. Even if we succeeded, the luminescence of those single spots was very low and noisy. The PL intensity was more stable in ethanol than in water, but both decreased significantly faster compared to Si-NCs in water with D-glucose.

In case of Si-NCs in water with NaCl we did not observe any single Si-NCs using the micro-spectroscopy apparatus. Even the observed Si-NCs agglomerates had very low PL intensity compared to other samples. The decrease of macroscopic PL intensity with time was fastest from all studied samples.

After discovering that Si-NCs treated with D-glucose have the most stable luminescence compared to other samples (it was stable even after 40 days), we decided to measure aging in another series of samples in solutions with different D-glucose concentrations. In addition we wanted to test whether the Si-NCs PL is sensitive to change of pH. Therefore, we prepared a series of Si-NCs samples treated in solutions of the same chemical composition but with different pH.

The unexpected blue-shift of PL peak maximum from 600 nm (for all Si-NC samples) was probably caused by saturation effects due to strong excitation of the samples. (This effect was also observed in literature [77]). As a consequence, the interpretation of PL peak position changes observed of Si-NCs is difficult. The emergence of a new Si-NCs PL maximum around 570 nm will be discussed at the end of this chapter.

3.4.2 Second PL-aging study

Si-NCs samples used in the 2nd aging study were treated the same way as samples used in the 1st aging report. The only difference was that an OD 1.5 filter was used for measuring with the micro-spectroscopy apparatus. Excitation energy in sample area was approximately 88 μW with this filter. The intensity was decreased compared to the 1st aging study to avoid the over-excitation problems (i.e. saturation and blue-shift of PL).

In this second report we describe three separate sets of colloidal suspensions. The first set of samples consisted of Si-NC dispersed in a buffer adjusted to different pH values. The second set used solutions of various D-glucose concentrations in water. For the third set we prepared samples as a complementary comparison to previous two sets. One sample had the same pH as the samples in the first set, but different chemical composition of the buffer. The other was prepared from D-glucose with the same concentration, but dissolved in mixture of water and ethanol.

a) Preparation of solutions

Solutions for the first set were prepared from the same two source solutions mixed in different ratios and with different final pH.

Source solution (S1) – was composed from Citric acid (2-hydroxypropane-1,2,3-tricarboxylic acid) 0.05 g in 10 ml H_2O with final pH 1.8.
Source solution (S2) – was prepared from of 0.034 g of $NaHPO_4.12H_2O$ in H_2O with final pH 8.0.

Samples A1, A2, A3 were prepared from Si-NCs dispersed in mixtures of S1:S2 with different ratios:

A1 in 4:1 ratio, resulting pH 4.5
A2 in 10:1 ratio, resulting pH 6.0
A3 in 40:1 ratio, resulting pH 7.0

Si-NC colloid in solution of NaOH and HCl in water (titrated to the same pH as sample A1) was prepared as a comparison sample.
A4 –NaOH and HCl in water titrated to resulting pH 4.5.

The second set of samples was Si-NCs in water with different concentration of D-glucose:

DG1 0.4 g/ 1ml, resulting pH 5.5
DG2 0.2 g/ 1ml, resulting pH 5.5
DG3 0.1 g/ 1 ml, resulting pH 6.5

The comparison sample was prepared as a Si-NCs colloid with D-glucose in ethanol with water (3:1 ratio):
DG4 0.1 g/1ml, resulting pH 6.5

b) Emission spectra from Si-NCs in solutions

The emission spectra of samples A1, A2, A3, DG1, DG2, DG3, DG4 and A4 are displayed in *Fig. 36*, *38*, *40*, *42*, *44*, *46*, *48*, and *50*, respectively. The emission spectra have been corrected for the apparatus sensitivity and background was subtracted.

The PL spectra of the Si-NCs (possibly single Si-NCs) measured with the micro-spectroscopy apparatus are displayed in *Fig. 37*, *39*, *41*, *43*, *45*, *47*, *49*, and *51* for samples A1, A2, A3, DG1, DG2, DG3, DG4 and A4, respectively. The PL spectra have been corrected for the apparatus spectral sensitivity and background signal coming from the solvents was subtracted.

Figure 36: Emission spectra of Si-NCs A1 solution measured after various duration of incubation (shown in the legend in days) with a) excitation wavelength 280 nm, b) excitation wavelength 360 nm.

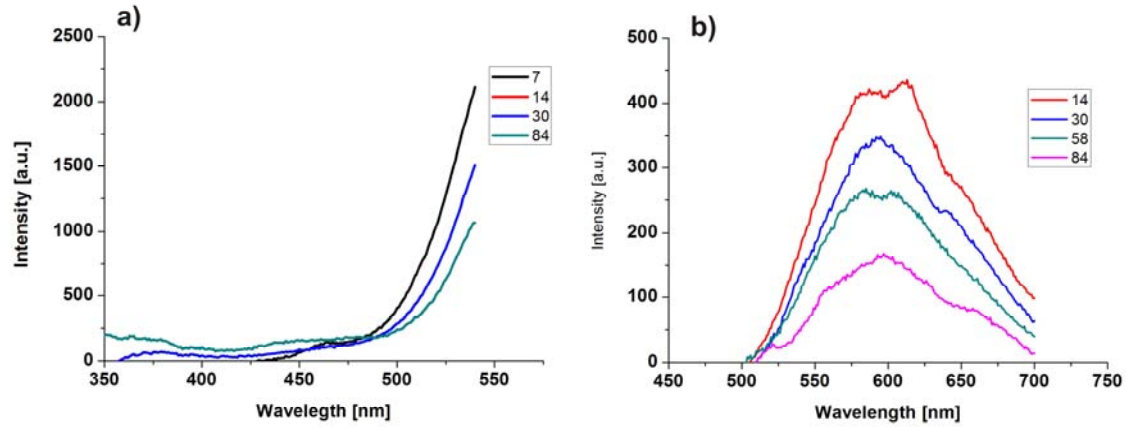

Comment: The intensity of PL peak (at 600 nm) decreased in time but did not reach the zero level as in some of the previous samples.

Figure 37: Emission spectrum of single Si-NCs in A1 solution measured by micro-spectroscopy apparatus (sample is excited with 405 nm diode laser) after: a) 10 days, b) 50 days. Spectra from various emitting spots in sample are presented to demonstrate the typical observations.

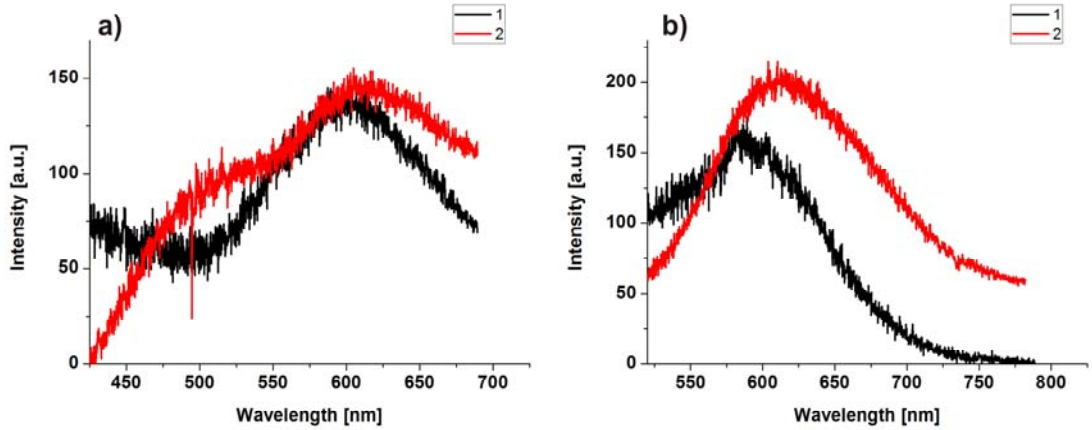

Comment: For sample A1, it was difficult to observe single-like Si-NCs even after 10 days of incubation and after 50 days it was practically impossible; only few big Si-NCs agglomerates have been detected. Majority of observed PL spectra was coming from huge agglomerates or grains of Si-NCs.

Figure 38: Emission spectra of Si-NCs A2 solution measured after various duration of incubation (shown in legend in days) with a) excitation wavelength 280 nm, b) excitation wavelength 360 nm.

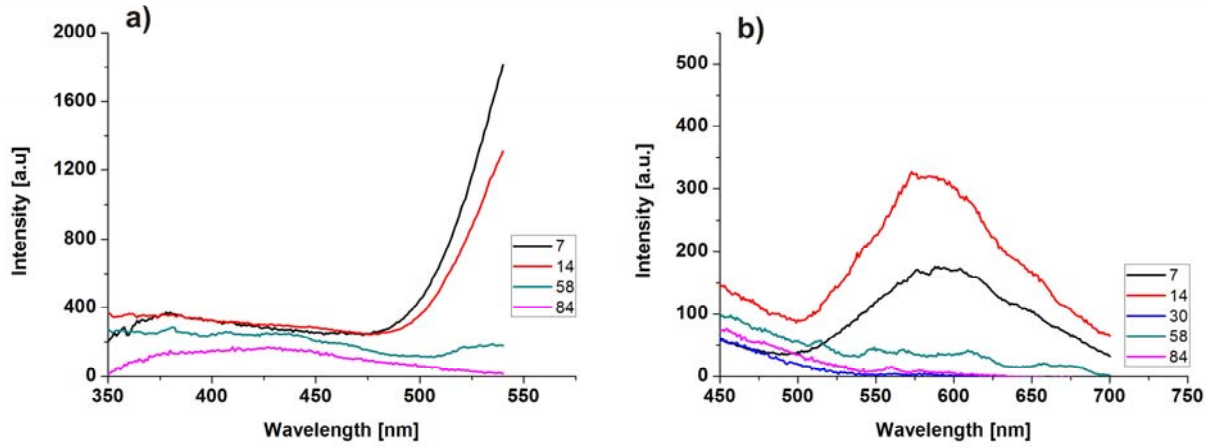

Comment: The PL intensity of the 600 nm peak decreases significantly with time compared to sample A1. After 30 days the emission was practically on the noise level.

Figure 39: Emission spectrum of single Si-NCs in A2 solution measured by the micro-spectroscopy apparature (sample is excited with 405 nm diode laser) after: a) 10 days, b) 50 days. Spectra from various emitting spots in sample are presented to demonstrate the typical observations.

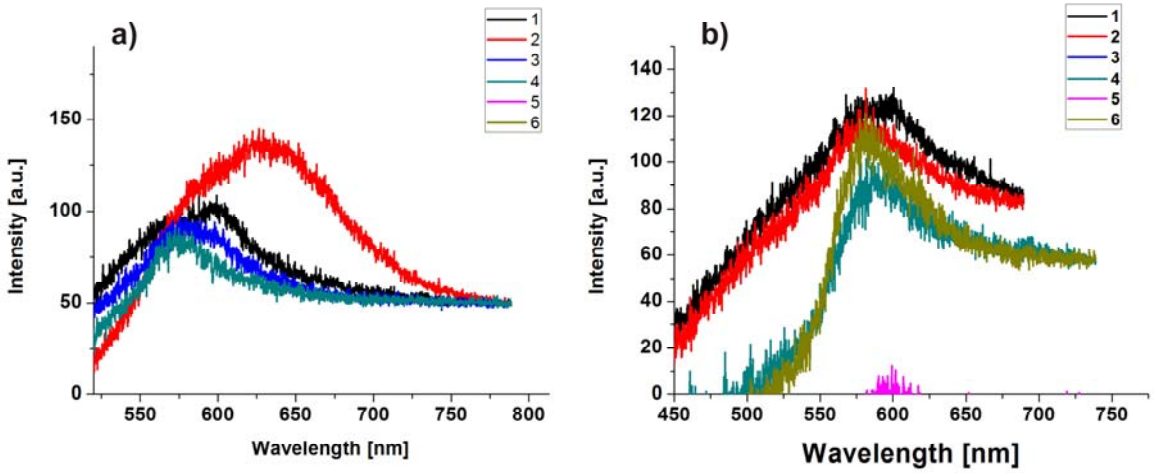

Comment: Although this sample was chemically identical as A1, the spectra were totally different. It was also difficult to find and measure "single-like" spectra of Si-NCs, but slightly easier than in case of sample A1. We observed emerging of a new PL peak which had maximum around 570 nm.

Figure 40: Emission spectra of Si-NCs A3 solution measured after various durations of incubation (shown in the legend in days) with a) excitation wavelength 280 nm, b) excitation wavelength 360 nm.

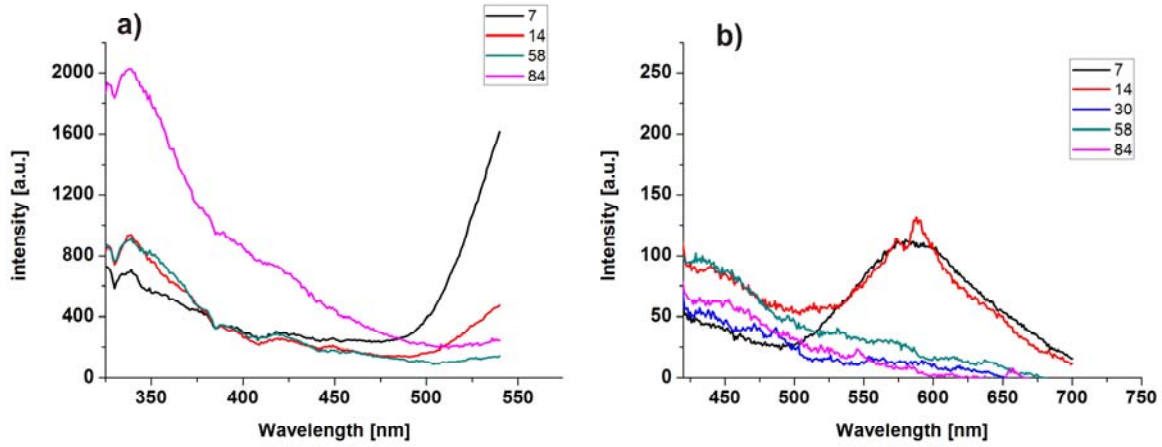

Comment: The sample looks similar to the previous A2 sample. The only difference was increase of PL at 350 nm under 280 nm excitation. This peak was assigned to the increased background signal of solution.

Figure 41: Emission spectrum of single Si-NCs in A3 solution measured by the micro-spectroscopy apparatus (sample is excited with 405 nm diode laser) after: a) 10 days, b) 50 days. Spectra from various emitting spots in sample are presented to demonstrate the typical observations.

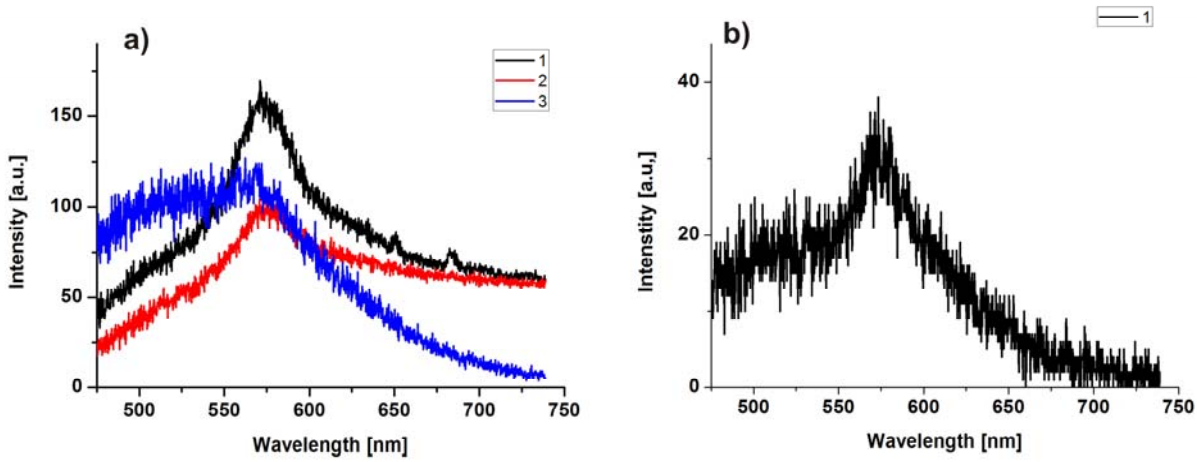

Comment: Although macroscopic PL intensity was very low compared to other chemically identical samples, it was not so difficult to observe and then measure single Si-NCs at 10th day. After 50 days ”single-like” PL spectra of Si-NCs were still observed but it was complicated to subtract PL signal from background due to low intensity. As in case of sample A2 we observed shift in the spectra of single Si-NCs to wavelengths around 570 nm

Figure 42: Emission spectra of Si-NCs in DG1 solution measured after various duration of incubation (shown in the legend in days) with a) excitation wavelength 280 nm, b) excitation wavelength 360 nm.

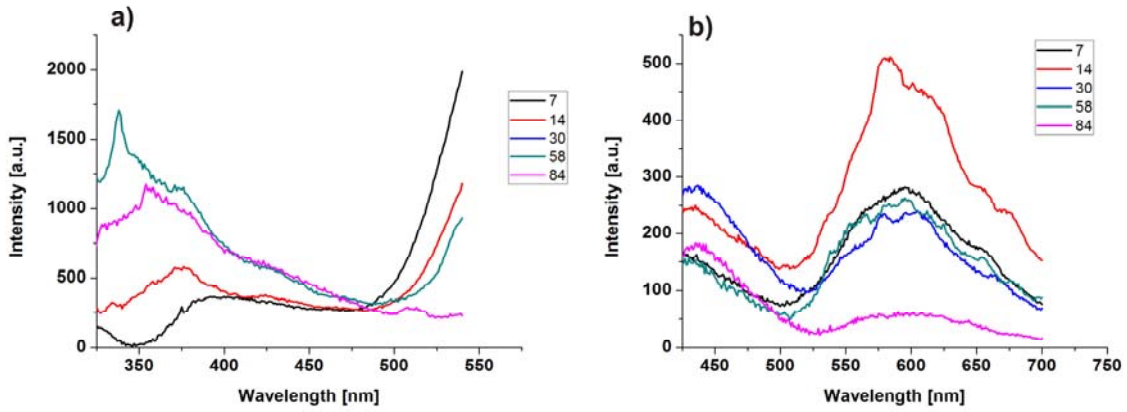

Comment: The intensity of 600 nm PL peak shows maximum on the 14th day. In general, this sample exhibit great PL stability during the first two months, similarly to the Si-NCs in water with D-glucose (*Fig. 29*) from previous set of aging samples. On the 84th day we observed decrease of PL but not as strong as for other A- series samples.

Figure 43: Emission spectrum of single emitting spots in DG1 solution measured by the micro-spectroscopy apparatus (sample is excited with 405 nm diode laser) after: a) 10 days, b) 50 days. Spectra from various emitting spots in sample are presented to demonstrate the typical observations.

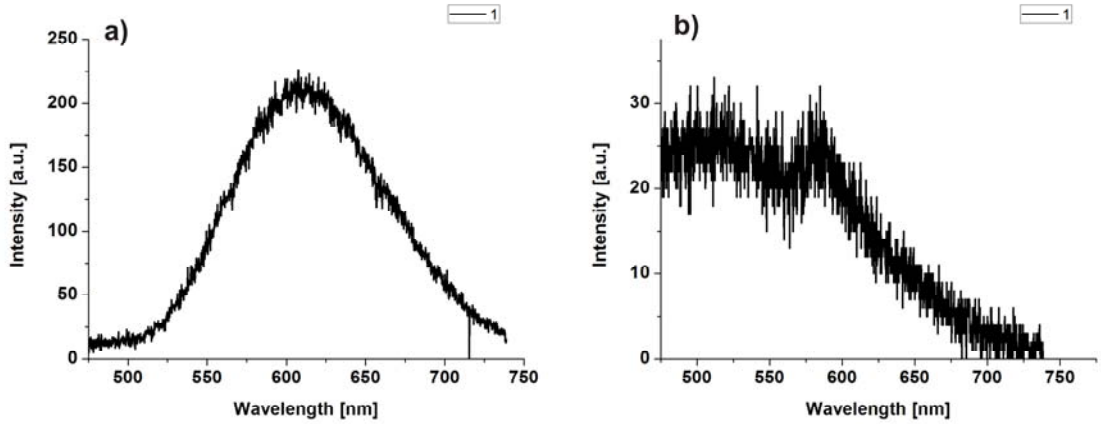

Comment: We observe several small Si-NCs agglomerates on the 10th day. The spectrum taken after 50 days of incubation was affected by the increased background signal from D-glucose. The problem was likely caused by a small water vapor leakage, which led to increase of concentration of D-glucose in the solution and higher luminescence. Although there were several single-like Si-NCs, we were not able to separate them from the background because of relatively strong emission of solution with high concentration of D-glucose.

Figure 44: Emission spectra of Si-NCs DG2 solution measured after various duration of incubation (shown in the legend in days) after a) excitation wavelength 280 nm, b) excitation wavelength 360 nm.

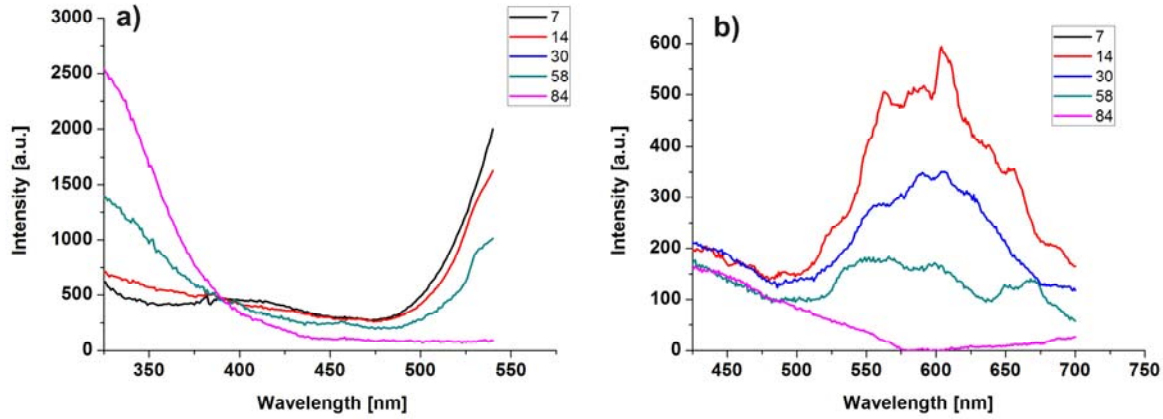

Comment: This sample behaves as the previous DG1 sample (*Fig. 42*). The only difference was absence of a period of PL stability; in this case PL was decreasing continuously.

Figure 45: Emission spectrum of single-like Si-NCs in DG2 solution measured using the micro-spectroscopy apparatus (sample is excited with 405 nm diode laser) after: a) 10 days, b) 50 days. Spectra from various emitting spots in sample are presented to demonstrate the typical observations.

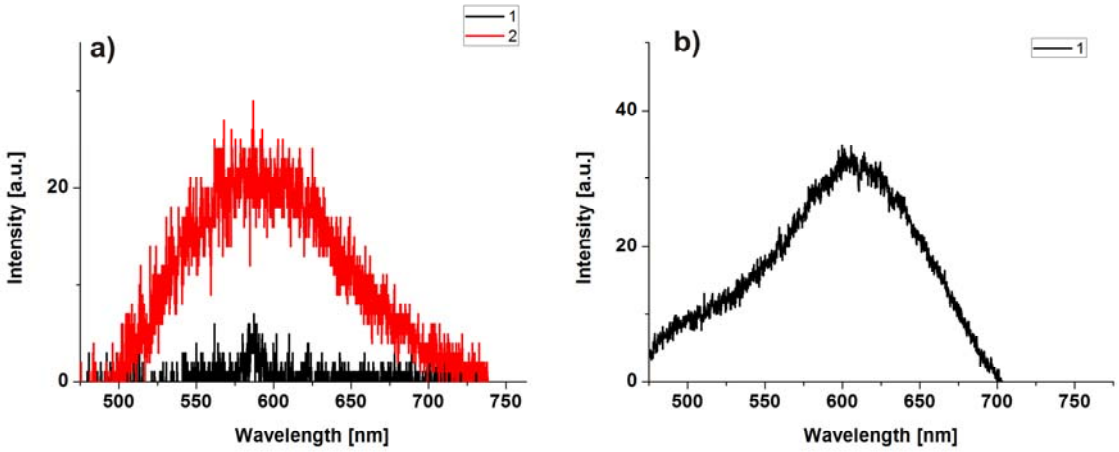

Comment: In this measurement we observed again small Si-NCs agglomerates. Because of that the observed PL emission peaks were wider than in case of single Si-NCs. Single Si-NCs were also observed, but their PL intensity was very low (*Fig. 45a* – black curve).

Figure 46: Emission spectra of Si-NCs in DG3 solution measured after various duration of incubation (shown in the legend in days) with a) excitation wavelength 280 nm, b) excitation wavelength 360 nm.

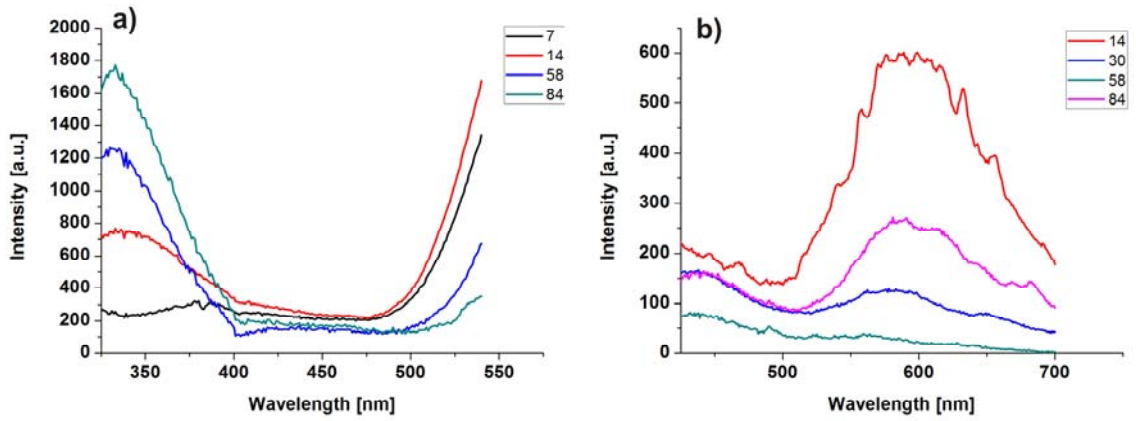

Comment: This sample had PL evolution similar to the previous sample DG2 (*Fig. 44*). Again we observed increase of PL for 350 nm peak (*Fig. 46a*) coming from concentrating of D-glucose in original solution due to evaporation of water.

Figure 47: Emission spectrum of single Si-NCs in DG3 solution measured using the micro-spectroscopy apparatus (sample was excited with 405 nm diode laser) after: a) 10 days, b) 50 days. Spectra from various emitting spots in sample are presented to demonstrate the typical observations.

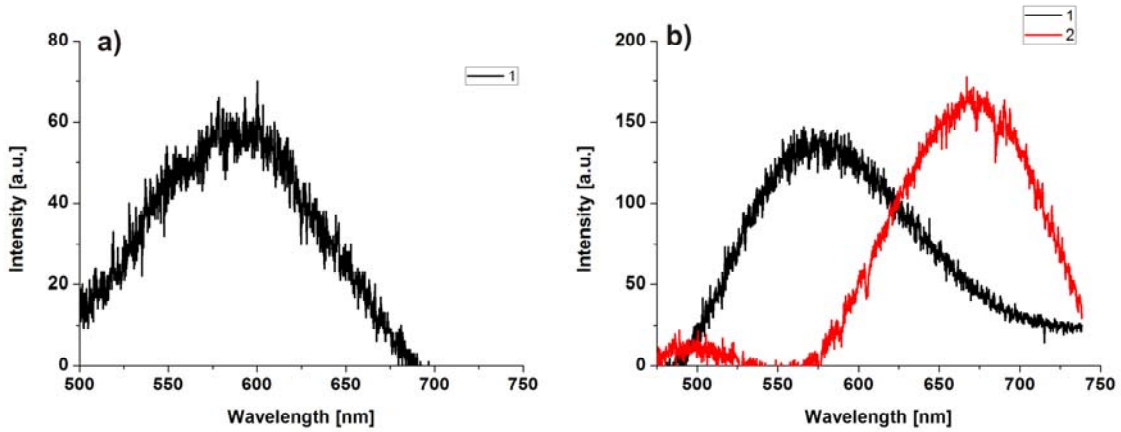

Comment: We did not observe single Si-NCs here, but agglomerates of few Si-NCs and so the PL emission peak was broadened a bit. On the 50th day we observed mainly peaks with maximum around 570 nm, but also a few peaks around 670 nm. Again they were probably not coming from single Si-NCs, but from agglomerates of a few NCs (presumably less than 10 as judged from the PL intensity).

Figure 48: Emission spectra of Si-NCs DG4 solution measured after various duration of incubation (shown in legend in days) after a) excitation wavelength 280 nm, b) excitation wavelength 360 nm.

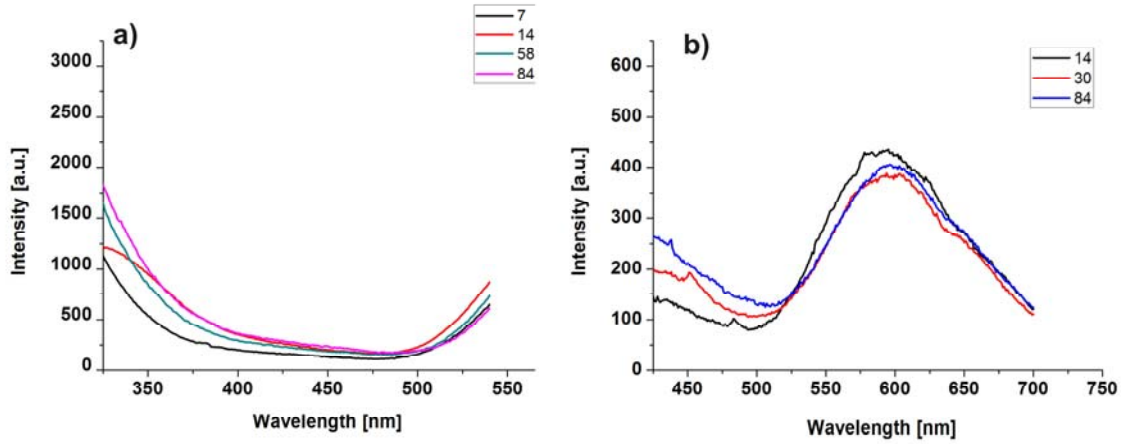

Comment: The intensity of the 600 nm PL peak was stable for the whole observation time. It was practically constant and, after two months of incubation, the intensity was the highest observed from all studied Si-NCs samples.

Figure 49: Emission spectrum of single Si-NCs in DG4 solution measured by the micro-spectroscopy apparatus (sample is excited with 405 nm diode laser) after: a) 10 days, b) 50 days. Spectra from various emitting spots in sample are presented to demonstrate the typical observations.

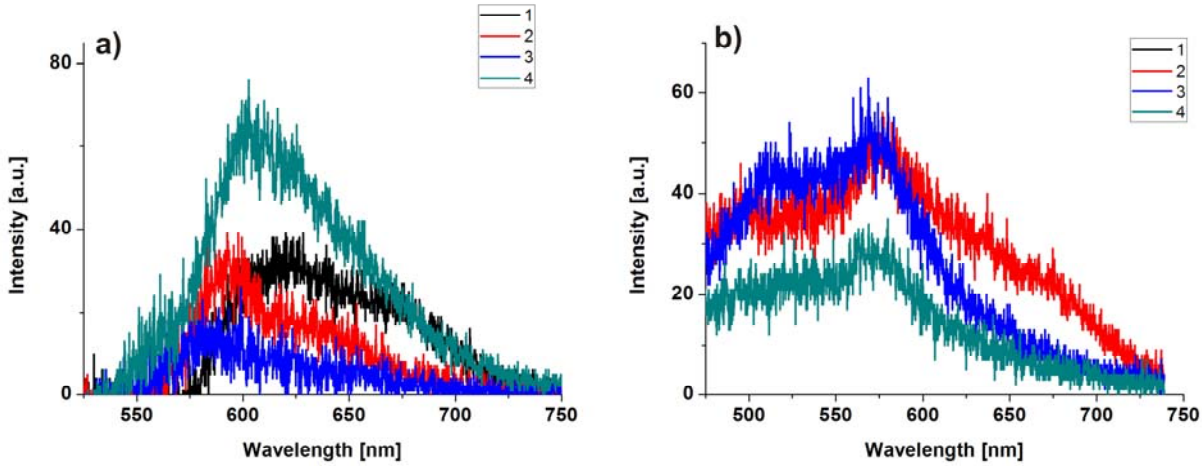

Comment: On the 10th day we observed PL from plenty of single Si-NCs with various peak positions (570 – 620 nm) but after 50 days of incubation there were only Si-NCs with emission maximum around 570 nm as was the case with Si-NCs treated with D-glucose in water (*Fig. 33*). As for the previous sample there was an increase of D-glucose concentration in the solution that caused stronger background on the blue side below the 570 nm maxima.

Figure 50: Emission spectra of Si-NCs in A4 solution measured after various duration of incubation (shown in legend in days) after a) excitation wavelength 280 nm, b) excitation wavelength 360 nm.

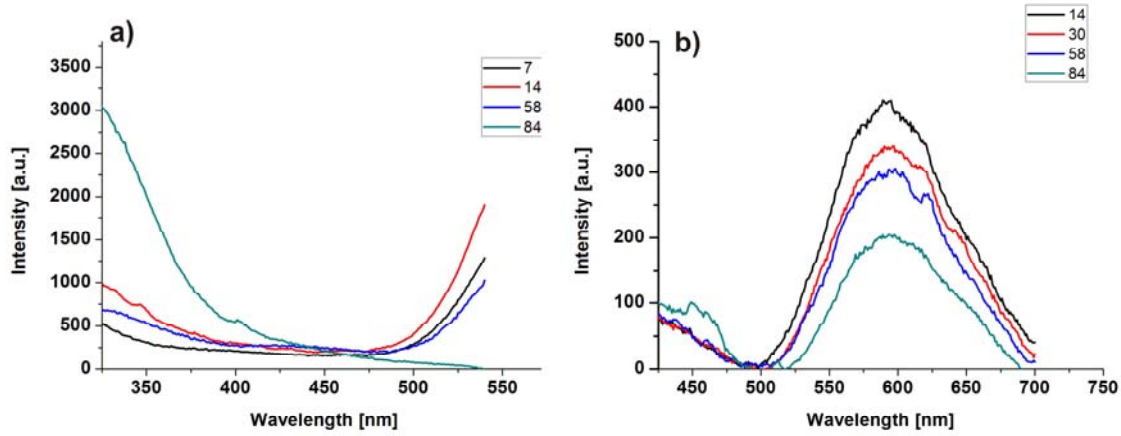

Comment: Intensity of the 600 nm PL peak of this sample decreased quite slowly compared to other Si-NCs samples mentioned above in the second aging report.

Figure 51: Emission spectrum of single Si-NCs in A4 solution measured by the micro-spectroscopy apparatus (sample is excited with 405 nm diode laser) after: a) 10 days, b) 50 days. Spectra from various emitting spots in sample are presented to demonstrate the typical observations.

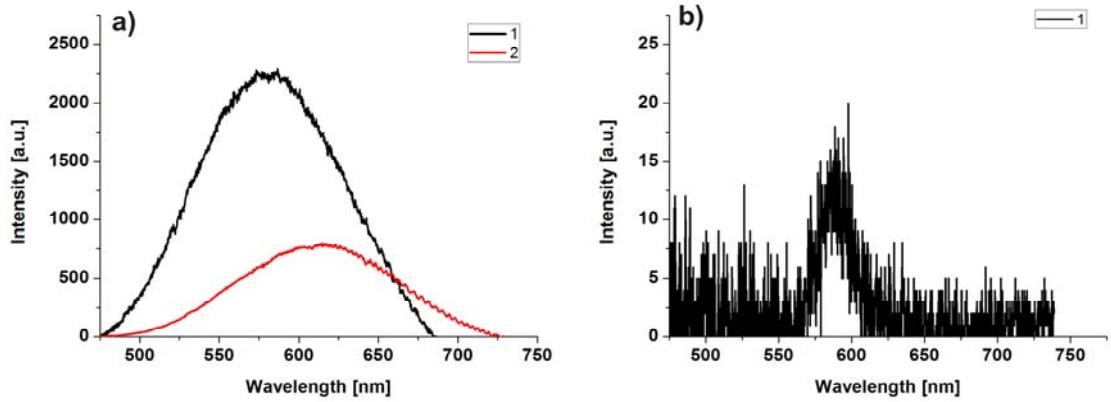

Comment: After 10 days of incubation we observed only PL from enormous Si-NCs agglomerates, while after 50 days there were only a few single Si-NCs. Their PL intensity was quite low and hard to distinguish from the background.

The strongest and most stable PL was observed for Si-NCs in mixture of ethanol and water with D-glucose (see *Tab. 7*). If we look at the sensitivity of PL intensity to changes of pH, it is evident that for lower pH PL intensities are higher. Samples A1 and A4, with the same pH of 4.5, had practically the same evolution of PL intensities in time. In contrast, samples with higher pH (6-7) showed the fastest decrease in PL intensity observed in this experiment. We were not able to measure single Si-NCs spectra for samples with this high pH, as they were

completely absent in the micro-PL images; instead we mainly observed huge Si-NCs agglomerates.

Table 7: Decrease of Si-NCs photoluminescence intensity of the 600-nm centered peak. The samples were excited at 360 nm and measured with the fluorescence spectrometer. The PL intensity observed on the 14th day was normalized as 100 % and the other values are related to this value (the same procedure was used for the 1st set of aging samples).

	Intensity [%]			
Sample name	14 days	30 days	58 days	84 days
A1	100	81	63	39
A2	100	5	11	2
A3	100	10	14	2
DG1	100	51	56	12
DG2	100	65	50	7
DG3	100	19	10	41
DG4	100	90	94	80
A4	100	89	59	42

c) The size-characterization of Si-NCs in colloidal suspensions

In micro-spectroscopy experiments we detected variously broadened PL emission peaks, which correspond to variously sized Si-NCs agglomerates. For better interpretation of these results, we need to know size distribution of Si-NCs agglomerates. Therefore, we measured the sizes of Si-NCs in samples from the 2nd aging report by the dynamic light scattering (DLS) method with Zetasizer Nano S (Malvern). (The samples from the 1st aging study were not measured due to inaccessibility of the DLS machine). The sizes of Si-NCs agglomerates are summarized in *Tab. 8*.

As in the case of DLS measurement described in Chapter 2.1.4, we needed to use centrifugation filters in order to detect particles smaller than 500 nm. We used 650 nm and 100 nm centrifugation filters from Millipore (Ultrafree-MC Centrifugal Filter Units with Microporous Durapore PVDF Membrane). The samples were centrifuged for 3 minutes at 1200 rpm in MiniSpin (Eppendorf) centrifuge.

For the first set – pH gradient from mixtures of citric acid and $NaHPO_4.12H_2O$ (samples A1, A2, A3) – the smallest Si-NCs grains were observed for sample A1. The biggest Si-NCs agglomerates were observed in sample A3 showing (without application of filtration) aggregates bigger than 800 nm. These results suggest that with higher pH the Si-NCs grains either tend to stay together in original agglomerates or there is further aggregation. The comparison sample with the same pH as sample A1 (sample A4) reveals slightly smaller size of the biggest Si-NCs agglomerates compared to the sample A2.

Table 8: Sizes and volume-fractions of Si-NCs in various colloidal suspensions determined by the dynamic light scattering. (Labels f650 and f100 indicate application of centrifugation filters with pores of 650 and 100 nm, respectively.)

Sample name	particle size [nm] / percentage [%]		particle size [nm] / volume [%]	
A1	170	90	170	6
	700	10	700	82
A1 - f650	13	90	13	60
	> 500	< 1	500	20
A2	90	90	120	30
	> 500	10	700	60
A2 - f650	40	90	40	60
	> 500	5	700	30
A3	50	80	50	20
	800	15	800	40
	> 1000	5	> 1000	10
A3 - f650	30	90	30	40
	50	10	50	60
DG1	80	80	80	30
	> 500	20	700	50
DG1 - f650	30	90	30	60
	50-60	10	50-60	20
DG1 100 filter	20	90	20	80
	60-150	10	60-150	20
DG2	120	80	120	10
	> 900	20	900	90
DG2 - f650	60	40	60	30
	> 70	60	> 100	70
DG2 - f100	20	80	20	40
	> 40	20	> 40	50
DG3	120	90	120	30
	> 120	10	900	60
DG3 - f650	70	90	70	40
	> 70	10	> 70	60
DG4	450	90	450	10
	> 450	10	800	80
DG4 - f650	60	80	60	20
	> 60	20	610	70
DG4 - f100	40	90	40	20
	> 40	10	> 40	70
A4	< 100	10	90	10
	600	80	600	90
A4 – f650	40	80	40	30
	> 50	10	> 50	60
A4 - f100	40	80	40	10
	> 50	10	> 50	80

The suspensions with D-glucose had practically the same sizes for all samples. The smallest agglomerates of 20 nm were observed in the sample DG1 and the average minimal size was around 40 nm. In general, we observed here smaller structures than in other samples (from the percentage point of view).

Let us note that very small particles (around 2-5 nm) were detected in some of DLS measurements, but in the final summary they have been omitted due to large experimental uncertainty (small particles have very low contribution to the scattered signal). However, presence of such small particles was not observed for the pH-gradient samples.

d) Influence of chemicals in solution on luminescence of Si-NCs

In case of samples treated with D-glucose we have had a suspicion that this molecule might interact with Si-NCs surface and cause increase of PL intensity and bigger size of agglomerates as well. The structural and conformational formulas of all used chemicals are summarized in *Fig. 52*. Especially we want to point out the structure of D-glucose which alternate between two conformations – envelope and twist. We are discussing the possible situations in sample and their influence on PL of Si-NCs later in this chapter.

Figure 52: Molecular structures of materials used in aging experiments. A – water, B – ethanol, C – NaCl, D – D-glucose in skeletal formula, E – two structural forms of D-glucose, F- citric acid, G - $NaHPO_4$, H- NaOH, I- HCl.

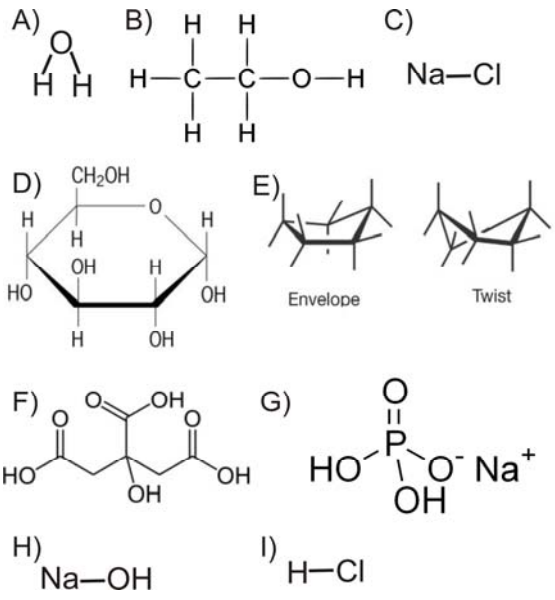

In Si-NCs samples with pH gradient were prepared from chemicals like NaCl, NaOH, HCl, citric acid and $NaHPO_4.12H_2O$. All of those compounds in water solution are in their radical form e.g. NaCl is there in form of Na^+ Cl^-. If the solution has higher pH, then there are more positively charged than negatively charged molecules in the Si-NCs colloid. This charging could be responsible for decrease of Si-NCs PL intensity via enhancement of Auger effect and also it can influence energy states of excitons in the crystal. To answer the question if dissolved compounds are also influencing PL by modifying Si-NCs surface bonds we applied another physical method - Fourier-transform infrared spectroscopy (FTIR) to study samples A1 (*Fig. 53*) and A4 (*Fig. 54*).

In case of Si-NCs samples in solutions with D-glucose the situation was a bit different; we observe stronger PL intensity in macro and micro-spectroscopy and also more "single-like" Si-NCs in micro-spectroscopy measurements. This is in disagreement with DLS measurement (*Tab. 8*) in which we observed big Si-NCs agglomerates rather than single Si-NCs. The D-glucose structure is more complicated compared to chemicals used in pH-gradient study. It can have open chain structure or a cyclic form. Moreover the cyclic form can flip between two conformations called "envelope" and "twist" (taking the form which is energetically more

favorable). This possibly could reduce charging of Si-NCs if the molecule is in closer proximity to the surface and increase PL efficiency by eliminating non-radiative Auger effect. By the micro-spectroscopy we observed plenty of single standing Si-NCs with some very small spacing between them. This led us to speculation that interactions of D-glucose with Si-NC aggregates induce their splitting, possibly down to single Si-NCs. For proving this idea we need to know if there is any structural change in D-glucose in presence of Si-NCs, for this we measure FTIR spectra of our samples: DG1 in *Fig. 55* and DG4 sample in *Fig. 56*.

e) FTIR measurement of Si-NC suspensions

FTIR measurement was done in the attenuated total-refection (ATR) mode. The FTIR spectra were collected using FTIR spectrometer Nicolet Nexus 860 equipped with an IR light source and a halogen lamp (20 W), KBr and CaF_2 beamsplitters, standard DTGS pyrodetector and high-sensitivity liquid-nitrogen-cooled MCT photodiode as detectors. To reduce H_2O and CO_2 absorption, the spectrometer was continuously purged with nitrogen blow. The ATR accessory Specac Gateway 6 Reflection Horizontal ATR with ZnSe prism was employed.

A droplet of studied suspension (50 µl) was placed on the measuring crystal and put in the FTIR apparatus for thermal and gas stabilization (nitrogen atmosphere). The sample dried slowly during the measurement, so we are able to measure also the signal from the base of solution and possibly identify components from speed of drying. In our case both Si-NCs sample and control solution were measured at the same time under the same conditions. The obtained infrared absorption spectrum allows us to identify chemical groups present in the sample and the control solution. We could also identify changes of their volumetric representation between sample and control solution.

We chose four representative samples from the 2nd aging study having the highest PL intensity in the time of measurement (after 60 days of aging). We have here one sample from the first pH gradient study – A1 sample, the D-glucose sample – DG1 and two comparative samples A4 (the same pH as A1) and DG4 (D-glucose in mixture of water and ethanol).

Figure 53: FTIR absorption spectra of Si-NCs in the A1 sample.

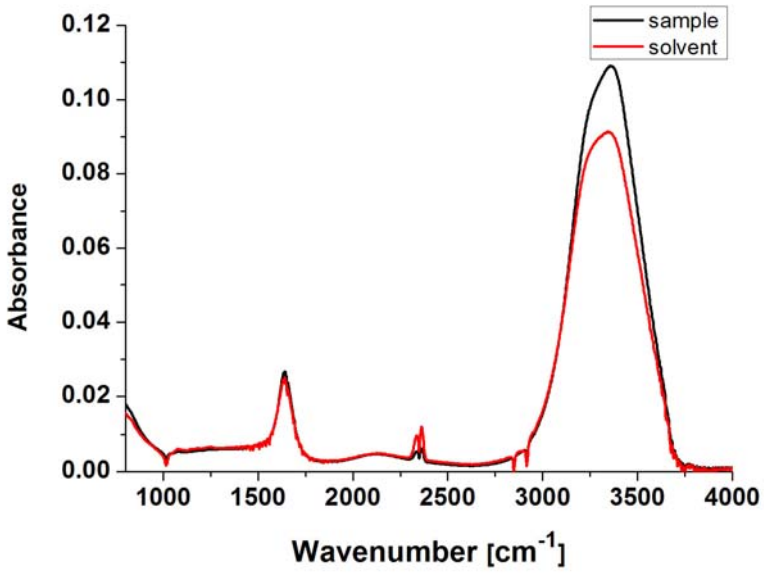

Comment: The FTIR spectra of the sample and solvent without Si-NCs are almost identical. The only change is observed in the 3400-3600 cm^{-1} peak which is higher in the presence of Si-NCs – i.e. there are more –OH groups.

Figure 54: FTIR absorption spectra of Si-NCs in the A4 sample.

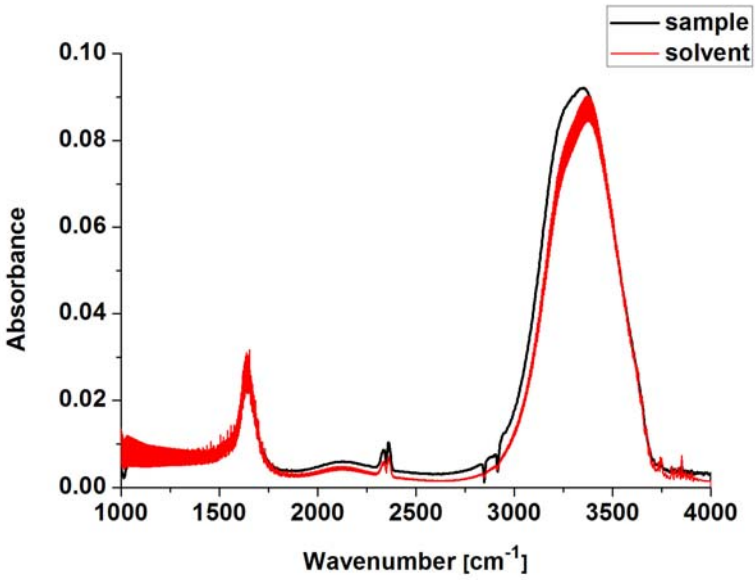

Comment: The FTIR spectra of the sample and solvent without Si-NCs are very similar; the only small change is in the 3400-3600 cm^{-1} peak. The increase of this peak means that we have slightly more –OH groups in the presence of Si-NCs. The solvent spectrum was quite noisy due to problems with excitation of the sample. Otherwise the sample and solution spectra are identical.

Figure 55: FTIR absorption spectra of Si-NCs in the DG1 sample.

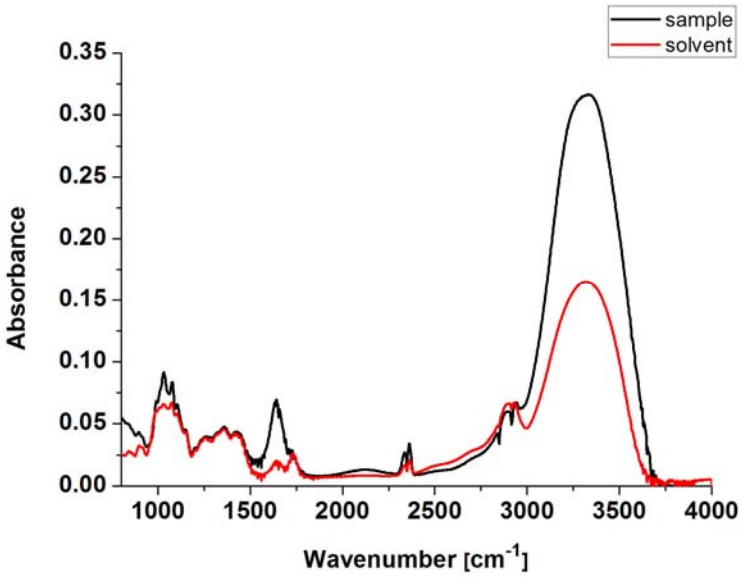

Comment: The FTIR spectra of the sample and solvent are quite different. The main change is observed in the 3400-3600 cm^{-1} peak (–OH groups), which has practically double absorbance in the presence of Si-NCs. Other significant changes are the stronger sample absorbance at peak 995-1090 cm^{-1} and also at 1590-1720 cm^{-1} peak. The signal from D-glucose is in the spectral range of 800-2000 cm^{-1} and (for pure solvent without Si-NCs) agree well with published FTIR spectra in literature [78]. It seems that the structural changes in the Si-NCs sample are mainly related to D-glucose structure.

The precise interpretation of peaks is difficult due to complicated structure of D-glucose molecule. The absorption at 1590-1720 cm^{-1} is related to carbon bonds (-CO, C=C, C=O). The peak at 995-1090 cm^{-1} can be assigned to Si-O-Si bonds (1080 cm^{-1}), but it is overlapped with another absorption by some different group. This peak can have origin in some 3R–C-O-H bond, where we are not sure what stands for R, but it can be also R-Si related.

Actually, the precise assignment of peaks was not our goal in this experiment; we just wanted to know if there is any structural change in D-glucose. Indeed, we observe significant changes which are probably related to the increased PL intensity of Si-NCs/D-glucose samples.

Deeper understanding could be achieved by nuclear magnetic resonance (NMR) studies.

Figure 56: FTIR absorption spectra of Si-NCs in the DG4 sample.

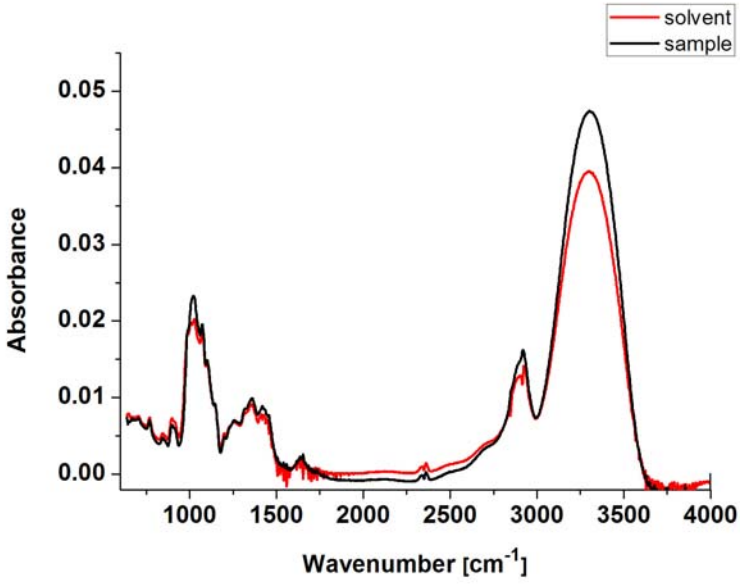

Comment: The FTIR spectra of the sample and solvent are again different in the region of the 3400-3600 cm^{-1} peak (representing -OH groups). Compared to the DG1 sample the difference is not so dramatical. The solvent absorbance from 800-2000 cm^{-1} is identical to the FTIR spectra of D-glucose found in literature [78]. Other slight changes are observed at 1000-1050 cm^{-1}, 1330-1470 cm^{-1} and 2890-2940 cm^{-1}.

We also observe small change at 1080 cm^{-1} peak which is related to Si-O-Si bonds. The 1000-1050 peak cm^{-1} is assigned to –COH or =C-O-C-3R bonds but we cannot exclude also bonds with silicon. The 1330-1470 cm^{-1} peak shows just a slight increase compared to solution, but its shape is not changed, than means that the bonds are already present in solution volumetric representation. Generally, this peak could be assigned to –COOR, $-CH_3$ or $-CH_2$ bonds, precise assignment is not possible due to broadness of the peak. Last significant peak was around 2890-2940 cm^{-1}; it is most probably related to –CH group but we cannot exclude – CH_2, $–CH_3$, –COH, -COOH groups.

f) AFM measurement of Si-NCs treated with D-glucose

In order to prove that we have single small Si-NCs surrounded by D-glucose as we deduced from micro-spectroscopy studies and FTIR, an AFM imaging was performed. The Agilent 5500 Scanning Probe Microscope operating in acoustic AC mode was used for measurements (10µm scan range). All post-processing was carried out using the PicoImage software. For this study we use the DG1 sample from the second aging study (see Chapter 3.6.2, emission spectra *Fig. 42*, micro-spectroscopy spectra *Fig. 43*, FTIR *Fig. 55*).

In *Fig. 57* we observe that there are two types of particles with distinct diameters as seen in *Fig. 58*. The smaller particles (which were in majority) had diameter around 8-12 nm and the bigger ones 20-30 nm. (The eventual bigger particles were removed from the original solution by gravitational forces – sedimentation).

Figure 57: 5x5µm AFM image of the DG1 sample deposited on HOPG.

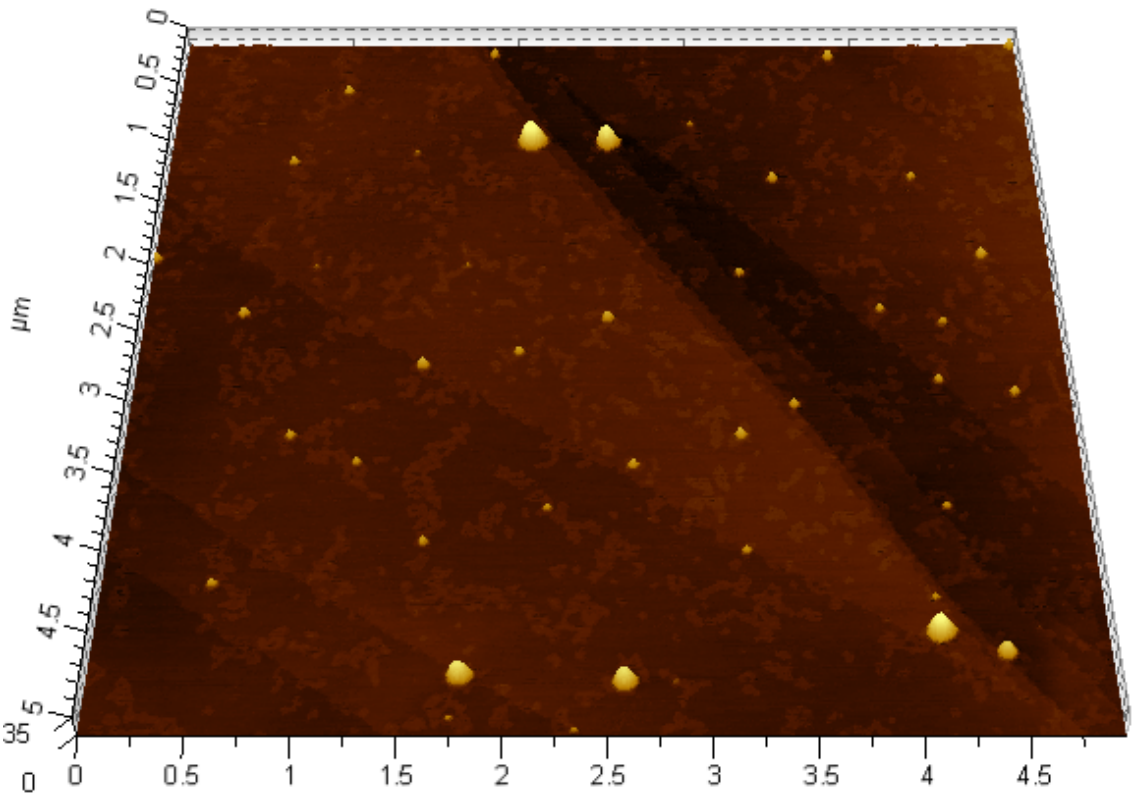

Figure 58: One cross-section of the AFM image revealing three particles whose diameters (the height of peaks) are between 8-10 nm.

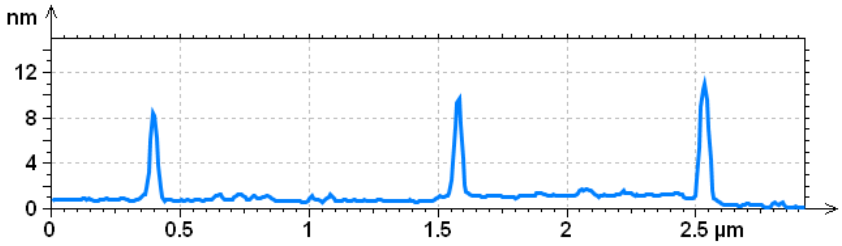

These results are in agreement with observation by micro-spectroscopy studies (chapter 3.4.1 and 3.4.2) where we detected small luminescent Si-NCs with relatively narrow PL spectra.

The size of closed D-glucose molecule is around 0.4-0.5 nm, while the length of the open chain D-glucose is around 0.9 nm. The Si-NCs emitting around 600 nm have size 1.5-2 nm (see Chapter 2.4 *Fig. 10*). Therefore the smallest particles (4 nm) can be formed by single nanocrystal surrounded by open-chain D-glucose molecules and the 12-nm particles can be formed by clusters containing up to three Si-NCs covered by one layer of D-glucose (or single nanocrystal covered by many glucose layers). The particles observed with AFM in *Fig. 57* are nicely rounded which suggest full covering of the surface by D-glucose molecules. This result proves our hypothesis that the D-glucose molecule is interacting with Si-NCs and forming Si-NCs particles embedded within D-glucose shell.

g) Summarization of the second aging study

In conclusion we observe degradation of Si-NCs PL intensity in time. The higher pH induce decreasing PL intensity due to charging of Si-NCs surface and consequent increase of Auger recombination. We did not observe any structural changes of the chemicals in pH gradient solutions (FTIR). In case of Si-NCs samples with D-glucose observed PL intensity was much stronger and more stable in time. We also observe significantly higher number of "single-like" Si-NCs (in the micro-spectroscopy experiments). Our hypothesis that D-glucose interacts strongly with Si-NC surface or even binds to that surface was supported with FTIR measurements, which revealed some structural changes of D-glucose in presence of Si-NCs and also AFM where we observe small Si-NCs. The changes in FTIR did include variety of bonds in which on the first place were various bonds containing carbon. The precise assignment of groups and final D-glucose conformation was impossible due to rather complicated structures and also broad FTIR peaks. Better structural information might be found with use of NMR techniques. Some structural changes and possible bonding of D-glucose to Si-NCs surface can also explain emerging of new PL band around 570 nm.

3.5 Photoluminescence quantum efficiency

Several research groups measured and reported quantum efficiency (QE) of Si-NCs fabricated by various techniques producing different passivation. The QE was mostly in the range of 5- 35 %, for example Kojima et al. found 23% efficiency [4]. QE of Si-NCs with oxidized surface is generally relatively low [79, 80], higher QE can be achieved for Si-NCs with activated surfaces; the highest reported QE was around 60 % [31].

Luminescence quantum efficiency (also called quantum yield) is simply defined as a ratio of emitted and absorbed photons in a certain sample (within certain (measurement) time interval) (3.1).

$$QE = \frac{PhotonEmitted(eV)}{PhotonAbsorbed(eV)} \tag{3.1}$$

3.5.1 QE measurement experimental setup

The experimental setup built in our laboratory is shown in *Fig. 59*. The Si-NCs colloidal suspensions were measured in 5x5 mm quartz cuvettes. A cuvette was placed vertically in an integration sphere. The excitation was provided by a series of light-emitting diodes (LED) with various emission wavelengths ranging from 240 nm up to 355 nm (Roithner Laser Technik GmbH). A LED was placed at an entrance port of the integration sphere opposite to the measured sample and powered by a stabilized laboratory source (P130R51D, Diametral).

The maximum allowed current for these LEDs was 20 mA and it was controlled with multi-metre (M-3890D, METEX). The signal from the integration sphere was collected by an optical fiber bundle, which was placed in right angle geometry. The output from the bundle was imaged by two quartz lenses to the entrance slit of a spectrometer (iHR 320, Horiba Jobin Yvon) and detected by an intensified CCD camera (PI-MAX 512RB, Princeton Instruments). Parameters of measurement and data collection were controlled using the WinSpec software.

Figure 59: Quantum efficiency setup: DS – diode power supply, MM – multi-meter , DH – diode holder with LED, IS – integration sphere, SH - sample holder with a cuvette, OC – optical cable, IT – imaging tube, SPE – spectrometer iHR 320, CAM - iCCD PI-MAX camera.

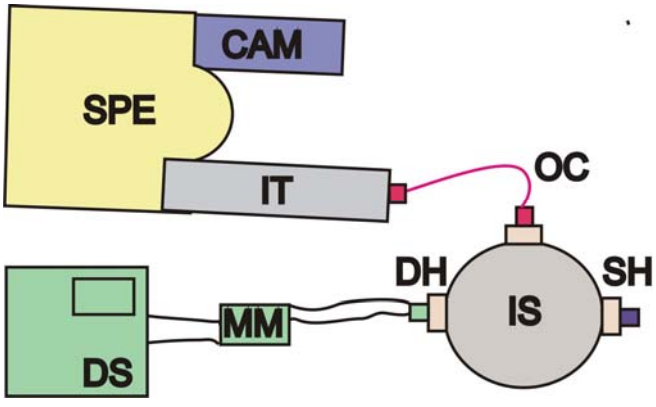

We excited the samples with a set of nine LEDs: 260 nm, 270 nm, 280 nm, 290 nm, 300 nm, 315 nm, 335 nm, 345 nm, and 355 nm. The LEDs had to be changed manually and each diode was let to stabilize for about 5 minutes.

Both Si-NCs colloidal solution and solution without Si-NCs were measured under the same conditions immediately after each other. The excitation part of signal was detected with central position of the spectrometer at 400 nm while the emission part of signal was detected at 600 nm. A neutral density filters (placed in the detection path between the two quartz lenses) were often used for excitation detection in order to avoid camera saturation when using stronger excitation.

During emission signal detection a long-pass filter was inserted in order to cut the scattered excitation light (often visible in its second order of diffraction). Both spectral windows were corrected for the apparatus spectral sensitivity (3.2). The QE calculation is based on comparison of signals from a sample with Si-NCs and a reference sample without Si-NCs (so called "blank"). The difference of both signals is corrected for spectral sensitivity C and filter transmission T, recalculated to number of photons, integrated (summed) within excitation and emission bands and finally divided (3.2). This calculation is expressed by the following equation and illustrated by *Fig. 60* and *Fig. 61* (concerning measurements of Si-NC multilayers deposited on a quartz substrate).

$$QE = \frac{\sum_{em.band} \left(I_{Si}^{em}(h\nu_{em}) - I_{blank}^{em}(h\nu_{em}) \right) \cdot C(h\nu_{em}) / T_{edgeFilter}(h\nu_{em}) / h\nu_{em}}{\sum_{ex.band} \left(I_{blank}^{ex}(h\nu_{ex}) - I_{Si}^{ex}(h\nu_{ex}) \right) \cdot C(h\nu_{ex}) / T_{grayFilter}(h\nu_{ex}) / h\nu_{ex}} \qquad (3.2)$$

Figure 60: The excitation (left) and emission (right) signals from a reference silica substrate (black lines) and a sample with deposited Si-NCs (red lines). The scattered light of exciting LED is decreased by absorption in the studied sample (left) while the background from a reference sample is overcome by photoluminescence from Si-NCs (right).

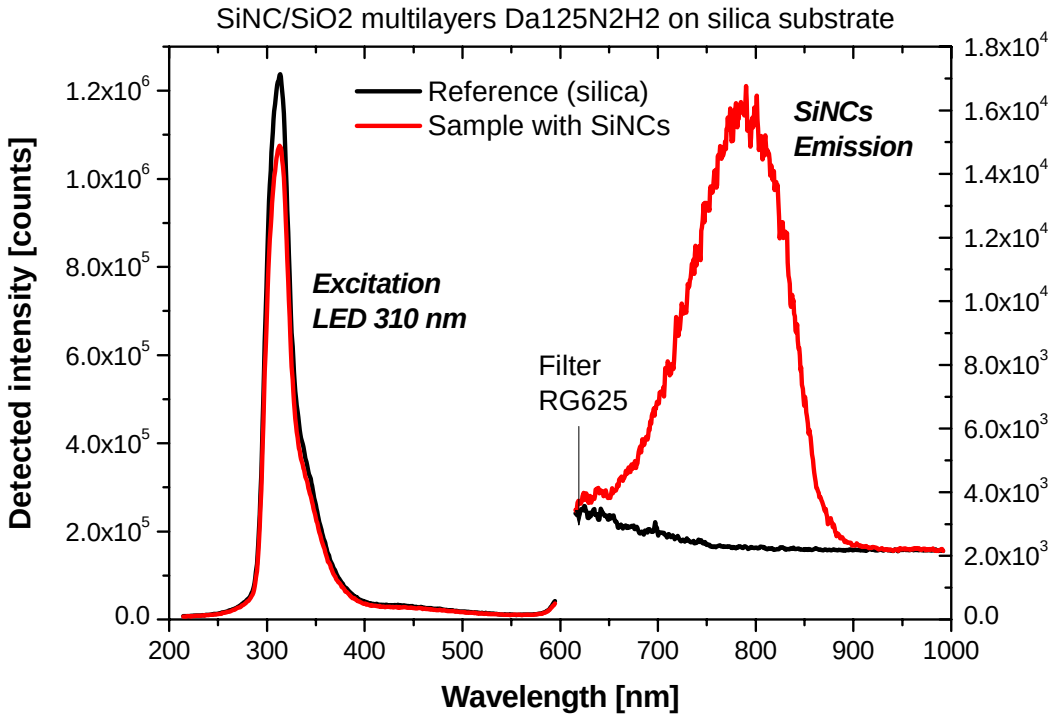

The measurement of QE was complicated by low absorption of photons in our Si-NCs colloidal samples (it is even decreasing for longer wavelengths - see excitation spectra in *Fig. 16*). The problem can be understood from the *Fig. 60*. When absorption is low, the two curves on the left side become very close (almost overlapping) and the QE uncertainty strongly increases as it is based on the difference of these two curves. In order to improve precision both excitation and emission curves were averaged over many measurements. Obviously, the stability of LED emission is crucial.

Figure 61: Data from *Fig. 60* after recalculation to photon energy and application of all corrections. The QE is then obtained by summing and dividing number of photons in both bands.

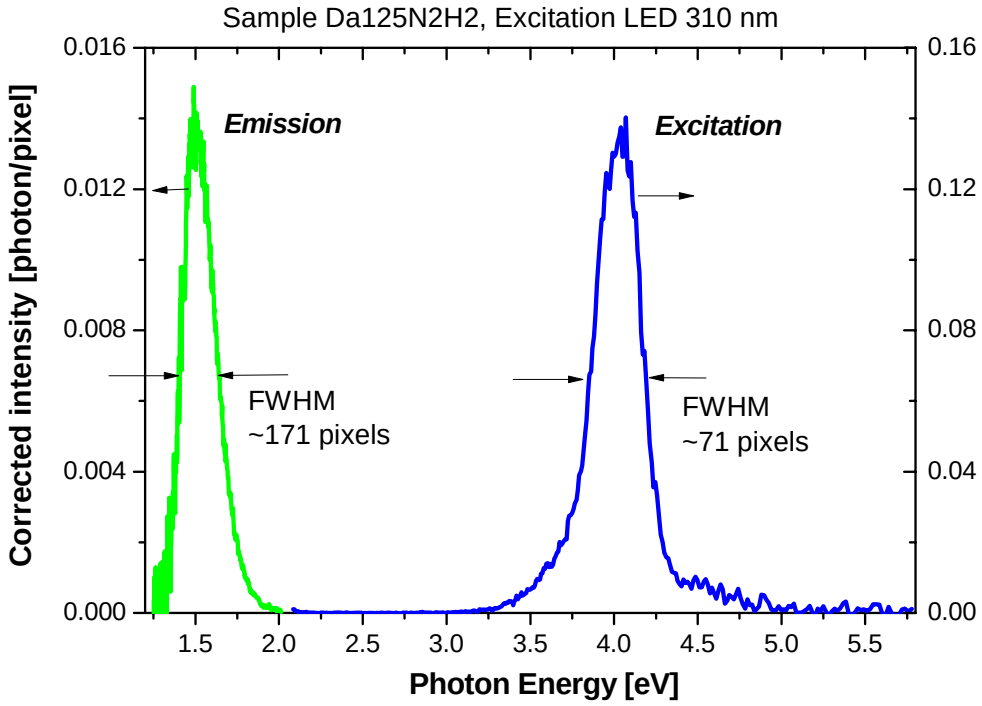

The QE of CQD was not measured because of fast degradation of PL intensity and also problems with cleaning of cuvettes after the measurement. The QE of ND was not measured because of very weak PL intensity.

3.5.2 Quantum efficiency of colloidal suspensions of Si-NCs

We measured Si-NCs samples from the 2nd aging study. (The samples from the 1st aging experiment were not measured because QE setup was built later). The preparation of measured Si-NCs samples and composition of solutions is described Chapter 3.4.2 in 2nd aging report. The samples were measured on the 110 day of aging. Due to low PL intensity of samples and their weak absorbance, we measured some of them only with diodes with short wavelengths (which are more absorbed). The spectra were measured 30 times each and then averaged. The final QE are summarized in *Tab. 9*. Due to very low absorbance of Si-NCs some QE could not be determined and the successfully measured QEs are burdened with experimental error as high as 30 %.

We need to take in account that the PL intensity of samples decreased with time so the starting QE had to be higher than the final one measured here. The ratio of final PL intensities between the samples corresponded to the ratio of QE values. The lowest QE was observed for sample A3. The QE values follow the decrease of PL intensity. For higher pH of the sample solvent, we observed lower PL intensity and also lower QE.

Table 9: Quantum efficiency of Si-NCs samples in various solutions after 110 days of aging process. The estimated maximal experimental error in this case is around 30 %.

	Sample quantum efficiency [%]							
Diode wavelength [nm]	A1	A2	A3	DG1	DG2	DG3	DG4	A4
240	~	~	< 0.5	~	×	6.0	8.3	1.5
250	2.5	~	< 0.5	4.4	7.6	6.5	8.1	1.4
260	2.8	0.5	< 0.5	~	7.4	×	7.9	1.5
270	~	2.0	< 0.5	11	7.2	3.9	10.2	1.2
280	~	~	< 0.5	5.1	7.0	~	11.1	0.2
290	0.7	0.9	0.6	3.1	7.0	17	8.6	0.15
300	~	3.1	0.4	1.8	< 6.0	~	5.6	0.1
315	1	0.3	< 0.1	1.6	~	~	5	< 0.1
325	~	0.4	< 0.1	1.5	1,4	8.3	3.1	< 0.1
345	×	< 0.2	~	1.7	~	7.7	2.3	< 0.1
355	< 1	< 0.2	< 0.1	1.8	×	5.0	×	×

~ - the signal was too noisy to determine the QE correctly
× - not measured due to problems with excitation diode

The sample with Si-NCs in D-glucose was at the time of measurement at about 40 % of the initial PL intensity value. That means that the maximal QE could be as high as 20-30 % (if the absorption did not change). QE values for Si-NCs with D-glucose were much higher than values measured for simple oxidized Si-NCs samples without any treatment (QE about 2-3 % [4A, 5A]). This high QE values together with results of FTIR measurements (*Fig. 55, 56*) indicates that interaction of D-glucose with surface of Si-NCs and structural changes of D-glucose molecule are responsible for the increase of PL intensity and QE. The specific changes of chemical groups could not be determined precisely, but the change was always connected with carbon atoms in the modified group. We cannot say if the D-glucose is directly connected (bonded) to Si-NC surface, but for sure there is some interaction between them as could be seen from AFM measurements Chapter 3.4.2. We also observed high increase of QE for particles activated with groups containing carbon atom (see Chapter 3.5.3).

3.5.3 Quantum efficiency of xylene-treated Si-NCs

QE of xylene treated Si-NCs was measured using OBB EasyLife V fluorescence System. The sample was excited with a 450 nm LED diode (for colloidal samples) or with a 355nm Nd:YAG (8 ns) laser (for naturally oxidized Si-NCs), and the emission detected by an intensified Andor CCD camera system. An interference filter was used to ensure detection at 550 nm for colloidal samples.

The measured QE for our organically CH_3 capped Si-NC was up to 20 % (at 550 nm). The Si-NCs samples before activation (naturally oxidized Si-NC) had the QE about 2-3 % [4A, 5A].

3.6 PL decay time of silicon nanocrystals

An excited state of a Si-NC (as any other type of luminescence center) can relax back to a ground state either radiatively or non-radiatively. These processes are described by characteristic lifetimes τ_r and τ_{nr}, respectively. The total lifetime of the excited state τ is a combination of those two lifetimes (3.3).

$$\frac{1}{\tau} = \frac{1}{\tau_r} + \frac{1}{\tau_{nr}} \tag{3.3}$$

This total lifetime of the excited state can be measured as PL decay. It is important to note that these lifetimes are directly related to luminescence QE, which is simply the ratio of the radiative relaxation rate to the total relaxation rate [71] (3.4).

$$QE = \frac{1/\tau_r}{1/\tau_r + 1/\tau_{nr}} = \frac{\tau}{\tau_r} \tag{3.4}$$

Therefore, by measuring PL decay time τ and QE we can calculate radiative and non-radiative lifetimes.

Si-NCs were prepared from the boron-doped Si wafers. This boron impurity probably resulted in further localization of excitons in nanocrystals and corresponding shortening of PL lifetime compared to intrinsic Si-NCs. The lifetime of excited state is influenced by non-homogeneity of impurities in Si-NCs and also by irregular shape and size-distribution of nanocrystals. Because of that the lifetime of excited state of measured colloids was determined with significant inaccuracy. Decay becomes faster with increasing temperature (two orders of magnitude when going from liquid-helium temperatures to room temperature). The non-radiative lifetime (related to dangling bonds etc.), which should take place also in our samples, is shorter than 1μs at low temperatures [81].

The PL intensity decay of Si-NCs is commonly described by the stretched exponential function (3.5)

$$I(t) = I_0 e^{\left(-\frac{t}{\tau}\right)^{-\beta}} \tag{3.5}$$

where τ is the characteristic lifetime and β □ (0,1) is the dispersion factor. This behavior of intensity has been attributed to exciton migration, carrier escape from Si dots, or distribution of shape of dots emitting at the same energy [7].

3.6.1 Experimental setup

Lifetimes of excited states were measured with the time-resolved spectroscopy apparatus displayed in *Fig. 62*. The excitation pulse was generated in optical parametric oscillator (PG 122/SH, EKSPLA) which was pumped by the second harmonic wave from a Nd:YAG laser (NL 3036, EKSPLA). Excitation pulse was guided with help of two mirrors into a quartz cuvette with Si-NCs colloidal sample. The emitted light was collected in right angle

geometry, focused by two lenses (forming an imaging tube) into an imaging spectrograph (TRIAX 320, HORIBA Jobin Yvon). The imaging spectrograph was controlled by Spectramax software. The signal from imaging spectrograph was collected on a cooled i-CCD camera (PI-MAX 512RB iCCD, Roper Scientic).

The synchronization of the detection time window and excitation pulses was done by a programmable time generator. The control of detection parameters of iCCD and signal recording was done in WinSpec software.

Figure 62: Time resolved spectroscopy apparatus: EKSPLA SHG – pumping laser (Second-harmonic generation) for OPO – optical parametric oscillator, imaging spectrograph – Triax 320, pulse generator – synchronization of the pulses, PTG – camera control, iCCD – CCD camera, imaging tube – collecting signal from the sample cuvette and focusing to a spectrograph, C – cuvette with the studied colloid, F – filter, M – mirror.

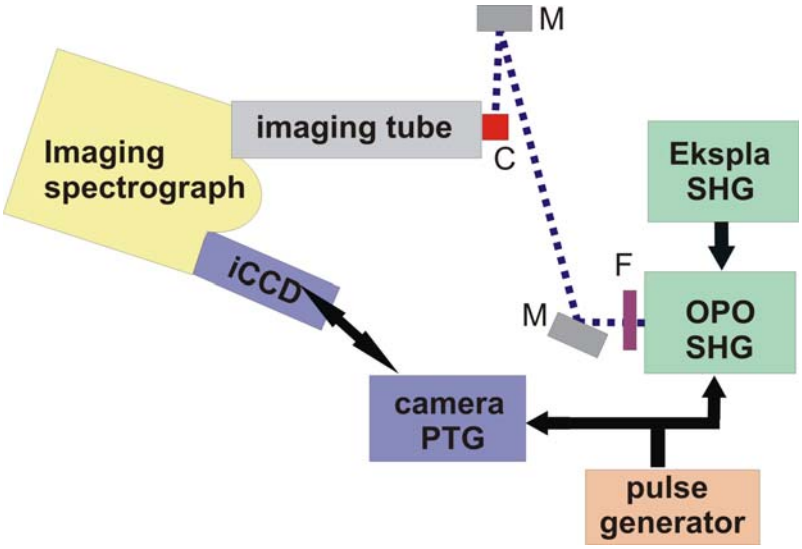

3.6.2 Time-resolved PL experiments

We used a mixture of blue (maximum at 420 nm) and orange (maximum at 600 nm) emitting Si-NCs treated with various solvents for measuring lifetime of excited states. The two types of Si-NCs were mixed in powder form and the same mixture was used in all solvents.

The samples were prepared as follows: Si-NCs with 19.6 mg of D-glucose in 1 ml of distilled water, Si-NCs with 17.5 mg of NaCl in 1 ml of distilled water, two samples of Si-NCs in ethanol (these samples denoted “ethanol I” and “ethanol II” were incubated for 2 and 5 weeks, respectively), and Si-NCs with 5.8 mg of D-glucose in 1 ml of ethanol. The samples were stirred continuously for 5 weeks in cuvette (one week in case of ethanol I) with a magnetic stirrer (Hei-Tec, Heidolph) at 220 rmp. This stirring was done at room temperature (22 °C) in ambient light.

The measured lifetimes of excited state of Si-NCs in various solvents are summarized in *Tab. 10*.

Table 10: Summary of the Si-NCs lifetimes of excited state in various solvents, each value is an average of at least 10 measurements, and is given with the standard deviation.

Sample	PL lifetime 420 nm [ns]	PL lifetime 600 nm [μs]
Si-NC in ethanol I.	6.0 ± 1.4	13.1 ± 0.4
Si-NC in ethanol II.	5.3 ± 1.4	11.1 ± 0.4
Si-NC in ethanol with D-glucose	5.9 ± 1.4	11.1 ± 0.4
Si-NC in water with D-glucose	9.3 ± 1.4	12. 2 ± 0.9
Si-NC in water with NaCl	6.5 ± 1.4	11. 8 ± 0.6

PL lifetimes at 420 nm were very similar for all samples. The only slight difference was observed for sample Si-NC with D-glucose in water, where the lifetime was approximately 50 % longer than for other Si-NCs samples. On the other hand, the PL lifetime at 600 nm (orange PL peak) of this sample was only slightly longer than for other samples. Lifetime of excited state of Si-NC in ethanol (emission at 600 nm) differs between sample I. and II. This difference was probably caused by further oxidation of Si-NCs in sample II which decreased the lifetime slightly.

We also measured PL lifetime for organically (CH_3) capped Si-NCs and found values of about 2 ns at 550 nm, which was significantly shorter compared to all other samples, indicating "direct-like" transitions of excitons in a NC core.

3.7 PL blinking of silicon nanocrystals

The single nanocrystal spectroscopy techniques enable to overcome inhomogeneous broadening of spectra inherently present in measurements of an ensemble of emitters (nanocrystals, molecules etc.) but it also reveals interesting new phenomena such as emission intermittency (ON–OFF blinking), spectral diffusion, polarization etc. [7A]. While the spectra of Si-NCs (possibly single nanocrystals or agglomerates of few Si-NCs) were studied by the wide-field imaging micro-spectroscopy, the ON-OFF blinking phenomenon is better studied by the confocal single-photon-counting microscopy which provides much better time resolution.

The ON-OFF statistics in Si-NCs has not been fully explored and understood yet (there is only couple of papers on this subject in literature) mainly due to difficulties of single Si-NCs preparation and low emission rate of the PL S-band of Si-NCs. The published reports can be briefly summarized as follows: Buratto's group reported that only a few percent of Si-NCs grains show detectable PL, but QE was estimated to be up to 88 % [82]. All their samples had the FWHM of PL band about 115 meV. The FWHM of pyrolysed Si-NCs particles from Chicos group was 100 eV or wider and in some cases exhibited a low-energy side-band shifted by 120-190 eV from the main PL peak [73]. The power-law distribution of OFF times was shown to be strongly related to the bleaching of Si-NCs PL [83]. Linros group observed Si nanopilars with QE up to 35 %, but only a few of Si-NCs on top of nanopilars were luminescent with FWHM of about 120 meV. The photoluminescent nanoparticle switches

randomly between ON and OFF states. The ON-time intervals shorten with the square of the excitation power, probably due to charging of nanoparticle and Auger effect [33].

Our Si-NCs were dispersed in ethanol then filtered with membrane pore 100 nm filter (Millex Millipore). A droplet (10 μL) of this suspension was deposited on the total-internal-reflective prism and the sample was excited with evanescence field from 442 nm laser beam from the He-Cd laser. The experimental setup is described in Chapter 3.3. We observed some spectral shifts and intensity variations of single Si-NCs PL spectra when detected a sequence of 9 spectra (each with 30 min acquisition-time). The results of measurement are shown in *Fig. 63*.

Figure 63: Changes of single Si-NCs PL spectra excited with evanescence wave (442 nm). a) Eight spectra taken from different diffraction-limited weakly emitting spots measured simultaneously during one 30 min acquisition at different locations on the sample. Some of the PL peaks are fitted with a Gaussian band (yellow lines) with the FWHM indicated, b) and c) sequence of nine 30 min acquisitions of photoluminescence spectra from two different emitting spots demonstrating the ON-OFF blinking and diffusion (Taken from [7A]).

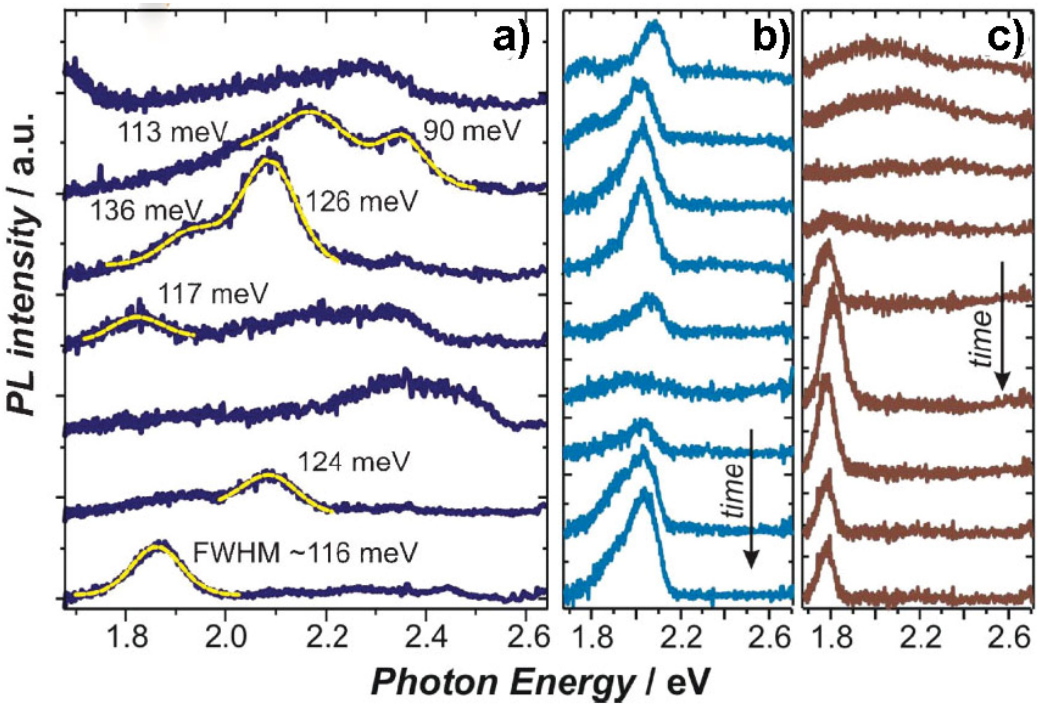

The ON-OFF blinking characteristics were measured with the single photon counting setup. It consisted from an inverted fluorescence microscope (Olymus IX-81 with UPlanS Apochromat 60 x magnifying objective with 1.2 numerical aperture) coupled to a photon-correlation detection system. The sample was placed on a quartz cover slide. The excitation was provided with the continuous-wave 444 nm diode-laser. The arrival times of emitted photons were detected with two avalanche photodiode counting modules (Perkin Elmer SPCM-AQR) for detection period from 5 to 15 min. The detection events were binned per selected time slots (optimal value was between 0.1 and 0.3 s) and plotted against time. The intensity time evolution revealed clear multilevel fluctuations with three states: OFF state, ON state and double ON state (see *Fig. 64*). This structure was also observed by Manson et al. in [84].

Figure 64: Blinking characteristics of single Si-NC grains. a) Typical time trace of one Si-NCs nanoparticle obtained by binning of the photon counting events per 300 ms slots (the most frequent signal levels are indicated by dashed lines) b) The occurrence histogram of intensities from the left panel (red line is a fit with three Gaussian peaks). Taken from [7A].

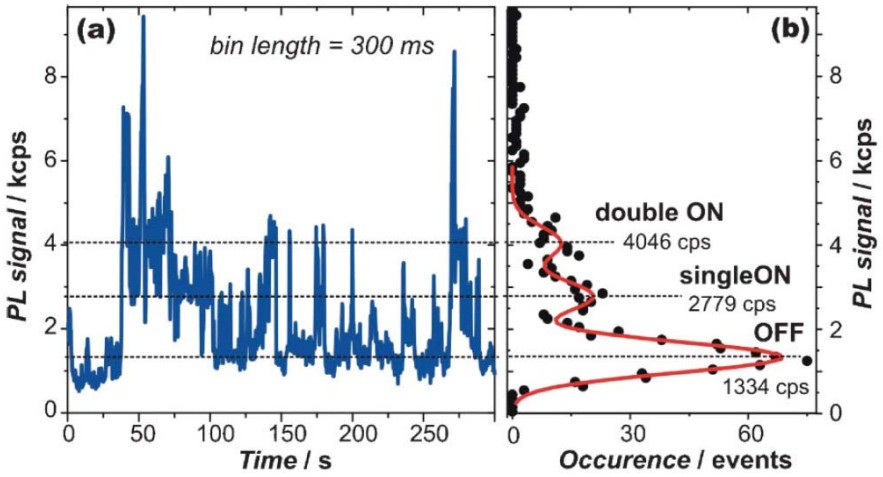

Due to the imperfect process of preparation we often had agglomerates of Si-NCs in the sample (containing from two up to several dozens of interconnected Si-NCs for non-filtered samples), but usually only one nanocrystal emitted in one single agglomerate and the others were in the OFF state. The double ON state is then explained as overlapping contributions from two nanocrystals emitting within the optically resolved spot.

There are various models explaining the distribution of ON and OFF states. For pillars with silicon nanocrystals on the top it seems that OFF and ON dwell times are distributed exponentially [85], which indicates the so called "random-telegraph" switching model [86]; other possible models are discussed in [7A]. In contrast, our Por-Si-based suspensions show ON and OFF time distribution in the form of power-law dependence $\sim t^{-\alpha}$, where the coefficient α is close to 1.5. Similar behavior was reported by Cichos et al. This type of dependence is usually explained to be due to distribution of trap states on the Si-NC interface, where a trapped carrier can diffuse until recombining back.

Figure 65: Schematic illustration of processes involved in the radiative and nonradiative recombination of electron-hole pairs in a single Si nanocrystal.

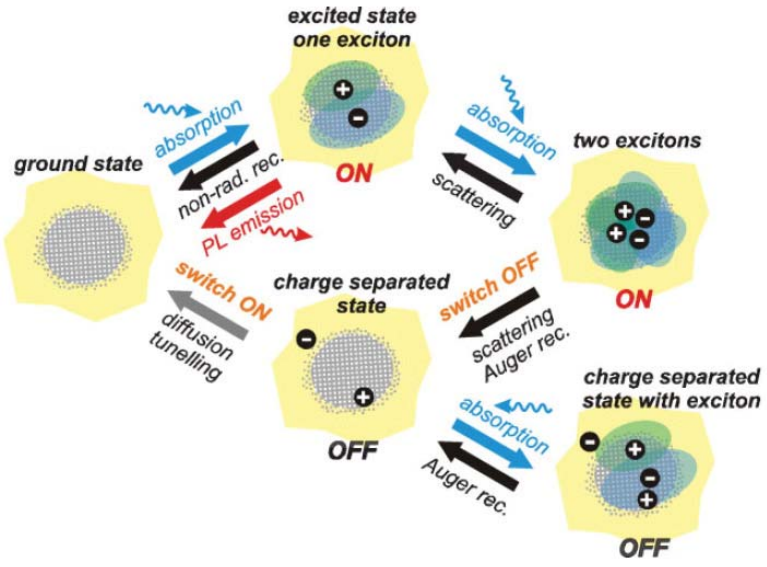

If we look on the microscopic model shown in *Fig. 65*, we can see that after absorption of photon an electron-hole pair (exciton) is formed in Si-NCs.

This exciton is strongly confined in small nanocrystals and also is influenced by interface between Si core and SiO_2 surface (this interface is connected to specific vibrations – phonons). The exciton can interact with

nonradiative centre [87] and this results in reduction of the average quantum efficiency of radiative recombination. Due to relatively long PL decay, a generation of second exciton is highly probable (under stronger excitation). The inelastic scattering can induce the nonradiative recombination of one exciton and excitation of the other one. The nanocrystal stays still ON because of presence of the first exciton, but the quantum efficiency is reduced due to the loss of the second exciton. If the exchanged energy is high enough and the energy landscape is favorable, the scattering can lead to a charge separation. In the charge-separated state, the Auger recombination efficiently quenches created excitons, hence causing the Si-NC to become dark until the charges recombine back [7A].

For high excitation, the excess of excitons is quenched by nonradiative processes. If we exclude the OFF states, then the QE (apparatus for measuring QE is described in Chapter 3.5.1) is up to 15 % for pumping rate of 2 x 10^4 photon.s^{-1} and decreases slowly as the 0.7^{th} power of excitation for another three orders of magnitude without clear saturation. Previously published low QE of a few percent was probably due to including the OFF states in the Si-NC ensemble measurement.

The above described blinking phenomenon is of course, detrimental to many applications, including fluorescence labeling for bio-applications. Deeper understanding of its mechanism is very important for developing of non-blinking quantum dots. Recently, it was shown that non-blinking nanocrystals of II-VI semiconductors are obtained by growing thick shells and/or creating smooth transition from the core to shell material CdZnSe/ZnSe [88]. We believe that similar improvement should be possible for Si-NCs too.

4. Biological studies

4.1 Introduction

One of the hot topics of current biological studies is the development of techniques to observe biological processes on a single molecule level, e.g. tracking of single proteins, various drug molecules, etc., without putting a high stress on a studied biological system by strong staining of observed molecules. The staining usually has considerable negative effects on cell development, starting already with a low stain concentration. The stain molecule usually also complicates movement of observed object (drug molecule, protein molecule, etc.) within the cell because of the size of the staining molecule, which is sometimes of the same size as studied object, but usually at least tree times bigger (e.g. Alexa Flor stain average size 0.1-0.3 nm without antibody, for stain with antibody at least twice bigger). Another complication connected with use of fluorescence dyes is their high cytotoxicity and majority of them is also suspected as cancerous agents. Quantum dots are used as an alternative to fluorescent dyes. Although they have high PL intensity and stability, they also have large size (around 25 nm and larger). They are usually at least 10 times bigger than the studied protein, because they need protective covering of the hydrophobic and often toxic core (majority of them is cadmium-chalcogenide based). Even though they have this protective covering, it can degrade in biological environment and toxic atoms are released to the surroundings.

The average diameter of Si-NCs (1-3 nm) is comparable to the length of phospholipids (2-4 nm) in a lipid bilayer of the cell. The ND and CQD are at least twice the size of bilayer. A thick shell is needed in case of cadmium-based CQD to prevent release of Cd atoms to the cell and that increases the size of particle to at least 25 nm (as it was in our test).

Although the Si based nano-particles are not organically based, they can be dissolved in the living body in a reasonable time [24, 89]. Biodegradability is an exclusive feature of Si-NCs. Moreover, they can be used as a florescent mark even for very sensitive measurements, because we can observe single nanocrystals also in living cells with our apparatus. On the other hand, even though ND and CQD are luminescent and usable for single molecule staining, there is no known pathway how to remove them from the living organism. We also need to take into account that possible aggregation of these particles in a living organism can be even more dangerous.

For practical application of nanoparticles in biology, it is crucial to be able to activate and functionalize the surface of single standing nanoparticles. This need is imposed not only by necessity to ensure specific addressing of the particle in the cell, but, in case of Si-NCs, also to prolongate duration of PL stability before their degradation in a living organism.

Many techniques for activation of silicon particles with surface covered by a layer of SiO_2 or Si-H are already developed (some of them tested only for macro-sized particles) [90, 91].

The CQD are usually covered with a shell formed by wider bandgap semiconductor and many protocols how to activate these surfaces for CQD exist. Separation methods for extracting activated CQD from the activation solvent can be used thanks to a large amount of particles, but significant losses cannot be avoided.

ND can be used also as markers in nanomagnetometry [92], where single fluorescent centers of ND (nitrogen vacancy) in single ND in HeLa cells were measured. This ND did not need

any special covering. Another use of non-covered ND was the two-photon imaging study (with NDs around 35 nm) in cell done by Chang's group [93]. Neugart et al. [94] prepared biotinylated 4 nm ND aggregates and bound them to streptavidin to study their motional dynamic in a living cell. Fu et al. [68] succeeded in preparation of 100 nm ND covered with carboxyl groups and their derivates; they can bind to non-specific nucleic acids and proteins, e.g. Polylysines covering of ND for DNA sensing. These nanoparticles are too large to be used in longtime studies in cells due to mechanical stress they can cause. The used ND activation technique is not usable for smaller ND particles, because the centrifugation cannot separate effectively and properly small particles from the activation solvent.

A few protocols for Si-NCs covered by SiO_2 were already developed. One of them is thermal carbonization. Carbonized Si-NCs are not able to penetrate intestinal walls, but when introduced directly to cells, they are highly inflammatory and cytotoxic [95]. Another example of activation is encapsulation of Si-NCs into pH-stable (4-10) phospholipids micelles [96] or covering them with 5'- amino-modified oligonucleotide, these samples were used for DNA studies [97]. Swihart´s group synthesized biocompatible luminescent composite nanosized vesicles (containing Si nanoparticles) for imaging cancer cells [96]; the covering was already part of a nano-vesicle itself.

Many techniques of activation already exist for surfaces covered with ND or Si-NC. Those materials with nanoparticles on the surface can be used as scaffolds for variety of cells without causing inflammatory reaction [76, 98]. Other general techniques for chemical activation of various quantum dots, including silicon nanocrystals and nano-surfaces, are summarized in [99, 100] and for Si-NCs discussed also in this work in Chapter 2.5.

Another advantage of luminescent nanoparticles in biological experiments is that they can be used in multicolor experiments. PL peak position depends mainly on size of particle and can cover large spectral range. In case of ND the PL shift depends not only on size, but also on doping. A mixture of such size-distributed nanoparticles can be excited by a single wavelength (laser line) with emission in several peaks, where each peak corresponds to one group of PL nanoparticles. That solves problem of simultaneous measurement of several biological indications – we can perform that with PL nanoparticles. Stains conventionally used in biology have broad emission spectra and also need several excitation wavelengths. The emission spectra of various dyes are then overlapping and we cannot distinguish which label is in a specific place of cell or is staining the studied biological process. Stains are not good for long time studies due to photo-bleaching; on the other hand, PL of nanoparticles is stable in long time. Additional disadvantage of stains is that distance between fluorophores must be larger than the resolution limit [101]; otherwise we cannot distinguish them et al..

Another important feature of Si-NCs is their big surface/volume ratio. That means that they could be, e.g., very good carriers of drug molecules, or can be used as probes in sensitive measurements, where it is crucial to have high amount of nanomaterials in a restricted area. Finally, we must keep in mind that for working with cells we must use safe excitation wavelength. Wavelengths in UV range cause significant damage to cells [102]. The lowest wavelength used in case of Si-NCs in cells was 320 nm.

In conclusion Si-NCs show all properties needed to be a good nano-sized label useful in biology: small size, PL stability, biocompatibility, and biodegradability in live organism.

In the Chapter 4 we study interaction of nanomaterials with biological environment in vitro. We focus on their cytotoxicity by applying various methods: cell-growth curves (Chapter 4.5), time-lapse microscopy (Chapter 4.6) and Lactate dehydrogenase test (Chapter 4.4). Morphological changes of cells interacting with nanoparticles were studied with optical microscopy using Gimsa-Ramanovskyi staining (Chapter 4.7), and scanning electron microscopy (Chapter 4.10). Finally interaction of nanomaterial with cells was studied by confocal fluorescent microscopy (Chapter 4.8) and micro-spectroscopy (Chapter 4.9).

4.2 Cell cultures and sample preparation

In this study we used cell lines representing both animals and humans: L929 mouse fibroblast cells, HeLa human cervical carcinoma cells (epithelial), SAOS-2 human osteosarcoma cell (osteoblast-like cell line). The cells were incubated in cell incubator with 5 % CO_2, at 37 °C, in nutrient media specific for each cell line. The composition of nutrient media is summarized in *Tab. 11*. The components of media for L929 and HeLa cell lines were from PAA company and SAOS-2 from BioConcept company (nutrient media line Amimed without phenol red).

Table 11: Composition of nutrient media for various cell lines

L929		**HeLa**		**SAOS-2**	
MEM with Eagle salt	92 %	EMEM	86%	McCoy's 5A with L-glutamine	500 ml
Newborn calf serum	5%	Newborn calf serum	10%	Fetal calf serum	75 ml
Antibiotics/antimicotics	1%	Antibiotics/antimicotics	1%	Penicillin	20 u/ml
$NaHCO_3$	1%	Non-essential amino acids	1%	Streptomycin	20 mg/ml
L-glutamine	1%	L-glutamine	1%		
		$NaHCO_3$	1%		

All the nanomaterials except CQD (which were excluded due to their light-sensitivity and the fact that they had been sterilized by the manufacturer) were sterilized by 25 minute illumination with a UV lamp (254 nm) for excluding cytotoxicity stemming from organic impurities. Then the nanomaterials were added to nutrient media in various concentrations and the incubation followed for various times depending on a specific experiment.

In case of optical experiments, we need to keep in mind that long time exposure of cells to excitation wavelengths in the UV range is significantly damaging the cells [102]. Therefore the exposure time was minimized and the lowest excitation wavelength used on live cells was 320 nm.

4.3 Cytotoxicity

Although silicon and diamond in form of a bulk material are non-toxic, nanoparticles prepared from those materials can cause toxic reaction. Not only the composition of nanoparticle plays crucial role in cytotoxicity, other parameters such as size, shape, its dispersion, composition, and surface properties of nanomaterials, contribute to the final toxicity, albeit the precise mechanisms are not known yet.

The chemical impurities arising from nanoparticle preparation or handling can also play an important role in the overall cytotoxicity. Impurities from preparation are usually toxic and could cause inflammatory reactions in cell or induce significant damage to cell functionality. Although Si-NCs in our study were prepared with highly toxic solvents, such as HF and H_2O_2, the final product was cleaned off them totally, without measurable traces left. The NDs in our study were prepared by various acids, but the presence of them in final product was beyond resolution of our measurement because of intensive cleaning procedure.

As was mentioned above [103] the shape and surface covering play important role in final cytotoxicity. We need to know all the above mentioned physical properties in order to be able to compare the measured cytotoxicity of nano-sized material with other published results. These are very difficult and time-consuming experiments that cannot be usually done for all parameters (mainly because of limited control on nanomaterial growth or manufacture). Small difference in one parameter can play crucial role for samples which are otherwise similar in all other parameters (e.g. oxygen vs. hydrogen termination of Si-NC or nanodiamonds). Small differences in sample parameters are usually reason of different experimental results obtained by different groups working with samples prepared seemingly "in the same way".

The Si-NCs sample closest in physical properties to our sample has the cytotoxicity level (i.e. the concentration of particles above which they start to have negative influence on cell proliferation) around 112 μg of Si-NCs per ml of nutrient media (data measured by Fujoka et al. [104]).

The typical size of human muscle cells is around 10 μm and larger. SAOS are in size around 30-50 μm, HeLa 30-60 μm, L929 15-25 μm. The cell is protected with a lipid bilayer membrane less than 10 nm thick. When we introduce to such cell object bigger than 100 nm, we can induce not only cytotoxicity, but also mechanical stress, followed by cell damage and death. Particles bigger than 10 nm present inside a living cell cause problems, which can be tolerated for low doses of particles but seriously endanger the cell functionality for high doses.

The nanomaterials can have also a specific type of toxicity – genotoxicity. Genotoxicity of Si-NCs has been studied by Jin et al. [105]; they proved that, although silicon particles enter inside cells, they are not entering the nucleus. Therefore, they are considered to be safe from the genotoxicity point of view. A care has to be taken in case of ND; there are emerging works about possible genotoxicity due to DNA damage caused by ND. So far, the studies have been done mainly on embryonic Stem cells, which are highly sensitive, and the genotoxicity might be connected only to a specific surface termination of ND, as in the case of ND with oxide on the surface in work of Xing et al. [106].

The CQD used in this study are cytotoxic due to presence of cadmium in the particle, which is covered only by a single carboxyl layer, and Cd atoms are released from the CQDs when embedded in a living cell. Even though we can use CQD covered with ZnS protective shell, they are not stable in biological environment and the cadmium-based core gets exposed anyway, followed by release of toxic atoms [107]. It is widely known that cadmium atoms are highly cytotoxic for living organism and genotoxic as well [108].

4.3.1 Generation of singlet oxygen by nanosized Si

Nanosized Si is, in special cases, able to produce chemically reactive molecules containing oxygen (e.g. oxygen ions and peroxides), which are grouped under the term "reactive oxygen species" (ROS). Origin of their reactivity is the presence of unpaired valence shell electrons. ROS are part of normal metabolism of oxygen in a cell, but when their concentration increases above certain limit which the cell can handle, then the cell could be significantly damaged due to oxidative stress produced by ROS.

ROS can be produced by Si-NCs under certain conditions, mainly by illumination of Si-H terminated porous silicon nanomaterials (summarized in [24, 109, 110]). Living cells do not adhere to materials with Si-H groups on the surface. Low et al. [109] observed ROS production in a cell culture cultivation media with Si-H terminated nanomaterials and, in agreement with other authors, found them cytotoxic. When the silicon surface is oxidized, the ROS production decreases to undetectable amounts and, therefore, brings no risk in using oxidized Si particles in biological experiments.

Kovalev and Fuji in [5] proved that nanoscale silicon is very efficient spin-flip activator of O_2 and explained observed production of ROS by Si-H terminated nanoscale silicon in biological environment [110, 5]. Si-NCs samples in our study had oxidized surface and because of that we did not observe any significant effects which might come from the ROS production (for preparation of Si-NCs see Chapter 2.1.1). The production of ROS is not only unwanted effect but it can be exploited for e.g. the photodynamic therapy of cancer [3A].

4.4 Lactase dehydrogenase cytotoxicity test

Lactase dehydrogenase (LDH) test is another possibility of empirical characterization of the viability of cells incubated with nanomaterials. LDH is stable cytoplasmic enzyme present in all living cells. When cell membrane is damaged, the LDH releases to the surrounding nutrient medium; the precise mechanism of this reaction is described in Appendices *Ap.2*. We let the SAOS-2 cells incubate with Si-NCs or ND for 24 hours and then performed LDH test; the results are shown in *Fig. 66*.

Figure 66: LDH cytotoxicity test of SAOS-2 cells incubated for 24 hours with various concentrations of Si-NCs or A-ND (Si in the graph stands for Si-NCs).

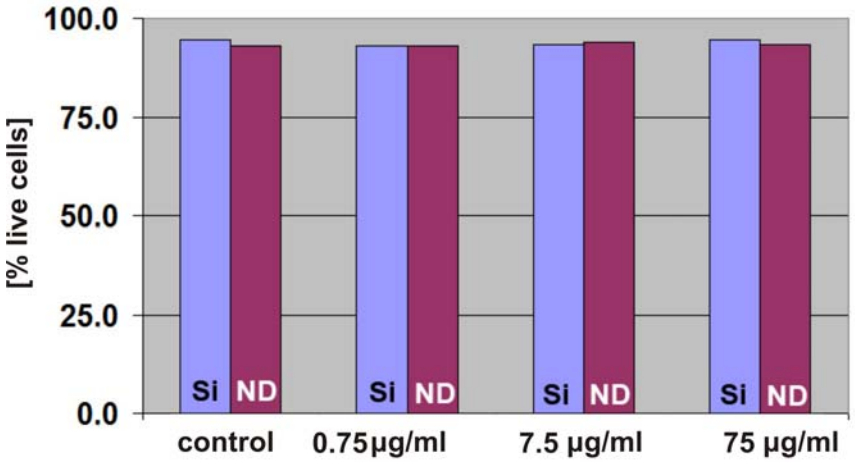

Comment: The columns show percentage of living cells from all cells in the sample. The values were quite similar for all samples. Only for concentration 75 µg in 1 ml of nutrient media we observed slightly higher number of living cells incubated with Si-NCs compared to A-ND.

Because this experiment did not show any significant difference in cytotoxicity of nanomaterials within 24 hours, we decided to do another LDH test for SAOS-2 cells incubated with Si-NCs or A-ND for 48 hours. The resulting cytotoxicity is displayed in *Fig. 67*. We had very limited amount of CQD, therefore we decided to measure LDH test only for lower concentrations of CQD (maximal concentration was about 5 μg/ml for 48 hours, for characterization see Chapter 2.3). The measured LDH data of cells incubated with CQD are displayed in *Fig. 68*.

Figure 67: LDH cytotoxicity test of SAOS-2 cells incubated for 48 hours with various concentrations of Si-NCs or A-ND (Si in the graph stands for Si-NCs).

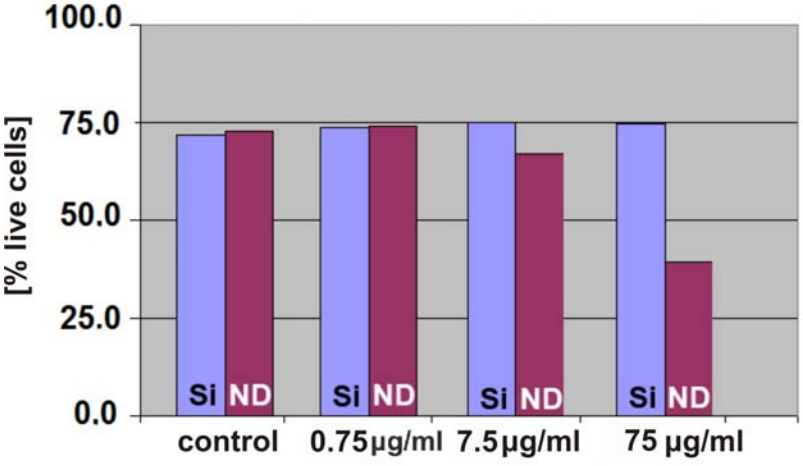

Comment: Significant difference between cytotoxicity of Si-NC and A-ND was observed for concentrations of 7.5 μg in 1 ml of nutrient media and higher. The LDH concentration outside the cells increased dramatically for the cells incubated with A-ND in correspondence to an increased number of dead cells. The percentage of living cells incubated with A-ND was just half of the percentage of living cells incubated with Si-NCs (which is close to the control sample). Illustration images of cells after 48 hour long incubation with nanomaterials are shown in Appendices *Ap.3*.

Figure 68: LDH cytotoxicity test of SAOS-2 cells incubated for 48 hours with various concentrations of CQD. The highest concentration was 5 μg of CQD in 1 ml of nutrient medium (different concentration than in previous cases).

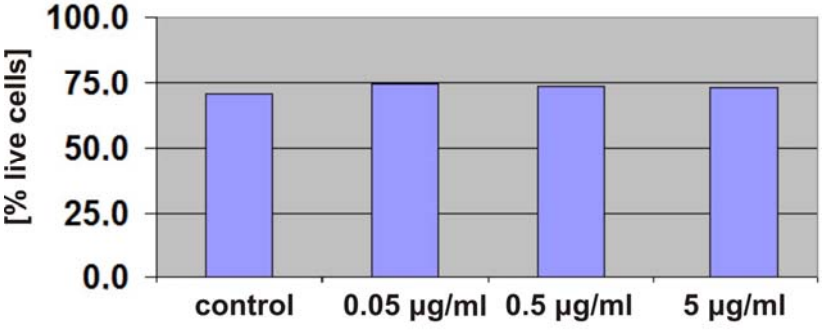

Comment: The percentage of living cells incubated with highest concentration of CQD is displayed in the last column. The percentage of living cells was more or less the same as in the control sample for all tested concentrations of CQD. The small variations are within the experimental error. Illustration images of cells after 48 hour long incubation with nanomaterial are shown in Appendices *Ap.3*.

In conclusion LDH test for cells incubated with nanomaterials for 24 hours showed that for low concentrations of Si-NCs or A-ND in nutrient media both samples behaved the same while for concentrations around 75 μg/ml cells incubated with Si-NCs did proliferate better than cells incubated with A-ND. These differences were even deeper for LDH test taken after 48 hours of cells incubation. In case of cells incubated with Si-NCs the numbers of cells were

practically the same as for the control sample. A-ND concentration of 7.5 μg or higher was strongly cytotoxic for the cells.

In case of CQD, we did not observe any significant change in cytotoxicity for all tested concentrations within 48 hours, but these samples were incubated with significantly lower concentration of nanomaterial than other samples. This is in agreement with Chapter 4.5, where we started to observe cytotoxicity of CQD after 50 hours of incubation with the cells.

4.5 Cell-growth curves

In order to characterize cell viability we need some empirical methods how to quantify it. One of these methods is the so-called growth curves method. We incubated cells with studied nanomaterials (nanomaterials were added immediately after the passage of cells) for about 80 hours and counted the number of living and dead cells in each sample in 8 hours intervals; each experiment was repeated 12 times. A growth curve represents number of living cells (observed within field of view of transmission optical microscope with 20x objective – approximately 0.5 mm^2) plotted against time. Growth curves were measured on both L929 and HeLa cells.

In the first experiment we studied influence of variously sized silicon nanomaterials (Si-NCs, M-Si) on L929 (*Fig. 69a*) and HeLa cells (*Fig. 69b*). The concentrations were as follows: 8 μg/ml of Si-NCs and 40 μg/ml of M-Si in nutrient medium (M-Si preparation is described in Chapter 2.1.3); the concentrations were chosen to result in about the same number of particles in each sample. The number of dead cells varied around 3% of the number of living cells for cells incubated with Si-NC or M-Si nanomaterials.

Figure 69: Growth curves of L929 (a) and HeLa (b) cells incubated with Si-NC, M-Si, and without nanomaterial (control sample).

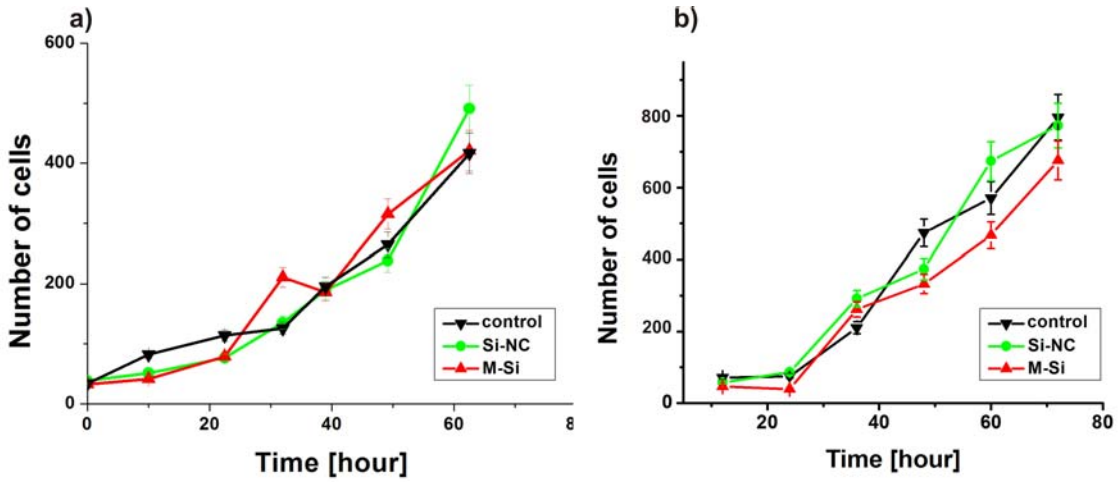

Comment: As we can see in *Fig. 69*, both cell lines grew nicely with both nanomaterials. The samples incubated with Si-NC grew slightly better than the control sample. In case of M-Si we observed slightly lower numbers of HeLa cells, but the ratio of the dead cells to live cells was the same as in the control sample and for cells incubated with Si-NCs (data not shown). That means that cells were just slowed down in proliferation due to presence of big crystallites.

Growth curves for ND, CQD and A-ND were measured only on HeLa cells due better response of these cells to nanoparticles as shown in *Fig. 69*. Growth curves for ND, CQD and A-ND are shown in *Fig. 70*. Concentrations of nanomaterials in nutrient media were: ND – 8 μg/ml, CQD – 8 μg/ml, and A-ND – 4 μg/ml (these concentrations were chosen so that the number of particles was about the same for all samples).

Figure 70: Growth curves of HeLa cells incubated with A-ND, CQD, or ND and of a control sample incubated without added nanomaterials.

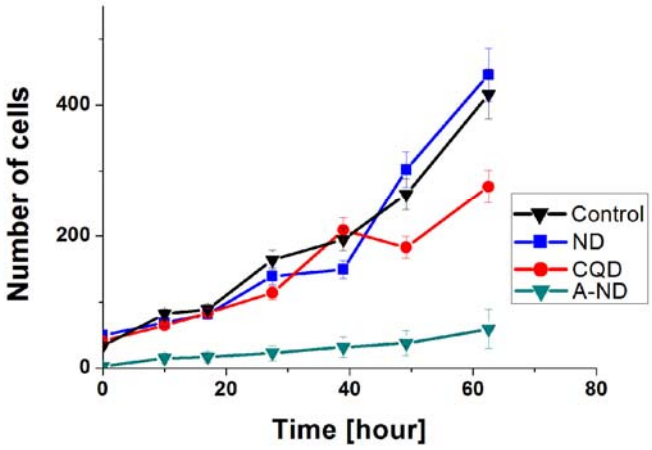

Comment: As we can see in *Fig. 70*, the cells incubated with ND grew like the control sample incubated without any nanomaterial. In case of CQD we observed slight decrease in number of cells compared to the control sample after 50 hours, this was probably due to the release of toxic compounds from CQD (mainly cadmium). Cells incubated with A-ND grew significantly worse compared to the control sample - the number of cells increased very slowly and after 60 hours the total number of cells incubated with A-ND was just on 1/10 of the control sample at the same time (the images of cells after 60 hour incubation are for illustration shown in Appendices *Ap.4*).

The number of dead cells was in case of CQD, ND, and control sample below 3 % of the number of living cells, in contrast to A-ND, where the number of dead cells was almost the same as number of living cells.

In conclusion, the cells incubated with Si-NCs and ND behaved practically the same as the control sample for nanoparticles incubated with L929. Slower proliferation of cells was observed for cells incubated with M-Si in case of incubation with HeLa cells. Small decrease of number of cells was observed for CQD just after 50 hours. The worst situation was observed in case of cells incubated with A-ND, cells did not proliferate well and exhibit high proportion of dead cells.

4.6 Time lapse microscopy of cells incubated with nanomaterials

4.6.1 Experimental setup

The experimental apparatus for time-lapse microscopy is shown in *Fig. 71*. The Petri dish with the cell sample was inserted in an inverted microscope (Olympus IX 51) equipped with an incubation chamber (36.8 °C and 5 % CO_2). A picture of sample was taken every 2 minutes; the sample was illuminated for 5 s before taking the picture. Although focusing was automatically controlled, some manual control was needed each 5-6 hours for correcting bigger focus shifts. A video was composed from taken pictures with 21 frames per second. With this technique, we are able to see how the cells proliferate in presence of various

nanomaterials and if there is any significant change in cell division. We can also observe the migration of cells and movement of cell filopodia.

Figure 71: Apparatus for the time-lapse microscopy observation of living cells.

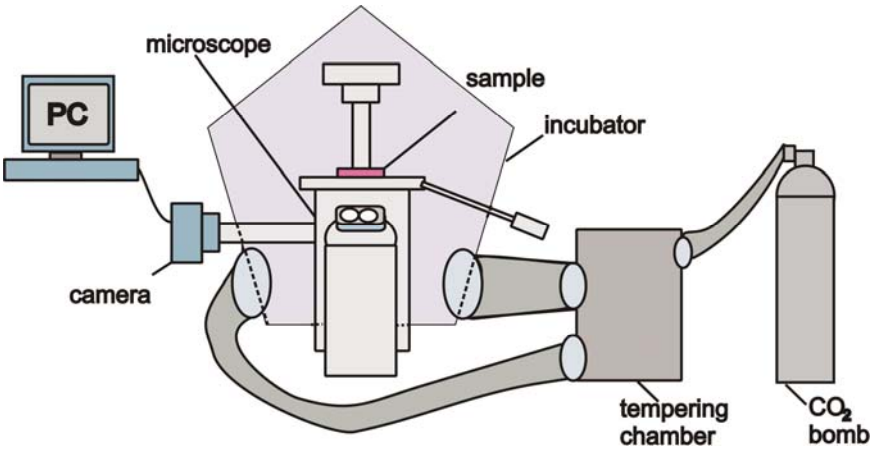

An objective lens with 20x magnification, and 0.4 numerical aperture (Olympus PLCN20x/0.40 C Plan Achromat) was used in our study. Pictures were taken with the digital camera Olympus C-7070 (7.1 megapixels), which was controlled by Quick Photo Micro 2.1 software.

The apparatus was placed in a dark room to exclude influence of light on the cell culture, although the inevitable illumination before taking a picture could have negative influence on cell proliferation in presence of nanomaterials. Main problems caused by illumination might be photodegradation of nanoparticles and also cells, production of reactive oxygen species etc.

4.6.2 Time lapse microscopy of L929 cells incubated with nanomaterials

Nanomaterials were added to nutrient media and then added to the cell samples immediately after passage. The whole volume of nutrient media in a Petri dish with cells was 3 ml. The Petri dish with studied sample was transferred to the lifetime lapse apparatus immediately after preparation. The cells were settling down during the first 30-60 minutes. Then we observed how fast the cells were attaching to the surface and also how often they were dividing. The average time of cell division for L929 cultures was 20-24 hours. We had to refocus the apparatus quite often (each 3-6 hours) due to random shifts produced by the apparature.

The concentrations of nanomaterials in 1 ml of nutrient media were as follows: Si-NCs 80 μg/ml, CQD 80 μg/ml, ND 80 μg/ml , M-Si 100 μg/ml, and A-ND 100 μg/ml mg. In the first experiment, when we added A-ND into nutrient solution immediately after cell passage, the cells died within two hours. Because of that a drop of source solution with A-ND particles was added on a cover glass, dried out, and sterilized for 25 minutes under 254 nm UV lamp. Then we put this glass on the bottom of Petri dish and added the cells with nutrient medium.

The cells incubated with Si-NCs and M-Si (already studied in our previous work [2A]) had been proliferating without significant change compared to a control sample.

Video files were created from the time-lapse sequences and they are recorded on the DVD accompanying this work. The filenames have form "4.6.2. L929-X", where X indicates the nanomaterial present in the nutrient medium, namely Si-NCs, control, M-Si, CQD, ND, and A-ND. Selected snapshots from the videos are presented below in *Fig. 72-76***,** with some comment. The general characteristics of cells incubated with nanomaterials revealed from time lapse microscopy are summarized in *Tab. 12*. The comparison was done strictly from attached videos, shown images are only illustrative.

Figure 72: Time lapse images of L929 cells incubated without any nanomaterial (control sample): a) after 2 hours, b) after 20 hours.

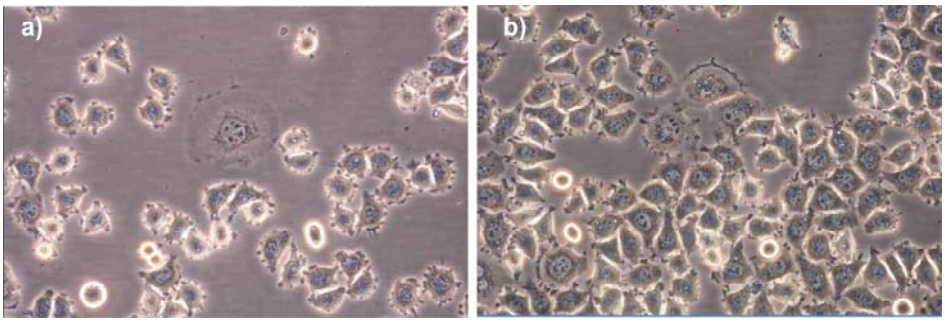

Comments (to the video file 4.6.2. L929-control): The video starts when cells already settled down on a glass coverslip. We could see that the cells were proliferating normally; they were dividing without significant number of death cells. The cells were not migrating within the frame and we saw normal fast movement of filopodia. Nucleus with nucleoli was clearly visible in majority of cells; there were no multinucleated cells.

Figure 73: Time lapse images of L929 cells incubated with Si-NCs after a) 2 hours, b) 20 hours, c) 40 hours, d) 60 hours.

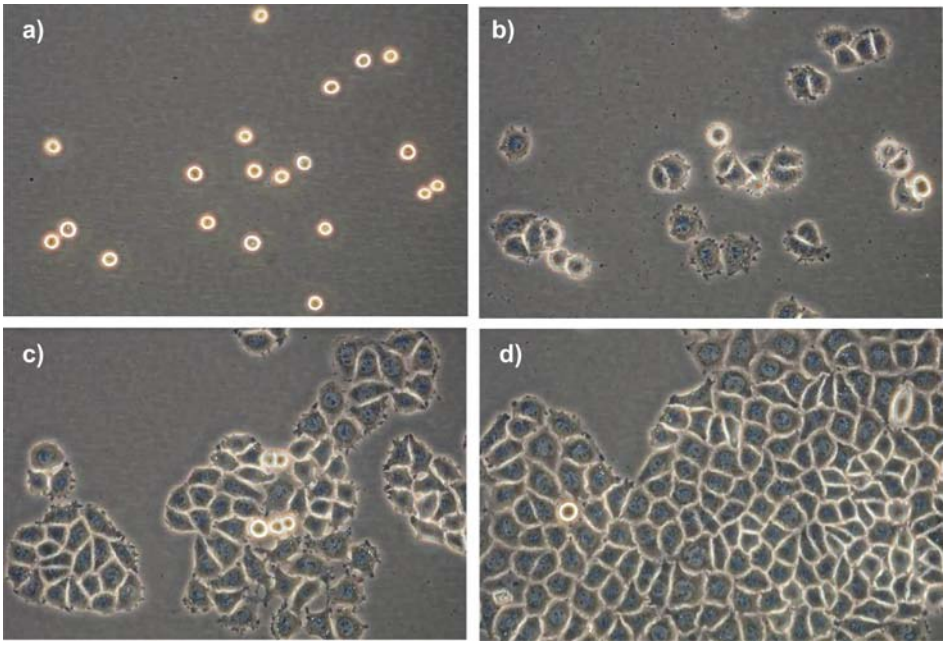

Comments (to the video file 4.6.2. L929-Si-NCs): Cells did not settle down immediately, however they did not undergo necrosis or apoptosis. In the first 24 hours they were unusually small compared to the control sample. After the adaptation time (around 20-24 hours – at which time we already had second generation of cells), the cells proliferated normally as the control sample (*Fig. 72*). We observed small objects in the medium; the objects were probably Si-NCs coated by components from the nutrient medium.

Figure 74: Time lapse images of L929 cells incubated with CQD a) after 2 hours, b) after 20 hours.

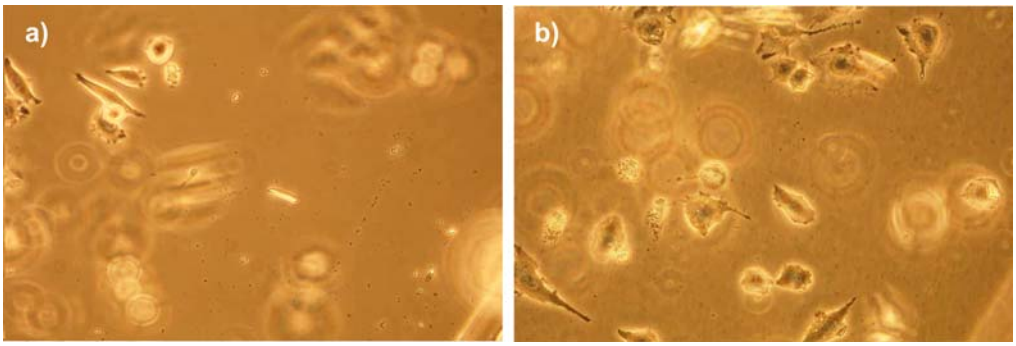

Comments (to the video file 4.6.2. L929-CQD): In this case we had problems with image focusing (in all 4 experiments); however, it is clear from the video that cells tend to migrate around the glass coverslip and had extremely long filopodia. About 20 % of observed cells within the video frame died within the first 15 hours. Cells divided and after the division they migrated rapidly around the surface. The video shows that cells were under extremely high stress and in an environment unfavorable for normal proliferation.

Figure 75: Time lapse images of L929 cells incubated with ND after a) 2 hours, b) 20 hours, c) 40 hours, d) 60 hours.

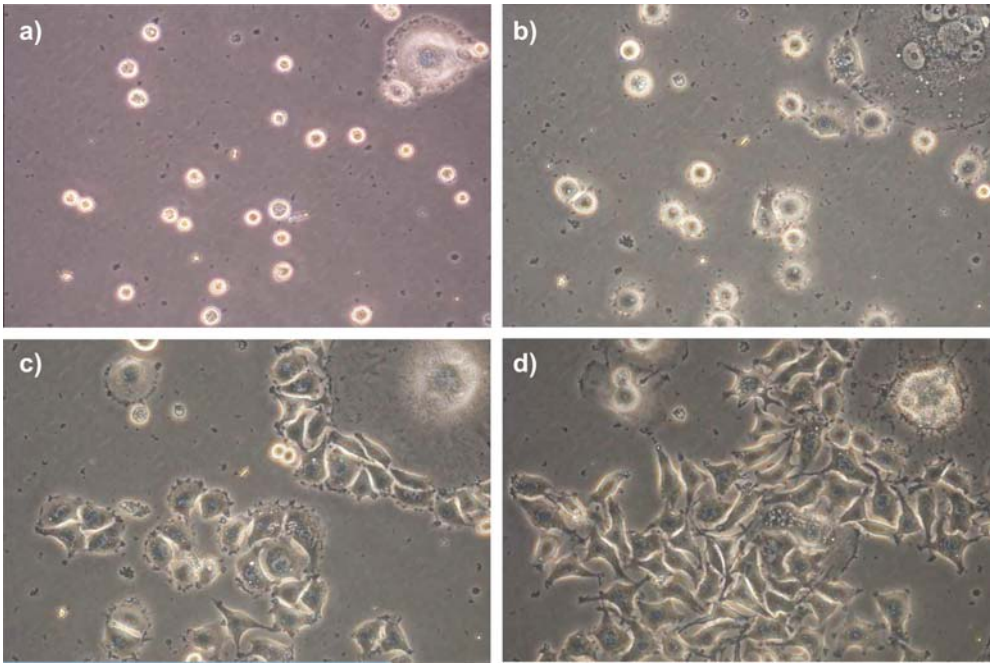

Comments (to the video file 4.6.2. L929-ND): From the start we observed high number of small object floating in the nutrient medium, probably ND particles covered by components of the medium. Again the cells stayed unusually long in the round form and it took more than 20 hours until they fully attached to the glass coverslip. We observed normal filopodia after this adaption time and cells divided normally and had normal size. During the whole observation time only about 4 % of cells died.

Figure 76: Time lapse images of L929 cells incubated on A-ND after a) 2 hours, b) 20 hours, c) 40 hours, d) 60 hours.

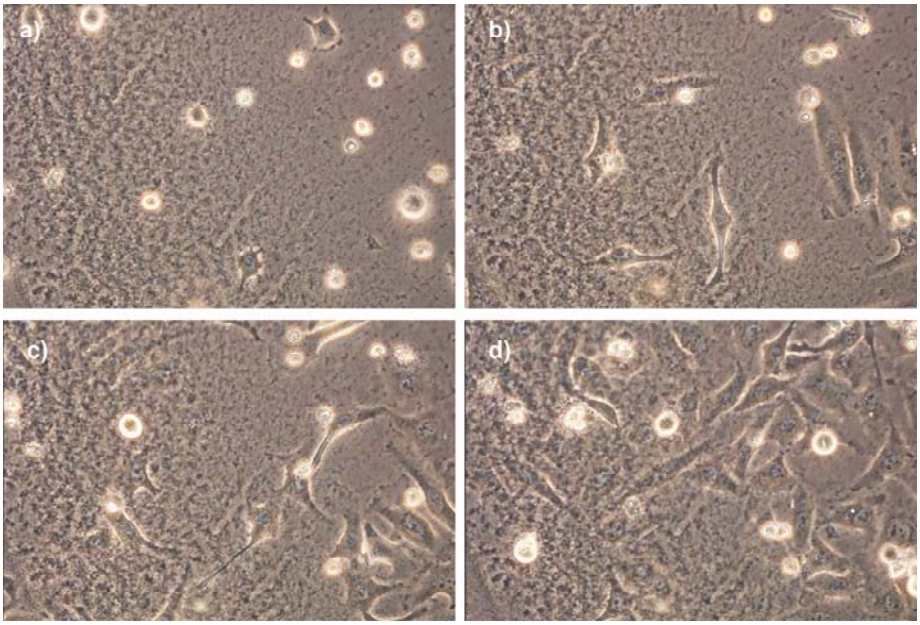

Comments (to the video file 4.6.2. L929-A-ND): Different setup was used: the nanomaterial (A-ND) was put in a droplet on a glass coverslip, let to dry and the cells were plated on it, because normal procedure (adding material directly to the medium after the cell passage) induced very fast death of cells. About 40 % of cells died within the first 3 hours, and the cells continued to die at a 10 % rate of the dead-to- living cells. After about 50 hours the cells started to undergo cell death in high numbers and we observed small object floating in the nutrient medium, most probably parts of dead cells and A-ND. Cells were unusually stretched in one direction with extremely long filopodia and they migrated rapidly around the surface. The percentage of dividing cells was lower than in the control sample as counted from the videos. The cytokinesis was extremely long (that could mean that the signals from outside of the cell were not favorable for cell division), about half of the cells in this phase undergo cell death. Although the cells were still alive, it is clear that they were under big stress caused by presence of A-ND.

Table 12: Parameters of cell proliferation for samples incubated with various nanomaterials.

Sample	Time of first cells spreading [hours]	Average percentage of cell divisions in first 24 hours [%]	Time of first cell division [hours]	Doubling time [hours]
Control	2.5 ± 0.5	22 ± 2	3 ± 1	15 ± 2
Si-NCs	3.0 ± 0.5	16 ± 2	4 ± 1	20 ± 2
CQD	2.7 ± 0.5	15 ± 2	4 ± 1	not available
ND	2.5 ± 0.5	18 ± 2	6 ± 1	not available
M-Si	3.5 ± 0.5	22 ± 2	5 ± 1	18 ± 2
A-ND*	3.0 ± 0.5	14 ± 2	4 ± 1	30 ± 2

Note: All data were counted from analysis of time lapse videos.
A-ND* different experimental setup due to fast cell death in normal setup

In conclusion we need to keep in mind that these samples were exposed to light compared to other biological experiments, this may influence the results. From the analysis of video

sequences it is clear, that cells had to adapt to presence of nanomaterials. The adaptation time was from a few hours up to 20-24 hours (one generation of cells). The longest adaptation time (when cells are strongly influenced by stress from environment), with significant death rate, was observed for cells incubated in presence of A-ND; in this case also another phases of cell life were significantly prolonged (cell division) and the cells continued to die during the incubation. The cells incubated with CQD did not proliferate well compared to control sample, but better than cells incubated with A-ND (due to technical difficulties we have not been able to obtain a good video sharpness). Cells did adapt relatively fast for samples incubated with M-Si. From videos it is clear that cells did endocytosed the M-Si crystals, and when the cell divided. Both new cells inherited the nanomaterial accumulated in the original cell (bright spots in videos). In case of incubation with Si-NCs, the cells did not settle down immediately, but there was adaptation time (up to 20 hours) after which they proliferate normally. It must be noted that used concentration of nanomaterial is at least 100 times higher than planed concentration in real experimental use. Although we observed accumulation of nanomaterial within the cells they proliferated quite normally and the nanomaterial was not causing significant stress for the cells. For cells incubated with ND, filaments were shorter compared to the control sample incubated without any nanomaterial and cells needed one generation to adapt to the new environment (presence of ND).

4.7 Optical microscopy

4.7.1 Giemsa-Romanowski staining of cells

Giemsa-Romanowski stain (G-R) is a mixture of eosin for staining cytoplasm and methylene blue for staining DNA and RNA containing organelles. This stain is mainly used for histological samples. The May-Grünwald (M-G) stain which has composition similar to G-R stain, was used for our cells to check if there was any bacterial infection.

Cell samples were incubated in the 24-wells plate with a cover glass slip on the bottom of each well. The samples were washed twice with phosphate buffer (PBS) after incubation with nanomaterials, and then dipped for 10 minutes in methanol and acetic acid (in ratio 3:1) to fix the cells. Then the cells with nanomaterials were again washed twice with PBS. The stock solution of M-G stain was filtered through cotton and then 10 µl of it was added to cells in each sample well for 5 minutes; afterwards the cells were washed with distilled water.
Stock solution of G-R stain was diluted in distilled water in 1:13 ratio and 0.5 ml of this solution was added to each sample well for 7 minutes. Then the sample was washed three times with distilled water. Samples were converted from water solution to xylene in five steps. The sample was transferred sequentially from one solution to the next one; the solutions were: acetone, acetone – xylene (1:1), acetone – xylene (1:2), acetone – xylene (1:4), xylene. Samples remained in each solution for 5 minutes. Then we prepared permanent specimens from our samples by fixing them to a glass slide with Canadian balsam.

4.7.2 Optical microscopy with Giemsa-Romanowski staining of cells

HeLa cells were incubated for 24 hours, and then nanomaterials were added to the cell culture and incubated for another 16 hours. After this incubation the cell samples were stained with G-R and M-G stain as described in section 4.7.1. With this stain we obtained initial information which that led to further investigation of nanomaterial influence on cells.

The concentrations of nanomaterials in 1 ml of nutrient media were as follows: M-Si 4 μg/ml, ND 4 μg/ml, A-ND 4 μg/ml, CQD 4 μg/ml, Si-NCs 4 μg/ml.

The fixed cell samples with nanomaterials were studied with optical microscope (Olympus C-8AC) with the oil-immersion objective 100x/1.25 and with 40x/0.66 objective. The pictures were recorded with Olympus C-7070 camera (7.1 megapixels). The cells incubated with various nanomaterials are displayed in *Fig. 77-82*.

Figure 77: Control sample of HeLa cells incubated without any nanomaterial, imaged with objective lenses: a) 40x (the scale bar is 20 μm), b) 100x (scale 10 μm).

a) b)

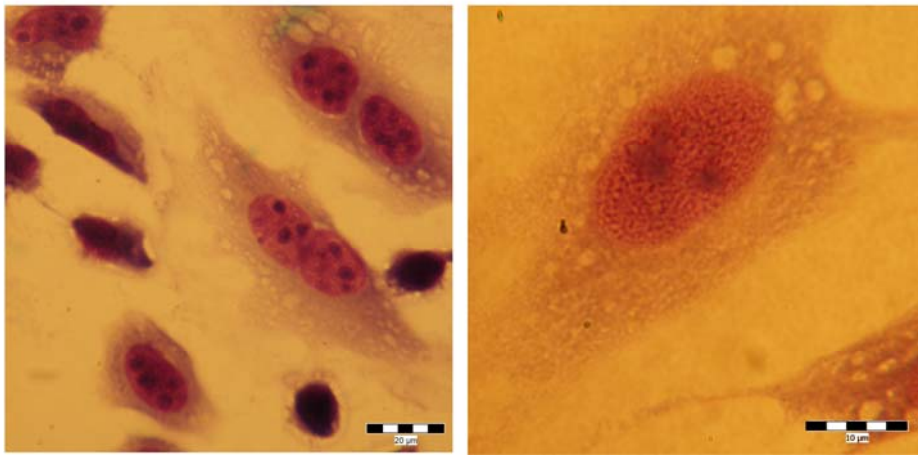

Comments: The cells had proper size with visible nucleus and nucleoli and the cytoplasm was without significant damage.

Figure 78: HeLa cells incubated with Si-NCs, imaged with objective lenses: a) 40x (scale bar 20 μm), b) 100x (scale 10 μm).

a) b)

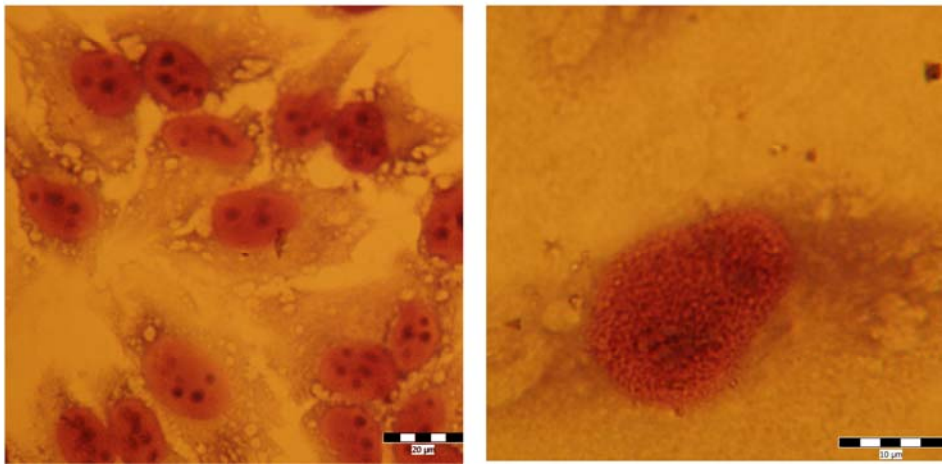

Comments: All images are well comparable with the control sample, revealing proper cell size, visible nucleus and nucleoli and the cytoplasm without significant changes.

Figure 79: HeLa cells incubated with CQD, imaged with objective lenses: a) 40x (scale 20 µm), b) 100x (scale 10 µm).

a) b)

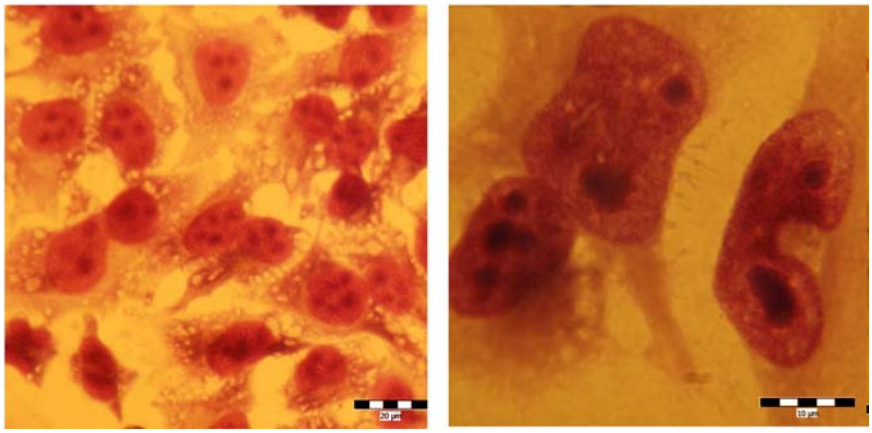

Comments: The cells were a bit smaller compared to the control sample. The nucleus and nucleoli were nicely visible, but they did not have clear round shape. Cytoplasm area seemed to be slightly smaller with respect to nucleus compared with the control sample.

Figure 80: HeLa cells incubated with ND, imaged with objective lenses: a) 40x (scale 20 µm), b) 100x (scale 10 µm).

a) b)

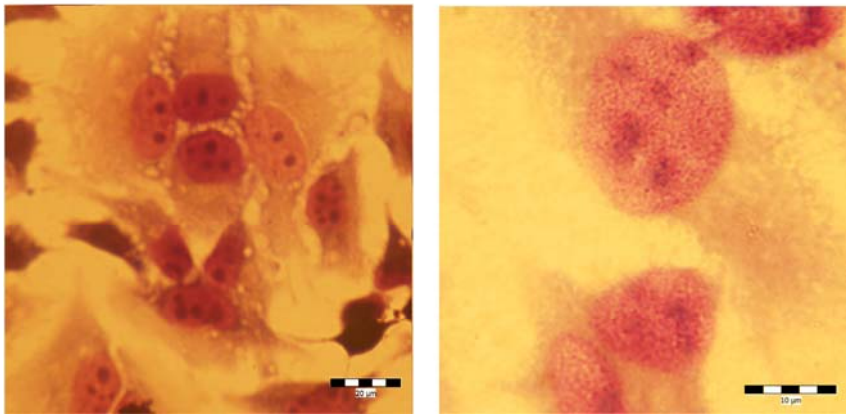

Comments: The cells had proper size, nucleus and nucleoli were nicely visible; the border between nucleus and cytoplasm was not delimited clearly. The cytoplasm looked normal.

Figure 81: HeLa cells incubated with A-ND, imaged with objective lenses: a) 40x (scale 20 µm), b) 100x (scale 10 µm).

a) b)

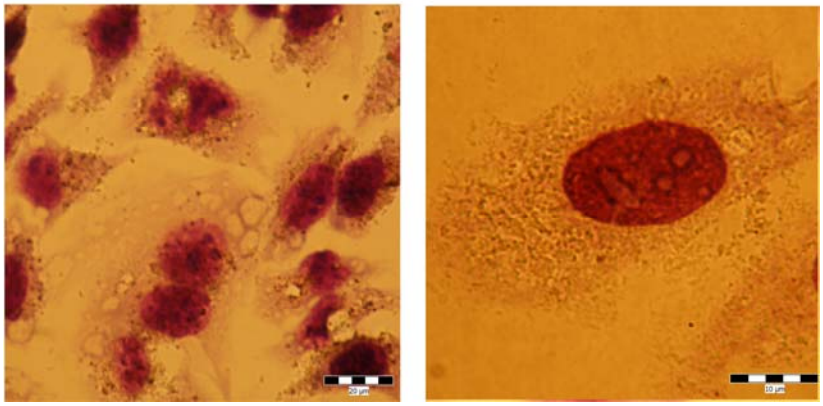

Comments: The cells had proper size and A-NDs were clearly visible in the cell as brown dots. The nucleus seemed to be damaged and nucleoli were not clearly visible. We did no observe smooth structure of cytoplasm, but rather a granular structure presumably with A-NDs in it (brown round dots).

Figure 82: HeLa cells incubated with M-Si, imaged with objective lenses: a) 40x (scale 20 μm), b) 100x (scale 10 μm).

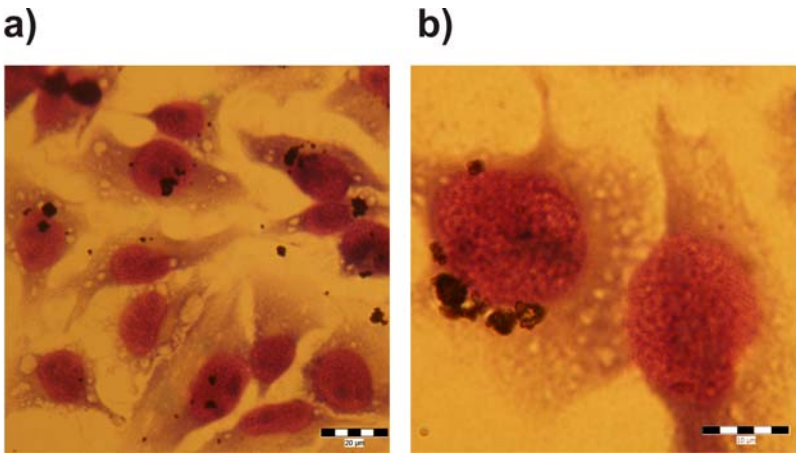

Comments: The cells had proper size. M-Si were clearly visible in the cell as black-brown dots. The nucleus was clearly visible but not the nucleoli. Although we observed M-Si in the cytoplasm and on the cell, the cytoplasm did not seem to be strongly influenced by presence of this nanomaterial.

In conclusion the sample of HeLa cells incubated with Si-NCs was the most similar to the control sample in all observed parameters. The shape and structure of nucleus was negatively influenced by presence of CQD or A-ND in the cell culture. Additionally, for cells incubated in presence of ND, the nucleoli were not visible at all. Cytoplasm was negatively influenced by presence of A-ND in the nutrient media; we observed a lot of A-ND with rips of cytoplasm between them with naked eye through the microscope. We also observed some big (Si) crystals in case of cells incubated with M-Si, but the cytoplasm seemed mostly unharmed. Even though we observed some M-Si inside cells, the cells seemed to proliferate quite well. Bacterial infection was not proved in any of the samples and, therefore, the observed responses of cell culture to presence of nanomaterials in nutrient media were assigned to the nanomaterials, although the negative effects of fixation may play minor role in observed damage of cells.

4.8 Laser-scanning confocal fluorescence microscopy

4.8.1 Experimental setup

Confocal microscopy enables us to study cells incubated with nanomaterials at better optical resolution and contrast compared to common (wide-field) fluorescence microscopy. The illumination and detection in a confocal microscope is done through a spatial pinhole (placed in an image plane) that nearly eliminates light coming from points out of the focal plane. The 3-D image can be obtained by combination of many 2-D images (cross-sections) detected by shifting the focal plane in Z-axis. In principle, the acquisition of an image with a laser-scanning confocal microscope takes longer time compared to a classical (wide-field) microscope, because the light is collected from each point in sequence. When we make prolonged observations or detailed Z-scans (series of 2-D images with different focus along the z-axis) of the cell, we need to take into account the limited photostability of stains or dyes; therefore, we have to either decrease the excitation intensity or shorten the signal accumulations time. The cells should be alive during the experiment as we want to observe nanomaterials entering the cell and other possible interactions of nanomaterials and cells. However, such living cells are moving so the experiment duration must be minimized. We can for example restrict the observed or use wider pinhole and detector slit in combination with shorter acquisition time.

Figure 83: Scanning confocal microscope setup for fluorescence microscopy, a) overview of whole setup, b) incubation chamber with microscope. Parameters of apparature are described below.

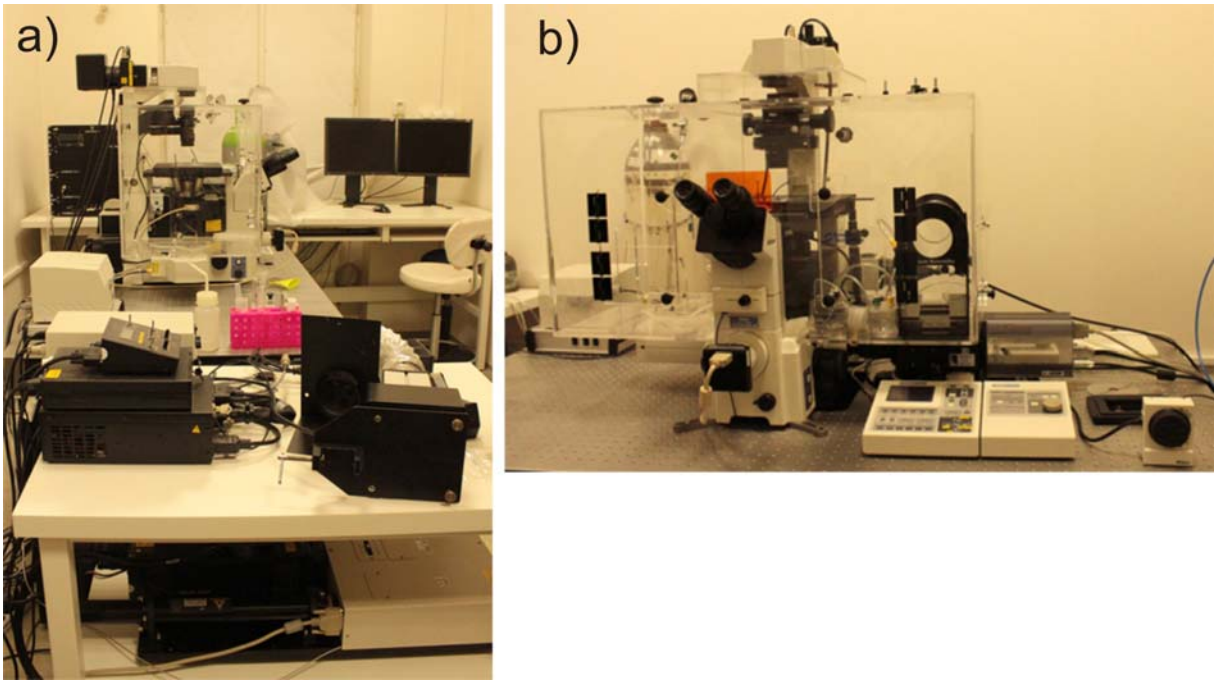

Our study was performed with a scanning confocal microscope (TE200E C1si, Nikon) using the 60x/1.49 oil-immersion objective with the total-internal reflection illumination (Apo TIRF, Nikon). The setup is shown in *Fig. 83*.The excitation of samples was done by a set of lasers: 405 nm (for all nanomaterials) and 488 nm (for actin structures in cell). The signal was detected by a CCD camera (CCD-1300, Vosskuhler). We use the dichroic mirror 405/488/543 nm with the band-pass filters (exciters) 450+/-15nm; 515+/-15nm. The spectral detection has 32 channels within 400-750 nm detection range and 2.5/5/10 nm resolution band-pass. A linear un-mixing algorithm based on the single value decomposition method is used to disentangle spectra. The microscope is equiped with a sample chamber which enables a temperature and atmosphere control (37°C, 5 % CO_2).

4.8.2 Sample preparation

We used SAOS-2 cells incubated in a standard nutrient medium (see *Tab. 11*). We also made an experiment where the cells were kept in a nutrient medium without the fetal bovine serum to see the influence of protein corona on the studied nanomaterials. The SAOS-2 cells were transfected with the pEYFP-N1/actin plasmid to see the fluorescently stained actin in living cells; the transfection is described in Appendices *Ap5*. These cells were incubated with various nanomaterials for various time intervals

SAOS-2 cells were incubated with two concentrations of Si-NCs or ND for times ranging from 10 minutes up to 30 hours. The concentrations were 7.5 µg/ml and 75 µg/ml of standard nutrient medium for SAOS-2 cells (see Tab. 11). After the first trial measurement we found out that single Si-NCs and ND were not observable under applied experimental conditions due to insufficient sensitivity of the microscope detection. We were able to observe only

agglomerates of Si-NCs (with estimated minimal content of ten Si-NCs) and only on a quartz slide (PL spectrum of such agglomerate is shown in *Fig. 21*). Then we decided to use a mixture of unfiltered Si-NCs (containing particles from single nanocrystals up to about 200-nm big agglomerates) and a mixture of ND and A-ND. Such aggregates of nanomaterials, could be formed from single nanoparticles inside a living body, not only in cells, but also in various organs of a living organism. Aggregates of nanomaterials react differently than single Si-NC or ND and may have different (mostly worse) cytotoxic effects. By using mixture of variously agglomerated nanomaterials, we simulate the worst-case scenario which might happen in a living organism.

We also studied the interaction of nanomaterials (concentrations were the same as mentioned above) with SAOS-2 cells in nutrient medium without fetal bovine serum in order to observe if the bovine serum plays a crucial role in uptake of nanomaterials by cells. The cells can live in the medium without fetal bovine serum for 2-3 hours, after this time our results might be compromised by starvation of cells.

The PL intensity of CQD bleached out rapidly when we tried to measure them with confocal microscope, as they did also in our micro-spectroscopy studies; therefore, we did not study them by this technique.

4.8.3 SAOS-2 cells incubated with Si-NCs

SAOS-2 cells were plated 24h before Si-NCs addition and then immediately put under the microscope. Within the first 20 minutes we observed Si-NCs agglomerates falling on the cells by gravitational forces while small Si-NCs were kept in liquid by Brownian motion (we observed them only later). This was observed for all concentrations of nanomaterials incubated with cells in standard nutrient media and also in nutrient media without fetal bovine serum.

We made several sequences of Z-scans each with 150 nm steps (for explanation see *Fig. 84*). Selected cross-sections from the most important Z-scans are shown in this chapter (the whole Z-scans, in form of the GIF animations, are included on the DVD attached to this thesis).

Figure 84: Illustrative image of Z-scan technique. A to C different focus planes along the z-axis with precise distance between them. Color coding: green – cell, blue – glass.

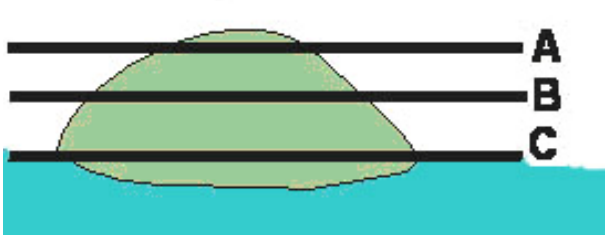

The fluorescence images from a control sample incubated without any nanomaterial are displayed in *Fig. 85*. The fluorescence images of SAOS-2 cells incubated for 2.5 hours with Si-NCs with concentration 7.5 µg/ml of nutrient medium are displayed in *Fig. 86* and for 10x higher concentration 75 µg/ml in *Fig. 87*. The SAOS-2 cells incubated for 24 hours with Si-NCs are displayed in *Fig. 88* and *Fig. 89*, for lower and higher concentrations, respectively. SAOS-2 cells incubated with Si-NCs with concentration 75 µg/ml of nutrient medium without fetal bovine serum after 1 hour long incubation are shown in *Fig. 90*.

Figure 85: Representative SAOS-2 cell incubated without any nanomaterial for 2 hours. a)-c) cross-sections of the cell with 1050 nm distance between each two images in the Z-axis. Green colour indicates actin. Image size 46.7x51.3 μm, scale is 10 μm.

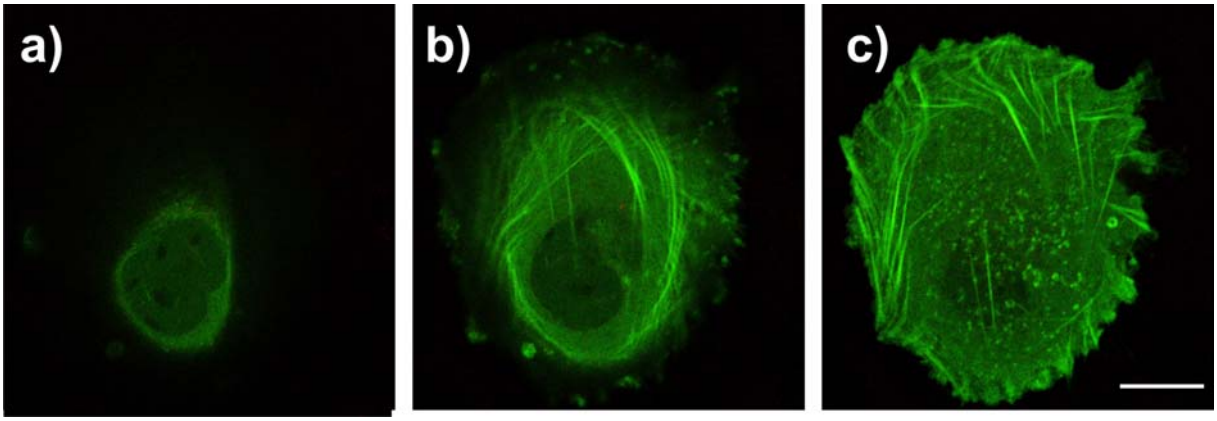

Comment: The actin structure was clearly visible and the size of the cell was normal.

Figure 86: Representative SAOS-2 cell incubated for 2.5 hour with Si-NCs (concentration 7.5 μg/ml). a)-c) cross-sections of the cell with 1050 nm Z-distance between the images, d) vertical cross-section of the cell, e) Blue line indicates position of the vertical cross-section shown in panel d). Colour coding: Green – actin, red – Si-NCs. Image size 44.8x71.1 μm, scale is 10 μm.

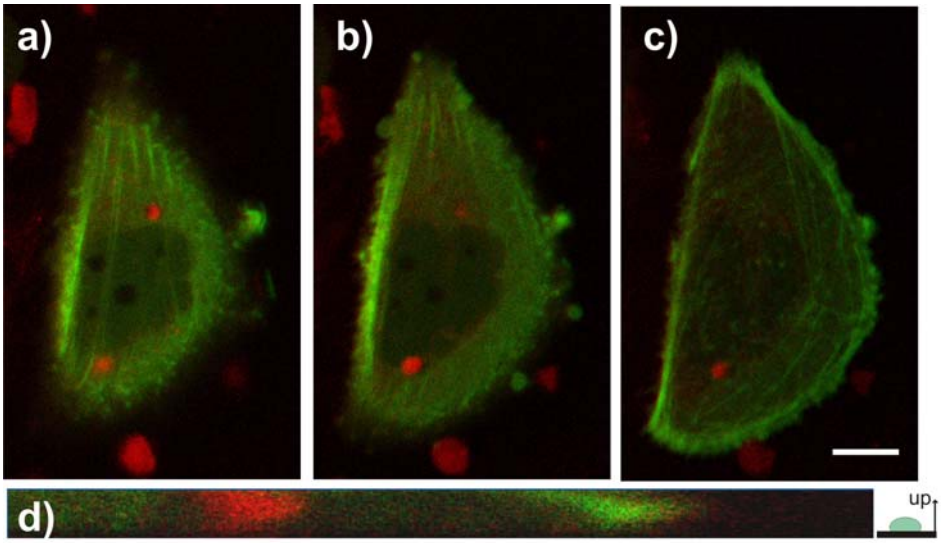

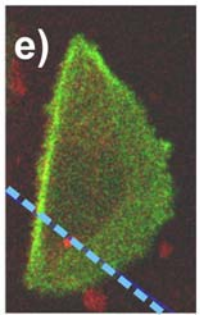

Comments: We observed Si-NCs agglomerates in the SAOS-2 cell (see cross-sections in *Fig. 86a)-c)*). We proved that this agglomerates were internalized in the cell by a vertical cross-section of the cell (see *Fig. 86d*)).

The actin filaments were clearly visible without any significant damage as in the control sample (see *Fig. 85*). Other cells from the same experiment in close time of incubation with Si-NCs were comparable to control cells.

Figure 87: Representative SAOS-2 cell incubated for 2.5 hour with Si-NCs (concentration 75 μg/ml). a)-c) cross-sections of the cell with 1050 nm Z-distance between the images, d) vertical cross-section of the cell, e) Blue line indicates position of the vertical cross-section shown in d). Colour coding:Green – actin, red – Si-NCs. Image size 78.1x103.1 μm, scale is 10 μm.

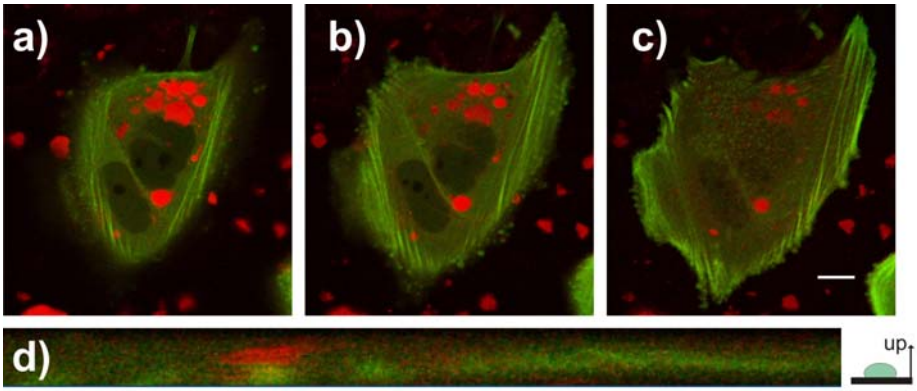

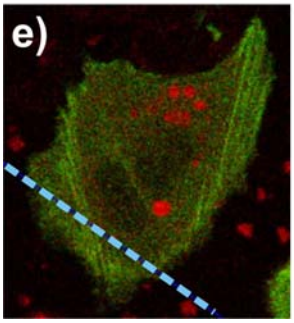

Comments: In this case we observed many Si-NCs agglomerates in the horizontal cross-sections of the SAOS-2 (*Fig. 87a)-c)*). We proved that those agglomerates were in the internal environment of cell by a vertical cross-section of the cell (*Fig. 87d)*). The actin filaments were clearly visible without significant damage as in the control sample despite the enormous number of Si-NCs in the cell. Other cells from the same experiment in close time of incubation with Si-NCs were comparable in the same way to control cells.

Figure 88: Representative SAOS-2 cell incubated for 24 hours with Si-NCs (concentration 7.5 μg/ml). a)-c) cross-sections of the cell with 1050 nm Z-distance between the images, d) vertical cross-section of the cell, e) Blue line indicates position of the vertical cross-section shown in d). Colour coding: Green – actin, red – Si-NCs. Image size 50.1x75.3 μm, scale is 10 μm.

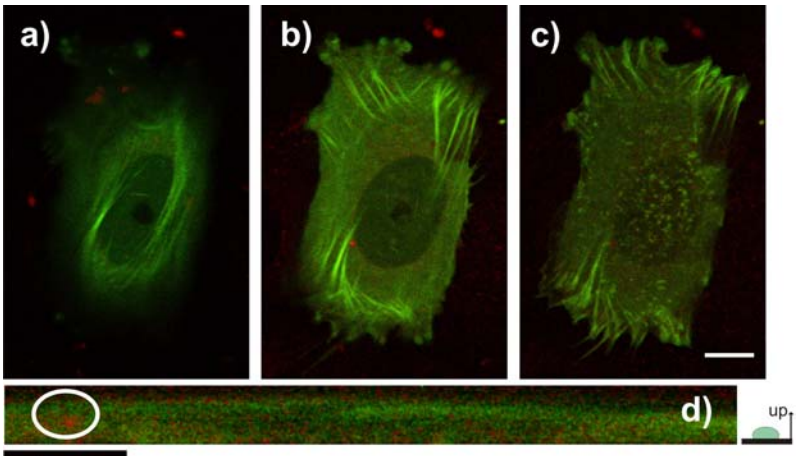

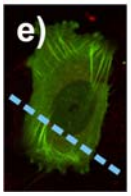

Comments: For this SAOS-2 cell we observed a few Si-NCs agglomerates in the cross-sections (*88a)-c)*), some of them were on the cell and (as shown in *Fig. 88d*) and other inside the cell. The actin filaments were clearly visible as in the SAOS cell incubated without any nanomaterial. Other cells from the same experiment in close time of incubation with Si-NCs were comparable to control cells.

Figure 89: Representative SAOS-2 cell incubated for 24 hours with Si-NCs (concentration 75 μg/ml). a)-c) cross-sections of the cell with 1050 nm Z-distance between the images, d) vertical cross-section of the cell, e) Blue line indicates position of the vertical cross-section shown in d). Colour coding: Green – actin, red – Si-NCs. Image size 67.1x57.2 μm, scale is 10 μm.

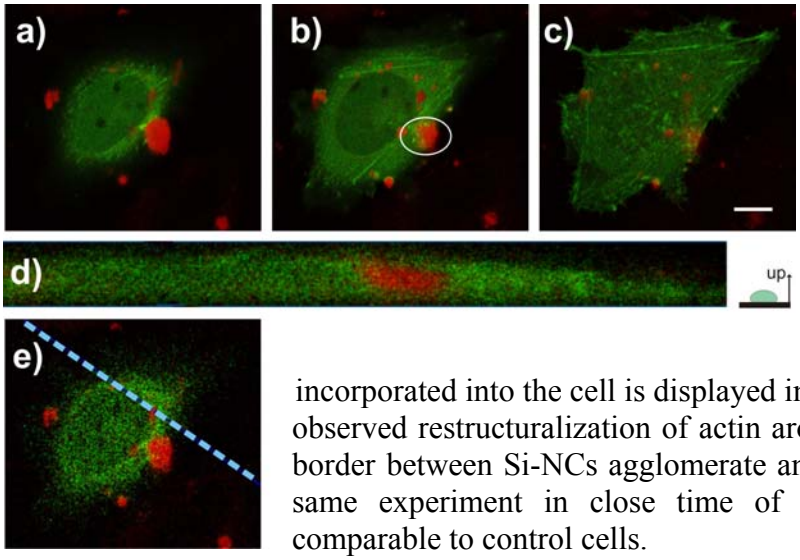

Comments: The cell had normal clearly visible actin filaments without any significant changes. Majority of the Si-NCs were found inside the cell (see the vertical cross-section in *Fig. 89d)*. An interesting example of a Si-NCs agglomerate just being incorporated into the cell is displayed in *Fig. 89b*) in white circle ; we observed restructuralization of actin around the Si-NCs particle on the border between Si-NCs agglomerate and the cell. Other cells from the same experiment in close time of incubation with Si-NCs were comparable to control cells.

Figure 90: Representative SAOS-2 cell incubated for 1 hour with Si-NCs (concentration 75 μg/ml in nutrient medium without fetal bovine serum). a)-c) cross-sections of the cell with 1050 nm Z-distance between the images, d) vertical cross-section of the cell, e) Blue line indicates position of the vertical cross-section shown in d). Colour coding: Green – actin, red – Si-NCs. Image size 57.9x57.9 μm, scale is 10 μm.

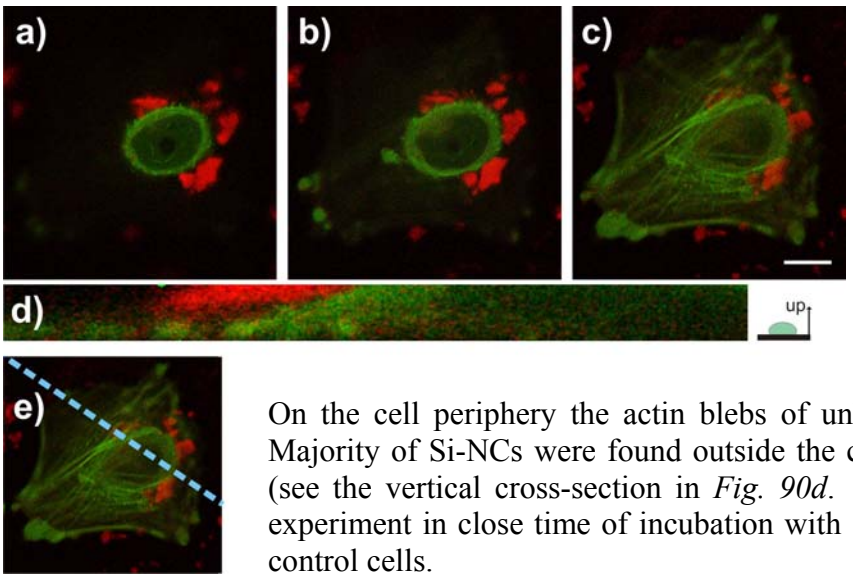

Comments: The cells in this time period of incubation had normal shape and size, actin filaments were clearly visible. Moreover this representative cell had actin ring around the nucleus.
On the cell periphery the actin blebs of unknown origin were visible. Majority of Si-NCs were found outside the cell sitting on its membrane (see the vertical cross-section in *Fig. 90d*. Other cells from the same experiment in close time of incubation with Si-NCs were comparable to control cells.

In conclusion the Si-NCs, even in form of very big agglomerates (20 Si-NCs and more), entered rapidly inside SAOS-2 cells (in case of incubation in the standard nutrient medium). However in medium without fetal bovine serum the big Si-NCs agglomerates stayed on the outer side of cell membrane, just touching the membrane. Smaller Si-NCs agglomerates penetrate into the cell after 3 hours of incubation (data not shown). This significant difference

indicates that Si-NCs are interacting with proteins and amino acids present in the bovine serum; the Si-NCs get covered with them and that eases entering in the cell.

In order to prove this model we made a mixture of around 80μg Si-NCs in 1 ml of bovine serum and this mixture was kept in a fridge (at 4°C). This experiment was done in low temperature in order to exclude possible contaminations. Two phases of suspension were formed within 24 hours: The upper phase was watery and clear, while the lower one was white consisting of agglomerated proteins. A droplet from each phase was observed under fluorescence microscope. Most of Si-NCs were in the lower protein containing phase but there were practically none in the upper phase (data not shown). This strengthens our hypothesis that Si-NCs are covered by proteins from fetal bovine serum.

We did not observe significant changes in actin structure for Si-NCs concentration of 7.5 μg/ml in any experiment (the longest was 28 hours). The cells in this time period of incubation had normal shape and size, actin filaments were clearly visible. In case of of cells incubated in media without fetal bovine serum representative cell had actin ring around the nucleus (see *Fig. 90*). On the cell periphery the actin blebs of unknown origin are visible. In case of higher concentration of 75 μg/ml, we observed only some small changes after 24 hours of incubation. In these experiments we detected small zones in cells with higher concentration of actin and a Si-NC was usually found in the middle of this actin zone. Otherwise the cell looked normally without any structural change.

4.8.4 SAOS-2 cells incubated with ND

Mixture of ND (8 nm) and A-ND (up to 450 nm) was added to the SAOS-2 cell sample pre-incubated for 24 hours under standard conditions and immediately transferred under the microscope. The small NDs maintained in liquid by Brownian motion and we observed them only later. Within the first 5-20 minutes we observed A-ND falling on the cell as a result of gravitational forces. This was observed for all concentrations of nanomaterials incubated with cells in standard nutrient medium and also in medium without fetal bovine serum.

We made sequences of Z-scans (focal plane cross-sections of the cell spanning the Z-axis with 150 nm steps) following consecutively after each other (from 15 up to 30). Selected cross-sections from the most important Z-scans are shown below in this chapter (the whole Z-scans, also in form of GIF animation, are included on the DVD attached to this thesis).

The fluorescence images of control SAOS-2 cells sample incubated without any nanomaterial are displayed in *Fig. 85*. The fluorescence images of SAOS-2 cells incubated for 3 hours with nanodiamonds with concentration 7.5 μg/ml in nutrient medium are displayed in *Fig. 91* and with concentration 75 μg/ml in nutrient medium after the same time of incubation in *Fig. 92*. The florescent images of SAOS-2 cell culture incubated for 22 hours with nanodiamonds with concentration 7.5 μg/ml in nutrient medium are displayed in *Fig. 93* and with concentration 75 μg/ml in standard nutrient medium in *Fig. 94*. SAOS-2 cells incubated for 1 hour with nanodiamonds with concentration 75 μg/ml in nutrient medium without fetal bovine serum are shown in *Fig. 95*.

Figure 91: Representative SAOS-2 cell incubated for 3 hours with nanodiamonds (concentration 7.5 μg/ml). a)-c) cross-sections of the cell with 1050 nm Z-distance between the images, d) vertical cross-section of the cell, e) blue line indicates position of the vertical cross-section shown in d). Colour coding: Green – actin, blue – nanodiamonds. Image size 61.9x43.1 μm, scale is 10 μm.

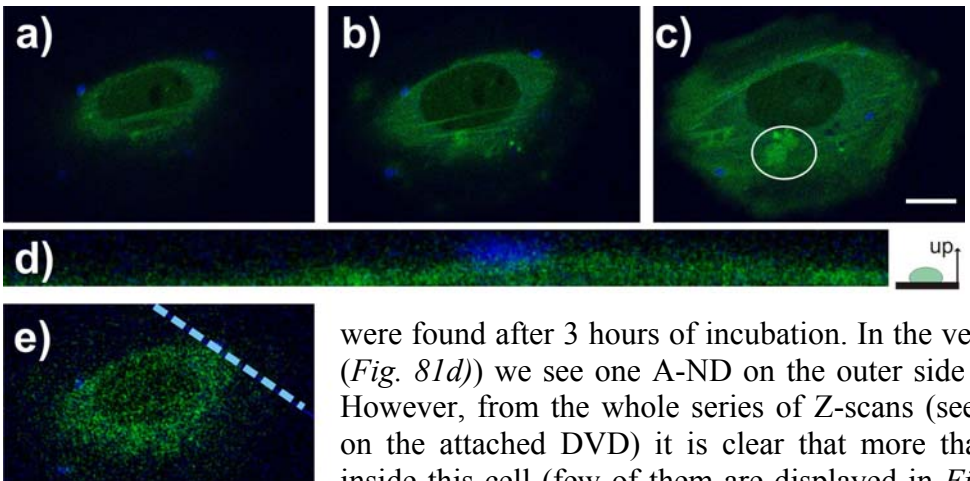

Comments: The size and shape of the cell were normal, as in the control sample (see *Fig. 85*). The first A-NDs inside the cell were found after 3 hours of incubation. In the vertical cross-section (*Fig. 81d)*) we see one A-ND on the outer side of cell membrane. However, from the whole series of Z-scans (see the gif animation on the attached DVD) it is clear that more than one A-ND was inside this cell (few of them are displayed in *Fig. 91b)*). We also observed accumulation of actin, intensive green spots (*Fig. 91c)* in ring); these were localized only in close proximity of A-ND. Except these anomalies, the actin structure looked normal for this duration of incubation.

Figure 92: Representative SAOS-2 cell incubated for 3 hours with nanodiamonds (concentration 75 μg/ml). a)-c) cross-sections of the cell with 1050 nm Z-distance between the images, d) vertical cross-section of the cell, e) blue line indicates position of the vertical cross-section shown in d). Colour coding: Green – actin, blue – nanodiamonds. Image size 65.6x67.7 μm, scale is 10 μm.

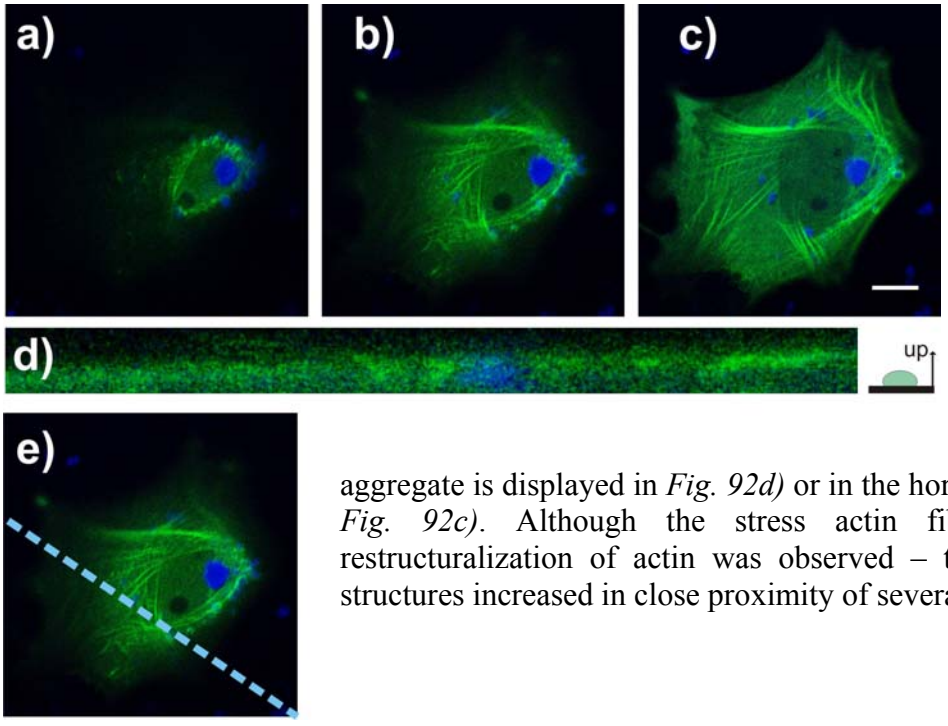

Comments: The size and shape of the cell was normal (similar to the control sample incubated without any nanomaterial). We observed plenty of A-ND in the cell as can be seen in the vertical cross-section (an aggregate is displayed in *Fig. 92d)* or in the horizontal cross-section *Fig. 92c)*. Although the stress actin fibers were visible, restructuralization of actin was observed – the density of actin structures increased in close proximity of several A-ND.

Figure 93: Representative SAOS-2 cell incubated for 22 hours with nanodiamonds (concentration 7.5 μg/ml). a)-c) cross-sections of the cell with 1050 nm Z-distance between the images, d) vertical cross-section of the cell, e) blue line indicates position of the vertical cross-section shown in d). Colour coding: Green – actin, blue – nanodiamonds. Image size 58.4x66.6 μm, scale is 10 μm.

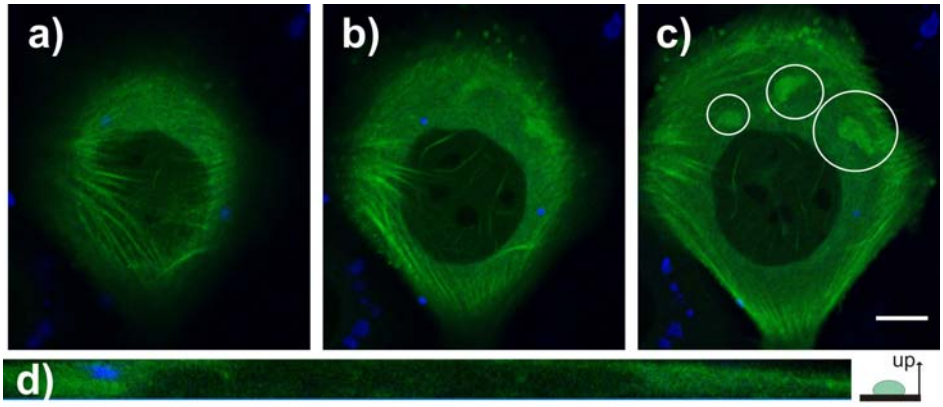

Comments: The cells in this time of incubation were slightly smaller than the cells in the control sample and also the shape was more rounded. We observed many A-ND inside the cell (see the vertical cross-section in panel d) or in the horizontal cross-section, panels b and c). Although the cell still kept its integrity, actin stress fibers were apparent, many areas of unorganized actin were present (as can be clearly seen in *Fig. 93b)* and *93c)* – in white rings). The number of those areas increased in time.

Figure 94: Representative SAOS-2 cell incubated for 22 hours with nanodiamonds (concentration 75 μg/ml). a)-c) cross-sections of the cell with 1050 nm Z-distance between the images, d) vertical cross-section of the cell, e) blue line indicates position of the vertical cross-section shown in d). Colour coding: Green – actin, blue – nanodiamonds. Image size 68.5x49.6 μm, scale is 10 μm.

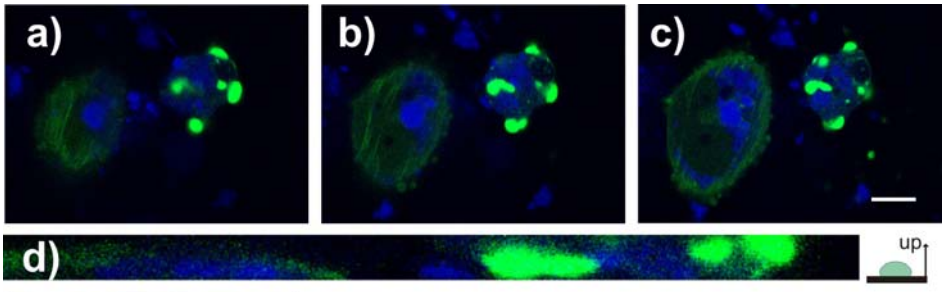

Comments: Two cells are shown in this figure. The one on the right side was already dead. An big aggregates of A-NDs was observed in the remains of this dead cell. The other cell was still living but smaller than the control cells. It was more shrunken than the well spread control cell. This effect was observed for majority of cells in this time period. There was almost no normal cell attached to the glass surface with normal filopodia. Most of A-ND was observed inside the cell and a bit less on the cell membrane as displayed in *Fig. 94d)* (the vertical cross-section). The actin structure was strongly affected by presence of A-NDs on the cell surface and also inside the cell. Other cells from the same experiment in close time of incubation were looking the same as this representative one.

Figure 95: Representative SAOS-2 cell incubated for 1 hour with nanodiamonds (concentration 75 µg/ml of nutrient medium without fetal bovine serum). a)-c) cross-sections of the cell with 1050 nm Z-distance between the images, d) vertical cross-section of the cell, e) blue line indicates position of the vertical cross-section shown in d). Colour coding: Green – actin, blue – nanodiamonds. Image size 65.1x69.4 µm, scale is 10 µm.

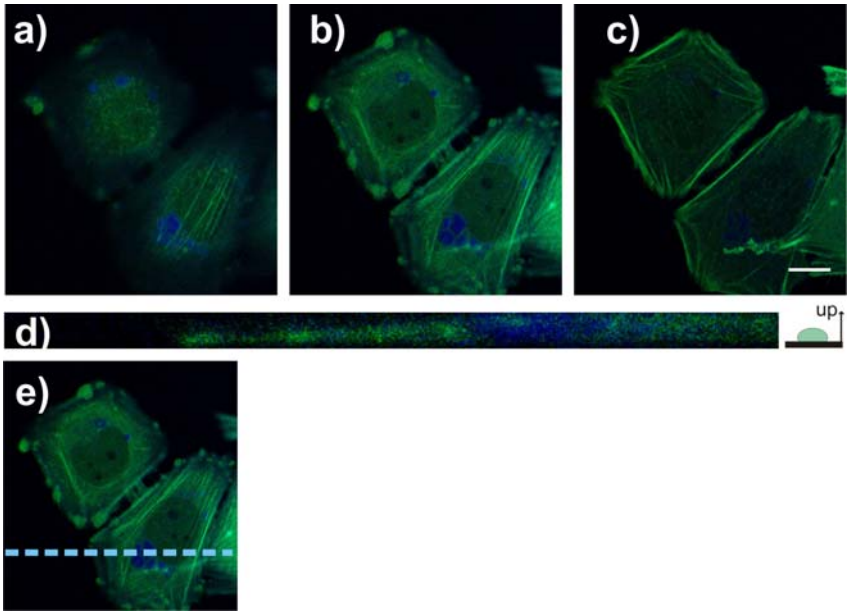

Comments: We observed fast integration of A-ND inside a cell even in case of cells incubated without fetal bovine serum. A-NDs were localized perinuclearly (this is clearly visible in the vertical cross-section, *Fig. 95d*) and in the horizontal cross-section in *Fig. 95b)*. The actin structure looked quite alike as in the control sample, with only slightly higher concentration on the borders of the cell. Majority of cells had normal size and shape as the control sample.

In conclusion A-NDs entered cells after longer incubation than Si-NCs. The first observed A-NDs in the cell was typically after 3 hours of incubation for cells incubated in standard medium. While for incubation in the medium without the fetal bovine serum, the first A-ND penetrated the cell after less than 1 hour. But in this case, we observed also a fast restructuralization of actin structure already after 3 hours of incubation. We propose that A-NDs might be driven to the cell by their charge and they were concentrated around the nucleus. The slower penetration of A-NDs into the cells incubated with bovine serum was in this light caused by a reaction of ND with the proteins and amino acids from the serum, which bound non-specifically to the A-ND surface and thus decreased the charge of A-ND.

The change of actin structure was observed after 8-10 hours of incubation for cells incubated with normal nutrient medium and with the highest ND concentration (data processed, not shown). A significant damage on the cell actin structure was observed after 24 hours of incubation with high concentration of ND, for lower concentration we observed a significant restructuralization of actin structures. We observed curled actin fibers with breaks instead of straight long fibers.

4.9 Micro-spectroscopy of nanomaterials in living cells

The micro-spectroscopy setup is described in Chapter 3.3.1. In this Chapter we study luminescence spectra of various nanomaterials (possibly single nanoparticle emitters) in living HeLa cells. Cells were incubated without nanomaterials for 24 hours, then nanomaterials were added and the cells were incubated with them for another 18 hours. The concentration was the same for each nanomaterial (ND, Si-NCs, and CQD), 8 μg/ml of standard nutrient medium for HeLa cells (for composition of the medium see *Tab. 11*). The cells were incubated with 2.5 ml of nutrient medium in Petri dishes (50x7mm), with a thin glass bottom to allow observation of the samples in a microscope directly, without further manipulation.

The micro-spectroscopy apparatus was not designed for measuring living cells so there is no possibility to control cell environment (i.e. there is room temperature and normal ~0.04% CO_2 concentration instead of 36.7 °C and 5% CO_2 preferred for cells incubation). The cells can survive under such conditions only about 30 minutes; after this time their metabolism slows down significantly and apoptosis begins. Therefore, we had limited time for measurements of micro-spectra as after 30 minutes the results might be compromised.

The main result of this chapter is the demonstration that we can distinguish PL signals from single luminescent nanoparticles within living cells in nutrient media. Cells had strong PL in the spectral region of 400-500 nm (sometimes called auto-fluorescence) and also the standard nutrient media were strongly luminescent in the 450-650 nm range. A PL spectrum of cells in standard nutrient medium is shown in *Fig. 96*.

Figure 96: Micro-PL spectrum of cells in nutrient media without any nanomaterial.

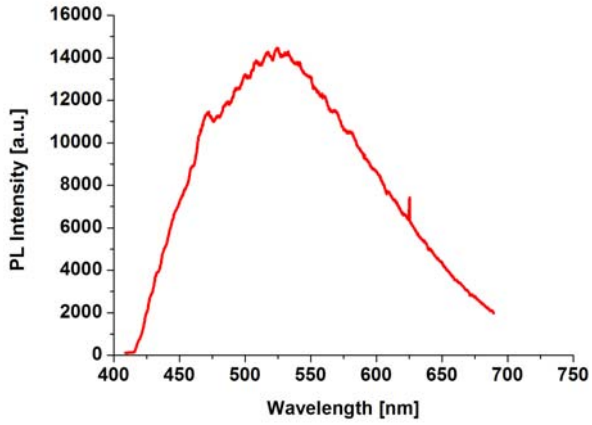

PL of small Si-NCs agglomerates within living cells was clearly visible by naked eye through the microscope. The single small nanocrystals were not visible to the naked eye, but we could detect them spectrally with use of the micro-spectroscopy apparatus. The procedure of the experiments was as follows: First, we found and focused a healthy cell in transmitted light (*Fig. 97a)*), then we took a fluorescence image of the cell under laser excitation (*Fig. 97b*)), and, finally, we took spectral image from a central vertical line (cross-section) of the cell image (*Fig. 97c*)). Luminescence spectra from single Si-NCs agglomerates (consisting of up to 10 nanocrystals, estimated from spectral shape and intensity) in the cell with subtracted background are shown in *Fig. 98*.

Images of HeLa cells incubated with CQD are shown in *Fig. 99* and spectra from CQD agglomerates are shown in *Fig. 100*. PL emission from big CQD aggregates within living cells was visible to the naked eye through the microscope. Images of HeLa cells incubated with ND are shown in *Fig. 101* and the spectrum from a ND agglomerate is shown in *Fig. 102*.

Figure 97: Images of HeLa cells incubated with Si-NCs (concentration 8 µg/ml) after 18 hours of incubation (images were taken with the micro-spectroscopy apparatus). a) transmission optical image of a living HeLa cell with Si-NCs, b) fluorescence image of the same HeLa cell with Si-NCs, c) spectral profile of a cross-section of the HeLa cell (lighter gray colour means higher intensity).

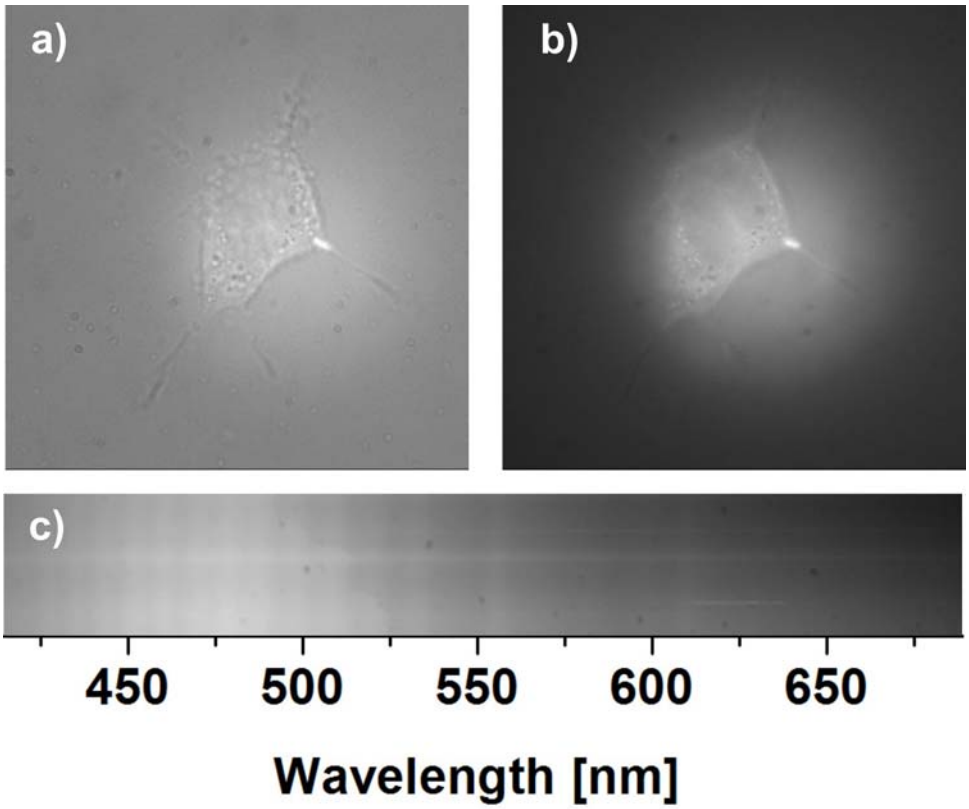

Comments: Agglomerates of Si-NCs were visible in the HeLa cell (very bright spots in *Fig. 97b*). A PL coming from a single Si-NCs with maximum around 600 nm is clearly resolvable on the right side of *Fig. 97c)*. The spectra from Si-NCs in the cell are displayed in *Fig. 98*. The images in full resolution are included on the DVD attached to this thesis.

Figure 98: Luminescence spectra from individual Si-NCs agglomerates (composed of at most 10 nanocrystals) from various spots in the HeLa cell.

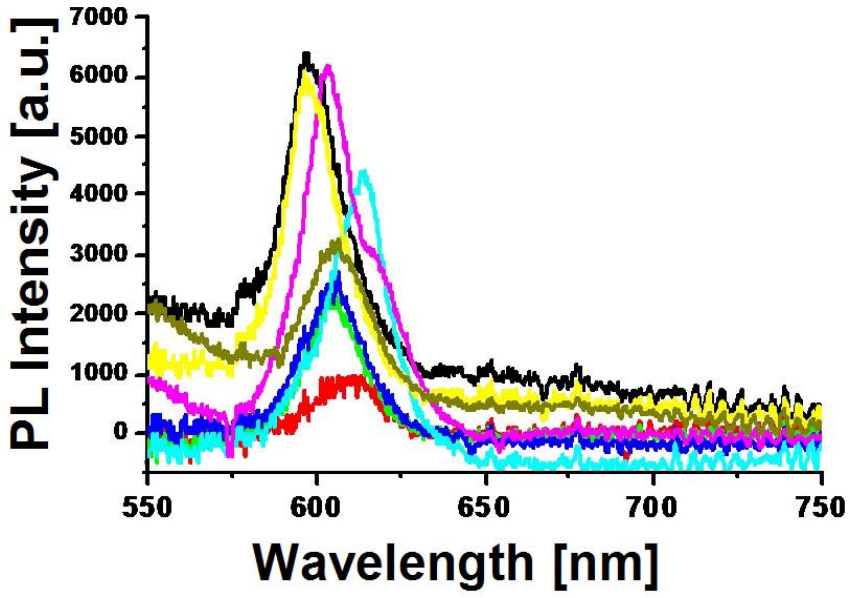

Comments: As we can see the PL peak position of Si-NCs spectra varied within certain range, this was either due to distribution of nanocrystals sizes or due to variable interaction of Si-NCs with surrounding cell environment.

Figure 99: Images of HeLa cells incubated with CQD (concentration 8 μg/ml) after 18 hours of incubation (images were taken with the micro-spectroscopy apparatus), a) transmission optical image of several living HeLa cells with CQD, b) fluorescence image of the HeLa cells with CQD, c) glass surface with CQD and without cells (b) and c) are images of the same cells from different focal planes), d) spectral profile of a vertical cross-section of the HeLa cell (lighter gray colour means higher intensity).

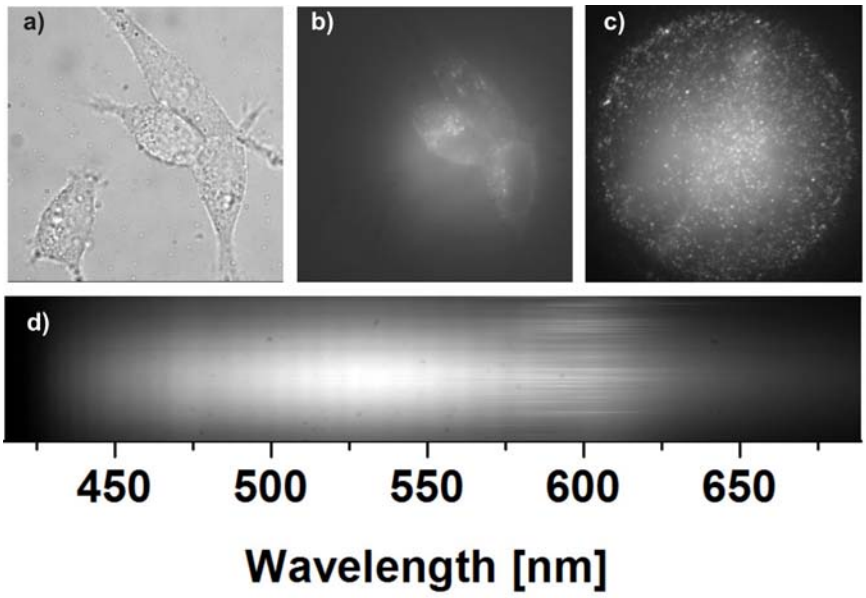

Comments: Aggregates of CQD were visible in the cell (very bright spots in *Fig. 99b)*. Bottom of a Petri dish with enormous amount of CQD aggregates is shown in *Fig. 99c)*, much less CQD aggregates were observed inside the cell (see *Fig. 99b)*). On the right side of *Fig. 99d)* we can see narrow PL peaks of many CQD aggregates emitting in spectral region around 600 nm. The images in full resolution are included on the DVD attached to this thesis.

Figure 100: Luminescence spectra of two single CQD aggregates in a HeLa cell (detected from different spots in the cell).

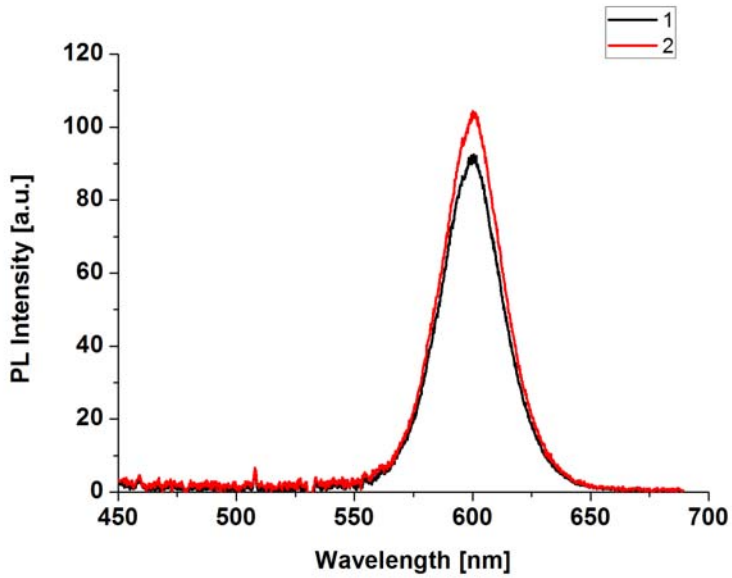

Comments: As we can see the PL peak position (around 605 nm) of CQD was not shifting at all. This is because the CQD size distribution is very narrow and because there are no observable interactions between cells and CQD leading to PL spectral shifts.

When trying to observe ND in living cells, we were facing two main problems: Luminescence of NDs was very broad (300-600 nm, PL spectra of NDs in water are shown in *Fig. 19*) and very weak. Therefore we were not able to clearly spectrally distinguish PL signal coming from ND and from the background (cell and media related) (see *Fig. 101c)*), although we could clearly observe them in fluorescence image as more intense spots (see *Fig. 101b)*). The

measured PL spectrum of A-ND in a cell (after subtraction of background) shown in *Fig. 102* demonstrates very low PL intensity which is close to the noise level.

Figure 101: Images of HeLa cells incubated with ND (concentration 8 μg/ml) after 18 hours of incubation (images were taken with the micro-spectroscopy apparatus). a) transmission optical image of a living HeLa cell with ND, b) fluorescence image of the same HeLa cell with aggregated NDs c) PL spectral profile from a vertical cross-section of the HeLa cell image (lighter gray colour means higher intensity).

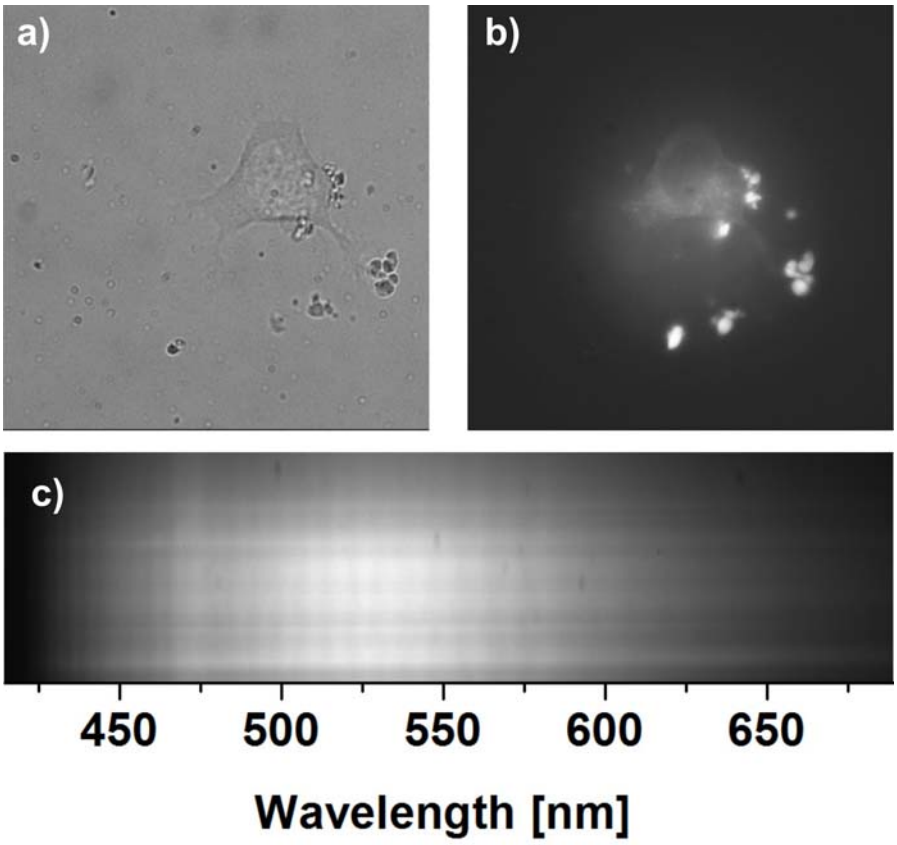

Comments: Although the ND aggregates were clearly visible in the florescence microscope (panel b) we were not able to separate their PL spectra from PL of the nutrient medium and the cell itself (see panel c). The images in full resolution are included on the DVD attached to the thesis.

Figure 102: Luminescence spectrum of one ND aggregate in a HeLa cell.

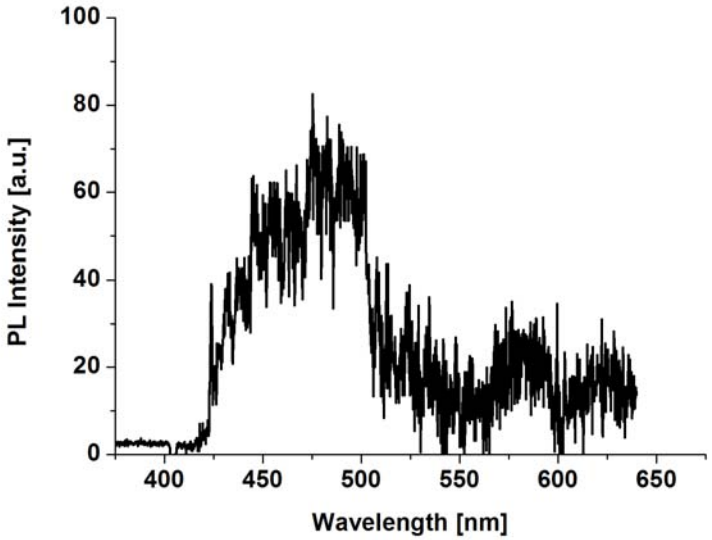

Comment: The extracted PL spectrum of a ND aggregate was more or less on the noise level, because of high background signal (from the cell and medium) and weak PL of ND in the spectral region between 400-600 nm.

To conclude, the results of the PL micro-spectroscopy experiments clearly show that the best nanomaterial from the spectral point of view is CQD (we observed plenty of single CQDs), but majority of CQDs did not enter the cell. The best nanomaterial from the biological point of view is Si-NC, because majority of Si-NCs were observed inside cells. We were able to subtract the strong PL background (originating from cells and nutrient media) from the emission spectra of Si-NCs, without significant problems; this was the case for CQD as well but not for NDs, because their PL signal is too weak and spectrally broad.

4.10 Scanning electron microscopy

We used scanning electron microscopy (SEM) for detailed observation of changes on the surface of cells incubated with nanomaterials. The fixed cell sample was scanned by a high-energy beam of electrons and secondary or back-scattered electrons are collected, which contain information about the sample surface.

The samples were measured with the JEOL JSM-6300 apparatus with accelerating voltage: 5 - 30 kV, cathode: thermoemission (W), image detector: Tescan 2048×1536×8bit, vacuum: 10^{-4} Pa); resolving power of this microscope is 11 nm. Even finer details were measured with another microscope having resolving power of 1 nm, JEOL JSM-7401F (accelerating voltage: 0.1 - 30 kV, cathode: field emission (W - single crystal), image capture: 1280×1024×8bit, vacuum: 10^{-7} Pa).

4.10.1 Sample preparation for SEM

The cells were fixed after incubation with various nanomaterials and transferred from nutrient media to organic solvents and then gilded. This procedure consisted of several steps. After incubation, the cells were washed with PBS, then dipped three times into a fresh solution of 3 % glutaraldehyde in phosphate buffer for 20 minutes each time and finally dipped once more, but this time for 1 hour. After this treatment the cells were dipped three times into 0.2 M phosphate buffer (pH 7.2) for 10 minutes each time. Then the cells were transferred form water to ethanol by dipping the sample three times in 50 % ethanol in water for 10 minutes each time and three times in 70 % ethanol in water for 10 minutes each time. Then the samples were transported to scanning the electron microscopy laboratory in Ceske Budejovice. Here they transferred the cell samples from 70 % ethanol to 100 % ethanol and afterwards to acetone. Finally, the samples were gilded.

4.10.2 SEM experiments

HeLa cells were used in this study (SEM results obtained on L929 cells incubated with various nanomaterials were published in [2A]). The cells were incubated in a 24-well plate. with a round glass coverslip on the bottom of each well. The first stage of incubation without any nanomaterial lasted for 6 hours (in order to let the cells attach to the coverslip), then the nanomaterials were added to the nutrient medium and incubated with cells for another 18 hours. The amount of nanomaterials was: 4 μg/ml for Si-NCs and CQD, and 10 μg/ml for A-ND and M-Si (the different concentration were chosen in order to have approximately the

same number of particles in the sample) in standard nutrient media for Hela cells, where each well was filled with 1.7 ml of nutrient medium.

Optical images of living HeLa cells incubated with nanomaterials before SEM preparation are shown in *Fig. 103*. The pictures were taken with the Olympus camera C-7070 attached to the CKX41 Olympus microscope with the 20x objective lens (numerical aperture 0.4).

Figure 103: Optical microscope images (in transmitted light) of living HeLa cells incubated with various nanomaterials before SEM preparation. a) control sample incubated without any nanomaterial, b) Si-NCs, c) ND, d) CQD e) A-ND , f) M-Si. (the scale bar is 100 μm)

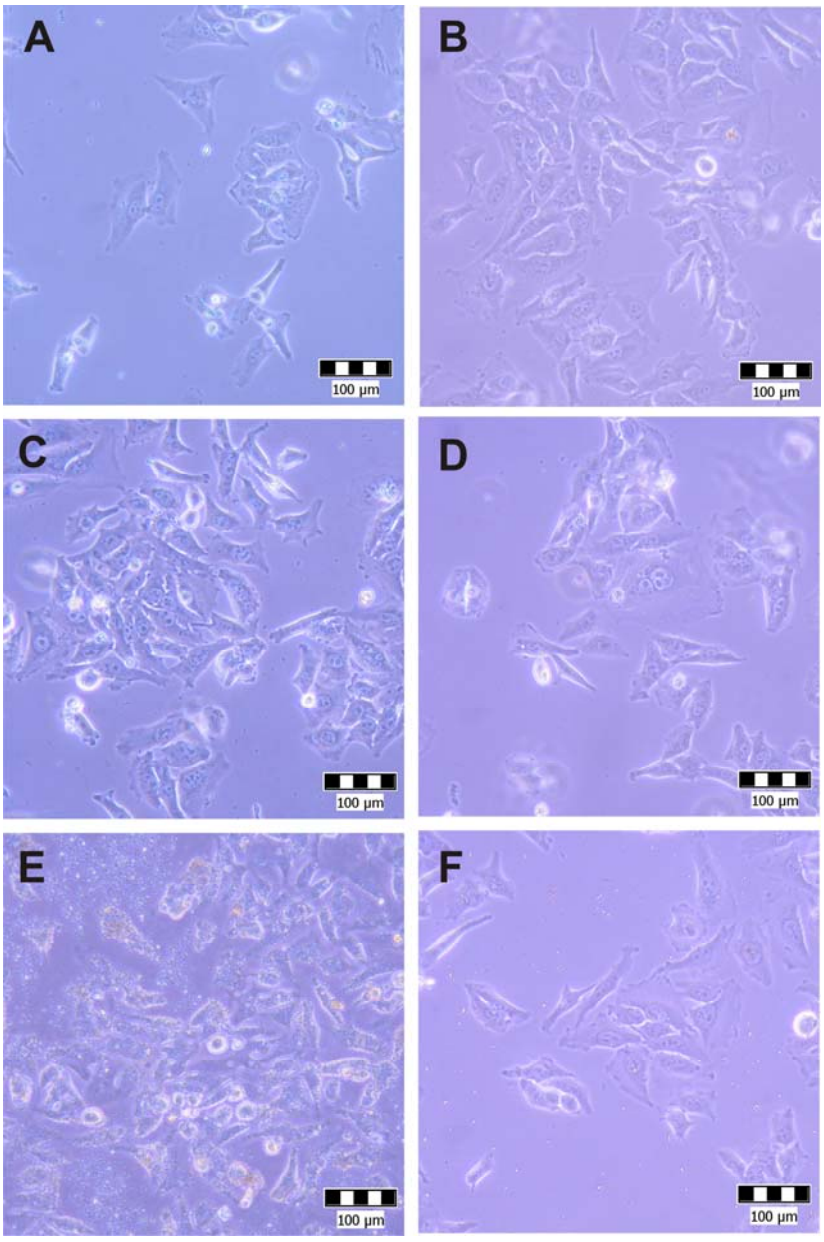

The SEM image of a control HeLa cell sample, which was incubated without any nanomaterial, is shown in *Fig. 104*. Images of HeLa cells incubated with Si-NCs, CQD, A-ND, and M-Si are displayed in *Fig. 105*, *106, 107* and 108, respectively.

Figure 104: SEM image of HeLa cells incubated without any nanomaterial (control sample). A – overview image (Scale is 2 μm), B – detail of cell membrane (Scale is 2 μm). (Image A and B was taken with the JSM-6300 microscope).

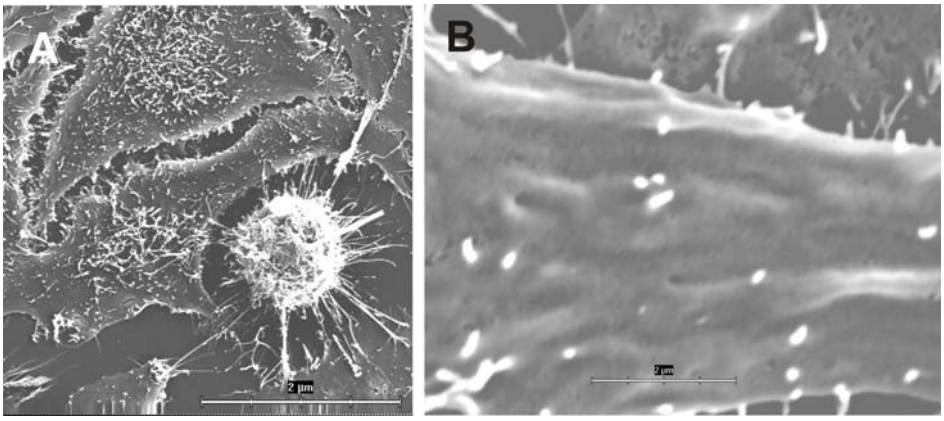

Comments: The cells had normal shape and size; normally looking filaments were on the outer cell membrane. An unspread bold shaped cell can be seen in the bottom right corner of *Fig. 104-A*. On *Fig. 104-B* is displayed smooth surface of cell membrane.

Figure 105: SEM image of HeLa cells incubated with Si-NCs. A - overview image (scale is 2 μm), B (scale is 500 nm) and C (scale is 1 μm) - details of cell outer membrane, D - interconnection between two cells (scale is 1 μm). (Images A and B were taken with the JSM-6300 microscope, while C and D with the JSM-7401F microscope).

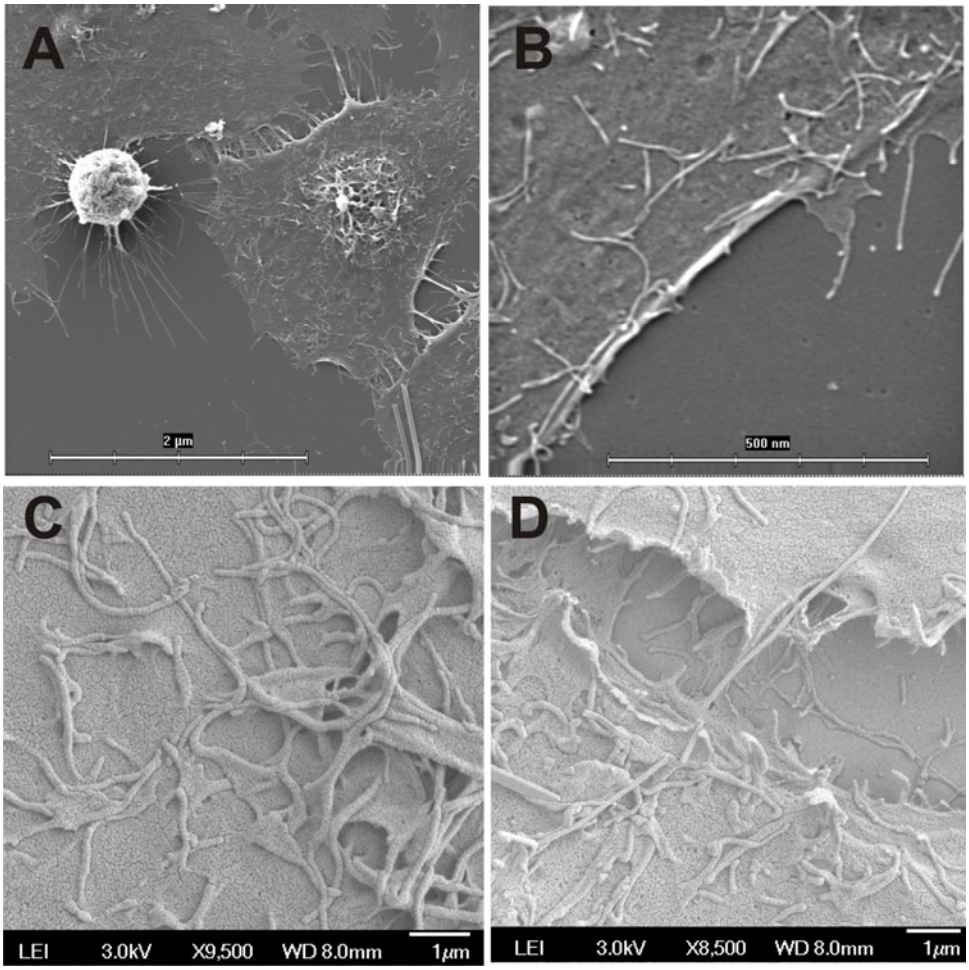

Comments: The cells had normal shape and the outer cell membrane was covered with visible filaments. Increased porosity of cell membrane was observed in *Fig. 105-B* and *105-D* (suggesting increased uptake of small objects). In *Fig. 105-B* we can see edge of the cell, in *105-C* surface of the cell close to center, in *105-D* border between two cells.

Figure 106: The SEM image of a HeLa cell incubated with CQD. A – overview image (scale is 1 μm), B - detail of cell outer membrane (scale is 1 μm) (taken with microscope JSM-7401F).

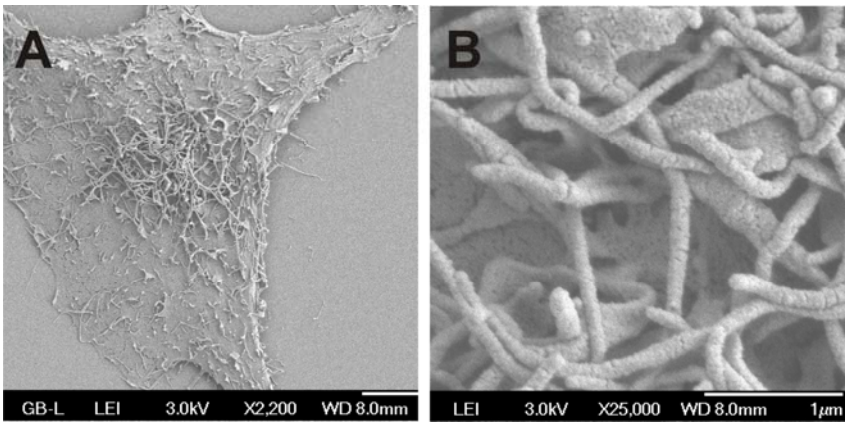

Comments: The cells had normal size and shape. We observed increased number of filaments, which were also longer than in the control sample. A detail of filaments is displayed in *Fig. 106-B*.

Figure 107: SEM images of HeLa cells incubated with A-ND. A - overview image (scale is 10 μm), B - detail of outer cell membrane (scale is 1 μm), C and D (scale is 1 μm) – details of a strangely prolongated HeLa cell (all pictures were taken with JSM-7401F microscope).

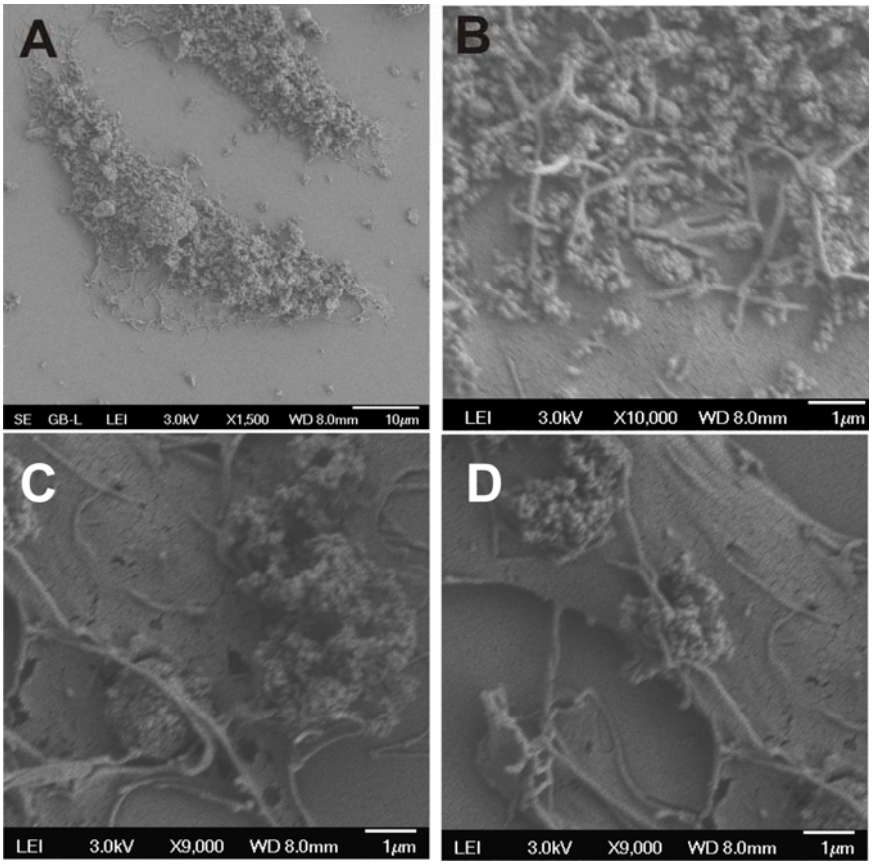

Comments: Majority of the observed cells were covered by A-NDs. The cells had not been dead yet, but severe damage to cell membranes was observed. The cell in *Fig. 107* was completely covered with A-ND and these aggregates of nanodiamonds were interweaved with filaments (detailed view of this phenomenon is shown in *Fig. 107-B*, In *Fig. 107-C* and *107-D*). Better images could not be obtained due to strong charging of sample.

Figure 108: SEM images of HeLa cells incubated with M-Si. A - overview image (scale is 2 μm), B - detail of HeLa cell with one M-Si crystal inside the cell (scale is 10 μm), C and D (scale is 1 μm) – detail of M-Si and filaments on the outer cell membrane. (The image A was taken with the JSM-6300 microscope and images B, C, and D with the JSM-7401F microscope).

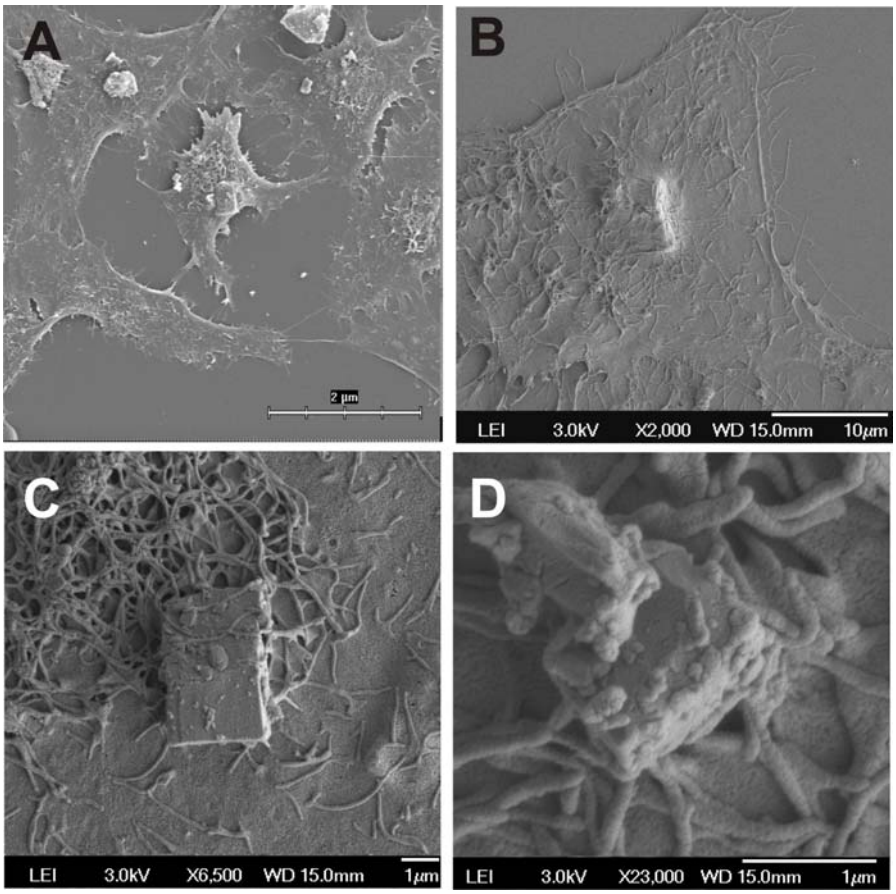

Comments: All cells had normal size and shape and majority of them had one or more M-Si on the outer membrane. We observed a lot of crystals being incorporated into the cell membrane or even inside the cell (*Fig. 108-A* and *108-B*). The details in *Fig. 108-B* and *108-C* show blocky crystalline fragments with filaments attached around them. Facets of M-Si crystals were not sharp, but covered by proteins originating from nutrient media or dead cells.

In conclusion although very small (up to 20 nm) Si-NCs, CQD, and ND cannot be resolved with the used SEM apparatuses, SEM imaging gives us important information about state of the outer cell membrane. We observed higher porosity of cell membranes for samples incubated with Si-NCs (see *Fig. 105*). We suppose the increased porosity was due to higher uptake of nanoparticles into the internal cell environment (presumably by endocytosis). The increased porosity was observed also in case of cells incubated with CQD (see *Fig. 106*). We also observed much higher number of filaments in samples incubated with CQD or ND compared to the control sample (see *Fig. 104*).

Significant structural changes of the outer cell membrane were induced in cells incubated with A-NDs (see *Fig. 107*). A-ND particles were observed attached to the outer cell membrane in huge aggregates interweaved with filaments. One HeLa cell, which is completely covered with A-ND, is shown in *Fig. 107-A*; the cell was probably still alive before fixation (see *Fig. 103*). Its future proliferation was unclear, because uptake of nutrients by the cell could be diminished due to the A-ND covering of the outer cell membrane. We can see the attachment

of A-ND to the outer cell membrane with filaments encircling A-ND in detail in *Fig. 107-C* and *107-D*.

The cells incubated with M-Si (*Fig. 108*) had normal shape and size, the number of filaments was slightly increased in close proximity to M-Si. M-Si was observed being incorporated into the cell membrane and also inside the cell (*Fig. 108-A* and *108-B*). Filaments tended to attach to the M-Si facets.

5. Summary and conclusions

This work would not be possible without cooperation of several Institutes; these Institutes are acknowledged in Appendices *Ap6*.

In this study we worked with tree different types of nanomaterials which are currently investigated as promising new fluorescent labels for use in biology. The main attention was devoted to Si-NCs, while the other two nanomaterials represented other two mainstream quantum dot based fluorescent labels. One was ND, which is still in the experimental phase of use, and the other was CQD - cadmium selenide based quantum dots, which are already commercially available and used.

Preparation of nanomaterials

Si-NCs were prepared by the electrochemical etching. We were able to tune PL emission through the large part of visible spectrum (see *Fig. 4*) by changing the parameters of etching. The desired PL band with maximum from 590 to 600 nm was achieved by etching with the standard hydrofluoric solution (see Chapter 2.1.1), additional treatment with peroxide for about 16 minutes, and then aging for about 2 days while exposed to air at room temperature (for details see [2A]). After transferring porous Si powder into colloidal suspension we had a mixture of single Si-NCs and grains of interconnected Si-NCs in agglomerates. In order to observe only small particles we had to filtrate the colloidal samples through 100 nm pore filters. The diameter of single Si-NCs was around 1.5-2 nm for those emitting around 600 nm, and smaller than 1.4 nm for those emitting around 400 nm, as was characterized by AFM and DLS (see Chapter 2.4).

This preparation method has very low production efficiency, but we obtain chemically pure nanocrystals in contrast to other preparation methods used by different groups (see Chapter 2.1.2). We developed and tested new method for production of Si-NCs by mechanical milling and laser-induced splitting (see Chapter 2.1.4). Although we did not obtain photoluminescent Si-NCs, we have come very close – the smallest Si-NCs particles were below 60 nm (see *Tab. 1*). The size of those nanocrystals might be further reduced chemically, but exploring this possibility was beyond the scope of this thesis. Ball milled silicon crystals were used in this work under the name M-Si as a comparison material in biological studies.

ND were prepared by our coworkers by combustion methods and treatments with various acids (see Chapter 2.2). Samples contained 8 nm ND particles and 460 nm aggregates (measured by DLS see [1A]) covered with various carboxy-, keto-, hydroxyl-, and oxygen groups (see [36]) in water. The ND aggregates were used in this work under the name A-ND as a comparison nanomaterial in biological studies.

CQD were used as purchased, the manufacturer claims that they have size around 8 nm and their surface is covered by various carboxyl groups (see Chapter 2.3). The PL maximum of CQD was around 605 nm. In reality, when we observed CQD with micro-spectroscopy apparatus, we observed a lot of single CQD, but majority of CQD were aggregated in clusters of ten CQD or more.

Chemical activation of nanomaterials

Not only the material composition of nanoparticles is determining their properties as fluorescent labels, but also the covering plays a crucial role. It has influence on the PL intensity and peak wavelength, but, more importantly, it also affects the biological and cytotoxic response of the cells incubated with these nanoparticles. The cell "sees" at first only the envelope of nanomaterial, until the envelope disintegrates. The application of common techniques of surface activation of bulk materials cannot be usually applied to their nano-sized form due to difficulties related to handling of so small particles. The cleaning treatment and unwanted aggregation of nanoparticles are inevitable. Even if we succeed in activation of nanoparticles, we would face great loses from the purification processes.

In our study we succeeded in activation of Si-NCs by treatment in xylene (see Chapter 2.5.1). Our patented procedure (see *Ap1*) produces Si-NCs with Si-CH_x groups on the surface, as proven by NMR and FTIR measurements (data have already been published [4A]). We also proved that the sample still consists of single Si-NCs with the diameter around 2-3 nm (DLS) and with the Si crystalline core conserved (HRTEM) (see *Fig. 13*). Although the xylene treated Si-NCs cannot be used in biological experiments, they hold exclusive features which are advantageous for applications in photonics (e.g. solid-state light emitting devices [1], quantum computing, solar cells etc). The capping influenced significantly the PL emission properties of single Si-NCs. We no longer observe one peak with PL peak at around 590-600 nm (see *Fig. 15*), but a double-peak structure with the first maximum at 510-570 nm and the second maximum at 570-620 nm (see Fig. 26). Similar double-peak structure was observed by other groups for Si-NCs with different capping [73, 74]. The origin of the PL double-peak structure was explained in literature as related to Si-O-Si vibration [73, 74].

This experimental result suggests that there is a deeper physical mechanism independent on preparation methods of Si-NCs and their organic capping. But the precise origin of this spectral shape is still under investigation.

This special capping affected not only the PL spectral shape but also the PL quantum efficiency. While the naturally oxidized Si-NCs have QE only about 2-3 % [4A, 5A], xylene-treated samples had QE up to 20 % (see Chapter 3.5.3 and [4A]). This innovative activation procedure was patented by our group (see details in Appendices *Ap1.*).

Observed activation of Si-NCs by treatment in solvent (water or ethanol) with D-glucose was a bit unexpected. This finding emerged from the aging experiment, where we wanted to know how the PL intensity of Si-NCs dispersed in various liquids mimicking the cell internal environment changes with time. The Si-NC suspensions were stirred continuously up to 120 days. The PL intensity was stable for certain D-glucose concentrations and did not decrease in contrast to other samples (see *Tab. 6* and *7*). In the micro-spectroscopical study we found that the PL emission peaks of single Si-NCs and smaller Si-NC agglomerates shifts from 600 nm to 570 nm, but the PL emission measured from the whole sample did not show any significant shift (see Chapter 3.4). Our first hypothesis was that this effect is due to flipping of D-glucose molecules attached to the Si-NC surface between two configurations (envelope and twist) to the more energetically favorable one in response to excitation, leading to a decrease of possible charge of Si-NCs and consequently to diminishing the Auger effect. This hypothesis can explain higher PL intensity, but it does not explain the spectral shift.

In order to study the origin of PL changes of Si-NCs treated with D-glucose, we performed FTIR measurements to prove if there is any structural change in D-glucose molecule (see Chapter 3.4.2). In contrast to Si-NCs treated with other solutions, we observed significant changes in D-glucose molecule in presence of Si-NCs (see *Fig. 55*). We observed changes which were assigned to several chemical groups: –COH, –CH, $–CH_2$, $–CH_3$, –COH, -COOH, -CO, C=C, C=O, 3R–C-O-H, or =C-O-C-3R (see Chapter 3.4.2). Although we were not able to determine precisely which of these groups really interacts with Si-NCs surface, they had one common parameter – all groups contain carbon atom. Thus we can expect that Si-C or Si-O-C bonds are probably formed. Another experimental technique, like NMR, would be needed to determine which one of those groups is actually responsible for the observed signal. However, such precise assignment of surface groups might require extended effort due to complicated structure of D-glucose with many similar groups. AFM images (*Fig. 57*) in Chapter 3.4.2 are showing that the D-Glucose is strongly interacting with surface and making an envelope around them.

The Si-NCs in solution with D-glucose had also significantly increased PL quantum efficiency (as high as 11 %, see *Tab. 9*), even though it was measured for aged samples with somewhat degraded PL intensity. If we estimate the QE of non-degraded PL intensity, then it could be about 20-30 %. In any case, the measured QE around 11 % is much higher than QE measured for naturally oxidized Si-NCs (2-3 % [4A, 5A]).

We did not attempt to activate comparison nanomaterials, ND and CQD, because of time constraints and limited supply of source materials.

Optical characterization of nanomaterials

Si-NCs used in this study had maximum of PL emission at around 600 nm (see *Fig. 15*). The purchased CQD comparison material had very similar PL peak position at around 605 nm (see *Fig. 17*), but the last studied material (ND) had PL maximum in the blue part of the visible spectrum at around 390-420 nm (see *Fig. 19*). The excitation was more efficient at shorter wavelengths for all samples (for Si-NCs see *Fig. 16*, for CQD see *Fig. 18*, the excitation spectra of ND were not measured due to limitations of our fluorescence spectrometer but the statement holds for NDs too).

The mechanism of PL is discussed for CQD in Chapter 3.1.2, and for ND in Chapter 3.1.3. Here we are going to summarize in more details only optical properties of Si-NCs which are in the main focus of our work.

Si-NCs have various emission bands (see *Tab. 5*). We are mostly interested in the S-Band with PL maximum in the yellow-orange-red region (600-800 nm) and PL decay time in the range of 1-100 μs. We also studied briefly the F-Band of Si-NCs with PL in the UV-blue region and characteristic lifetimes of excited state in the range of a few ns (see Chapter 3.2.1). We found out that the origin of the F-band luminescence lies most probably in the Si-NC core (our studies of the F-Band are summarized in the paper [6A]). We also observed anomalous behavior of PL Stokes shifts for particles with diameters around 1.4 nm and smaller; this observation is in agreement with numerical calculations published in [71].

The optical properties of Si-NCs were also studied on the single nanocrystal level. PL properties of single nanocrystals were studied with our micro-spectroscopy apparatus (the principle of measurement and experimental setup is described in Chapter 3.3).

Micro-spectroscopy study of our xylene treated Si-NCs (see Chapter 3.3.3) revealed double peak PL spectra (*Fig. 26*). The PL intensity maximum of the main peak was positioned around 525 nm and the second PL peak between 560-620 nm. This double-peak emission structure was observed also by other groups for variously treated Si-NCs [73, 74]. Our results indicate a slightly different model of the double-peak structure than what was proposed by other groups. The precise origin of the double peak is hard to find because the 150-meV splitting (distances between both PL peaks) is much larger than any phonon energies in bulk silicon. Authors of articles [73, 74] propose that the origin of PL in their Si-NCs is related to the interaction of excitons with Si-O-Si surface vibrations, but presence of those vibration bands in our samples is very low. This phenomenon is still under investigation. Optical properties of our xylene treated Si-NCs are summarized in our publication [4A].

When studying standard oxidized Si-NCs in living cells by micro-spectroscopy, we discovered that there is a shift in the PL intensity maxima (*Fig. 27*). We treated our Si-NCs with various solutions, which are found in cells, to discover the origin of this shift. The Si-NCs colloids were observed for up to 120 days in order to study not only the spectral shift but also change of PL intensity and possible degradation of Si-NCs (see Chapter 3.4). We found out that the most stable PL emission intensity was observed for Si-NCs treated with various concentration of D-glucose in water or ethanol. The standard sample, Si-NCs in ethanol, have been studied in our laboratory for over 5 years. In this sample the PL intensity is relatively stable for 2-3 months, but if we look at the micro-PL spectra from single Si-NCs in ethanol, then we observe constant decrease in PL intensity with time (*Fig. 32*). Si-NCs in water showed similar PL results (*Fig. 30* and *34*) as Si-NCs in ethanol. The fastest decrease of PL intensity was observed in Si-NCs treated with water solution of NaCl (*Fig. 31*) where we were not able to measure any micro-PL spectra from single Si-NCs (*Fig. 35*) after the first week of study.

The investigation of PL dependence on pH (Chapter 3.4.2) revealed that PL intensity decreases faster for higher pH (*Tab. 7*) and that it is hard to measure micro-PL spectra from single Si-NCs for those samples. Si-NCs samples treated with acid solution had slower decrease of PL intensity (*Fig. 50*) and we were able to measure PL emission spectra from single Si-NCs even after 50 days (*Fig. 51*). The pH had influence on size of Si-NC agglomerates in the solution (*Tab. 8*) - bigger agglomerates were observed for higher pH. The smallest Si-NCs agglomerates were observed for Si-NCs treated with D-glucose in water. Although the average size of the smallest Si-NCs in this solution was around 30 nm, much smaller Si-NCs (size around 2-5 nm) were also observed during DLS measurement. However, their contribution to the overall scattering was very small and get lost in the averaging of DLS measurements. Presence of those small Si-NCs was not observed in any DLS measurements of Si-NCs treated with different solutions as described in Chapter 3.4.

In order to find out if there was any chemical interaction between Si-NC surface and D-glucose molecules, which would explain the strong PL intensity of those samples, FTIR measurements were done (Chapter 3.4.2). It was clear from *Fig. 55* and *Fig. 56* that the D-glucose molecule changed significantly and these changes mainly involve carbon atoms. This suggests that the D-glucose molecule was interacting with Si-NCs surface and formed a nanocrystal shell as it is clear from AFM measurements (*Fig. 57*). This is also in agreement

with our micro-PL spectroscopy measurements, where we observed many Si-NCs with some spacing between them and very low number of Si-NCs agglomerates compared to other studied samples (except xylene treated Si-NCs).

PL quantum efficiency of our samples was studied in Chapter 3.5. Naturally oxidized samples have QE around 2-3 % [5A] while the xylene treated Si-NCs had QE up to 20 % (at 550 nm). The second highest measured QE was around 11 % (*Tab. 9*) and was observed for Si-NCs sample treated with D-glucose in water. However, this QE was measured when the samples were very old and their PL intensity was only at about 40 % of the PL intensity plateau value (*Tab. 7*). So the estimated QE of Si-NCs in D-glucose in water could be as high as 25-30 % for samples in the best condition. The PL decay time for Si-NCs treated with D-glucose in water was around 12 μs (at 600 nm), which was very close to Si-NCs in ethanol 11 μs (at 600 nm) for the same age of sample (*Tab. 10*). Measured lifetimes of Si-NCs (Chapter 3.6) are in agreement with results published by other groups [9]. The relatively long PL lifetimes in the range of tens μs can be in principle used to differentiate the faster autofluorescence of cells from the slower photoluminescence of Si-NCs, when pulsed excitation and time correlated detection is used [1A, 111].

The QE of Si-NCs treated with solutions with various pH copied the trend observed in PL intensity of Si-NCs. The lowest QE was observed for high pH and the highest was observed for low pH (*Tab. 9*). Low QE and PL intensity of Si-NCs can be both assigned to charging of Si-NCs and increased Auger effect, which is even enhanced by the stronger tendency of Si-NCs to stay together in environment with higher pH (shown by DLS measurement, see *Tab. 8*).

Si nanocrystals (as other quantum emitters like single molecules) do not emit PL continuously (under constant excitation), but their PL reveals intermittency – switching between ON and OFF phases. Study of PL intermittency is summarized in Chapter 3.7 and was published in our paper [7A]. The effect is probably related to charging of nanoparticles due to Auger effect [33]. The possible excitation-relaxation processes in Si-NCs are summarized in the schema in *Fig. 65*. The exciton is strongly confined in small nanocrystals and is influenced by interface between Si core and SiO_2 surface (this interface is connected to specific vibrations – phonons). The exciton can interact with a non-radiative centre as in [87] and this reduces the average quantum efficiency of radiative recombination. Due to relatively long excited state lifetime a generation of second exciton is highly probable (under stronger excitation). Interaction of two excitons (inelastic scattering) within one nanocrystal probably plays a crucial role in non-radiative and radiative processes within Si-NCs. The inelastic scattering can induce the non-radiative recombination of one exciton and excitation of the other one. Another way of non-radiative recombination is the Auger recombination, when an electron-hole pair interacts with a third quasiparticle. All these effects reduce PL QE. If the exchanged energy between excitons is high enough and the energy landscape is favorable, the scattering can lead to a charge separation and their capture in trap states near the interface. In such charge-separated state, the Auger recombination efficiently quenches created excitons, hence causing the Si-NC to become dark until the charges recombine back [7A].

Previously published low QE values of a few percent were probably influenced by including OFF periods in the final result. When we removed the dark periods, then the quantum efficiency was 10-20 % for the pumping rate corresponding to population of one exciton per quantum dot or lower. The QE decreases slowly for higher pumping rates. This is most likely caused by stronger Auger recombination.

Interaction of nanomaterials with cells

The last experimental chapter (Chapter 4) is devoted to studies of nanomaterial interaction with cells. Our nanoparticles can be used as very good single fluorescent marks in biology, e.g. in single protein tracking, due to their small size. They can replace staining molecules, which are currently used, but which are usually toxic and applied in high doses. Presence of such staining molecules negatively influences functionality of cell and might compromise results of studied processes. Commercially available quantum dots are usually based on cadmium which is very toxic for the biological environment. Even though the CQDs are covered by protective shells, the shells disintegrate in time and the cadmium based core gets exposed [107]. These particles are also very big (smallest are around 25 nm with protective covering) compared to, for example, a lipid bilayer protecting the cell (usually around 6 nm thick). Si-NC particles are just about 1-5 nm big and their PL in a cell is very stable.

The biological studies were done on HeLa, L929, and SAOS-2 cell lines. The cell treatment and preparation is described in Chapter 4.2. Nanomaterials can be toxic to the biological environment as summarized in Chapter 4.3. Not only the composition of nanoparticles plays crucial role, but their size and shape influence the cytotoxicity as well.

Although nanodiamonds are biologically inert in bulk (e.g. nanocrystalline layers), they can induce stress to a cell by accumulation of nanoparticles, which do not degrade in the living organism. On the other hand, Si-NCs are biodegradable to nontoxic silic acids in reasonable time spent in a living organism ([24, 89]). Many studies indicate that non-activated nanocrystalline silicon is removed from the body by urine system (particles of sizes less than 20 nm [89]) and this process is quite fast (days in case of oxidized particles <120 nm based on Por-Si). To prolog the presence of silicon nanoparticles within a living body the aggregates of them can be used, as well as activation of Si-NCs surface by less degradable chemical compounds, e.g. by thermal carbonization [95].

Internal organs such as liver, spleen, and kidney showed neither significant change in morphology nor significant inflammatory reaction to Si materials used in [89, 95] within the time scale of 4 weeks; consequences of a long-term influence spanning the lifetime of an organism are not yet known. We can presume that the organism will not show significant changes in functionality, because silicon nanocrystals are biodegradable. The only question is if significant accumulation in specific organs takes place before the degradation occurs [3A].

Information that Si-NCs are genotoxic [105] or have big cytotoxicity due to production of ROS appears from time to time in literature (Chapter 4.3.1). Those results are observed only for Si-NCs with hydrogenated surface as showed by Kovalev et al. in [5]. The production of ROS by Si-NCs with oxide on the surface is below measurable levels. On the other hand, production of ROS in hydrogenated Si-NCs can be exploited in the photodynamic therapy of cancer [3A].

Commercially available fluorescent labels were represented in this work by cadmium selenide based CQD from eBioscience. This company makes the quantum dots covered by protective shells and already tagged with specific antibodies. In this case we had the opportunity to work with a cadmium selenide core covered by a layer of carboxyl groups on the surface. With this CQD we studied cytotoxicity and observed the reaction of cells to released cadmium atoms.

We used also ball milled M-Si (for preparation see 2.1.3) in biological studies as another comparative material, with non-luminescent particles of around 500-800 nm in diameter. The last comparative material was A-ND, which comprised of luminescent agglomerates of NDs (see preparation described in Chapter 2.2). These materials were used for testing if there is any difference in cell interaction with nano-sized and semi-bulk materials of the same composition. They can also simulate situation when a cell is overdosed with the corresponding nanomaterial.

Three independent methods were used for testing the cytotoxicity of nanomaterials. The first was LDH test done on SAOS-2 cell, which gives us the information about the cell membrane damage (see description of method in Chapter 4.4). Si-NCs had the best results in this test; there was no significant change, compared to the control sample incubated without any nanomaterial, for both 24 and 48 hour long incubations and for all tested concentrations. NDs behaved like the control sample for all concentration in 24 hour long incubation, but in the 48 hour test they started to be very cytotoxic for concentrations of 7.5 μg/ml and higher. For ND concentration of 75 μg/ml almost half of the overall number of cells were dead compared to the control sample. The CQD did not show any cytotoxic reaction in 48 hour long incubation even for the highest tested concentration (5 μg/ml). The highest concentration comparable to that used in case of ND and Si-NCs could not be tested due to lack of this sample. The interpretation of cytotoxic result for CQD is a bit tricky, because the release of cadmium from this particle takes time and also the subsequent toxic reaction is not immediate.

The method of growth-curves was used for studies of nanomaterial cytotoxic influence at longer time-scale (Chapter 4.5). This test consists in counting the number of live and dead cells from images taken by optical microscopy in precise time intervals. We used this test on HeLa cells and the results are in agreement with our previously measured growth curves on L929 cells (published in our paper [1A]). The used concentrations were the same for Si-NCs, ND, and CQD (8 μg/ml in standard nutrient medium) and for A-ND and M-Si (4 μg/ml). The used materials had the same effect (on number of living cells), the only difference in development of cells was observed for cells incubated with CQD and A-ND. Decrease in numbers of living cells compared to the control cell sample was observed after 50 hours in case of cells incubated with CQD (*Fig. 70*), when the release of cadmium atoms was probably poisoning the cell culture. In case of cells incubated with A-ND, a big reduction of living cells was observed from the beginning of incubation. After 60 hours just around 10 % of cells was alive (*Fig. 70*).

More complex information, not only about cytotoxicity of nanomaterials but also about their precise influence on cell development, was obtained with time-lapse microscopy (Chapter 4.6). Cell cultures incubated with various nanomaterials were photographed in microscope in 2 minutes intervals and video sequences were composed from these pictures (the videos are included on the DVD attached to this thesis). The parameters of cell proliferation are summarized in *Tab. 12*. It is clear that the sample incubated with Si-NCs was identical to the control sample. Although there was a bit longer cell adaption for high doses of Si-NCs, the second generation showed normal parameters of viability. The least viable sample were cells incubated with A-ND; it exhibited the longest time between consecutive cell divisions and the division itself lasted almost 3 times longer than in the control sample. Moreover, the A-ND caused immediate cell death when added to freshly passaged cells, therefore the cells had to be incubated on a surface with a droplet of A-ND on it (see Chapter 4.6.2).

Staining with G-R stain was used to observe morphological changes of cells (Chapter 4.7). The sample closest to the control cell culture was again that one with Si-NCs. For cells incubated with CQD and ND we observed slight deformation of cell nucleus (*Fig. 79*, *Fig. 80*). In case of cells incubated with A-ND the nucleus was not clearly visible and the cell cytoplasm was severely damaged, with clearly visible A-ND in it. In case of cells incubated with M-Si the cell looked normal and M-Si were visible in them.

Laser-scanning fluorescence confocal microscopy was applied to study the dynamic reaction of cell cultures to presence of nanomaterials (Chapter 4.8). We used transfected SAOS-2 cells (which have luminescent actin structures) with Si-NCs and ND/A-ND mixture; the CQD were not studied due to fast photobleaching of their PL intensity. First Si-NCs were observed within the cell after 1 hour long incubation in standard nutrient medium. We did not observe any significant damage to actin structure even for the highest concentration within the 24 hours long incubation. The cells had normal shape and size even though the concentration of nanomaterial within them was very high (*Fig. 87*). When the cells with Si-NCs were incubated in nutrient medium without fetal bovine serum, the penetration of nanomaterial into the cell was slowed down significantly (up to 3 hours). This strengthens our hypothesis that proteins and amino acids from bovine serum bond non-specifically to Si-NCs surface, and such enveloped Si-NCs enter a cell without problems.

In case of cells incubated with mixture of ND and A-ND, the first ND were observed in cells after 3 hours of incubation in standard nutrient medium. First changes of actin structure were observed after 3 hours long incubation for concentration of 75 μg/ml nanodiamonds in standard nutrient medium. Small unorganized areas of extraneous actin fibrous structures were observed in close proximity to nanodiamonds (*Fig. 93*). Severe damage of actin structure was observed for the same concentration of nanodiamonds after 24 hour long incubation (Fig. 94). About half of cells were dead and plenty of nanodiamonds were found in their remains. The still alive cells were significantly smaller than cells in the control sample; they had round shape and were not properly attached to the glass surface. Actin fibrous structures in close proximity to nanodiamonds had breaks in them and a lot of curls. When the cells were incubated with nanodiamonds in nutrient medium without fetal bovine serum, the NDs went inside the cells almost immediately after addition to the cell culture (*Fig. 95*) and accumulated around the cell nucleus. Such fast penetration of nanodiamonds was probably driven by charge of nanodiamonds.

The nanomaterials in living cells were also studied with the micro-spectroscopy apparatus (Chapter 4.9). We were able to extract PL spectra of Si-NCs (possibly single Si-NCs particles) and CQDs from interior of living cells, even though the cell and nutrient medium themselves are strongly luminescent (*Fig. 98* and *Fig. 100*, respectively). But it was not possible for cells incubated with NDs (*Fig. 102*) due to weak and broad PL signal from NDs, spectrally overlapped with PL from cells and nutrient medium (although we were able to image NDs in cells as spots with increased PL intensity, *Fig. 101*).

SEM imaging was performed to observe structural changes of outer cell membranes (Chapter 4.10). The morphological changes observed in cells incubated in presence of A-ND (*Fig. 107*) by SEM shaded light on results obtained by other methods. A-NDs covered cell membrane and were interweaved with filopodia. The damage to the cell membrane and to actin structures around A-NDs observed by SEM looked the same as the damage of actin structures inside cells containing A-ND observed by fluorescence microscopy. Therefore, we can conclude that the damage to the actin structures inside cells was likely caused by A-ND as well. Cells

incubated with CQD and Si-NCs looked the same as the control sample with exception of higher porosity of cell membrane. In case of cells incubated with M-Si we observed M-Si on the outer cell membrane, being incorporated into the cell, and some particles already inside the cell.

Endocytosis is considered as the dominant uptake mechanism of extracellular materials with size up to about 150 nm [112]. Faklaris et. al [112] showed that non-activated, 46 nm big NDs enter HeLa cells by endocytosis. According to our observations and similar results for similar materials in above mentioned studies we presume the same uptake mechanism – endocytosis.

In conclusion, Si-NCs are the most promising nanomaterial of all nanomaterials studied in this work for application as new florescent labels in biology and also as single dot trackers [8A]. They have several exclusive features: efficient PL, biodegradability, small size, and low toxicity. NDs were stable, but they caused cytotoxic reaction and damage to actin structure of the cell when used in higher concentrations. Cytotoxic reaction was also observed in case of lower concentrations, but in long time incubations. A-ND had strongly negative influence on cell cultures; they were highly cytotoxic after 24 hours of incubation even at mild concentrations and caused significant damage to the actin structure of cells. Moreover, there is no known pathway so far, how to remove them from living bodies. Although CQDs have bright PL, they need very thick shells in order to keep the efficient PL also in biological environment which increases their size to at least 25 nm. Also the core of CQD gets exposed with time and release of toxic cadmium poisons the cell, as we observed in our long time studies. M-Si is dangerous for cells only at high concentrations (5 particles per cell or more). Here the negative influence is not caused by the composition of particles, but by the mechanical stress that these micro-crystals induce in the cell membrane [1A, 9A].

Considered all together the Si-NCs are very promising nanomaterial for a new fluorescent mark without any side effect on cell proliferation. They are clearly detectable inside living cells - we were able to measure PL spectra coming from single particles inside a cell and the PL intensity was rather stable during all our measurements. Moreover, a living body has mechanisms for removing excess of Si-NCs [76]. This exceptional advantage allows application of Si-NCs particles in human medicine without any concern. The second material of choice is ND. Although they have a mild negative effect on cell cultures, they can be used as a very good fluorescent, long term stable marks for in vitro experiments, if precaution is taken.

6. Appendices

Ap1. Patent details

Name: Method for the preparation of optically clear solution of silicon nanocrystals with short-wavelength luminescence.

Autors: K. Kusova, O. Cibulka, K. Dohnalova, K. Zidek, A. Fucikova, I. Pelant

Application Number: CZ2009/000053

Publication Date: 10/29/2009

Filing Date: 04/17/2009

International Classes: C09K11/59

Abstract: The method of the preparation of optically clear solution of silicon nanocrystals is based on the preparation of silicon nanocrystals by electrochemical etching of silicon wafers yielding a porous-silicon layer with subsequent post-etching and ageing procedure. The layer of porous silicon is then mechanically pulverized for the crystalline substrate, yielding powder composed of large agglomerates of silicon nanocrystals. These agglomerates are exploited for the preparation of an optically clear solution of single silicon nanocrystals with bright and yellow photoluminescence, stable in the long-term, by long-term stirring in a suitable organic solvent.

Ap2. LDH cytotoxicity assay reactions

This procedure has two phases – in the first phase LDH catalyzes the reduction of NAD^+ to NADH and H^+ by oxidation of lactate to pyruvate. In the second phase diaphorase uses NADH and H^+ to catalyze the reduction of a tetrazolium salt to highly colorful formazan. Formazan absorbs strongly at 490 – 520 nm and can be measured by fluorescence spectroscopy. The PL intensity of formazan then corresponds to the amount of LDH released into nutrient medium. That enables us to estimate cytotoxic effects for low concentrations of nanomaterials incubated with cells.

Ap3. **Illustration images of cells in LDH test**

Illustration images of cells after 48 hour long incubation with nanomaterials from LDH test (see Chapter 4.4). LDH graphs for Si-NCs and A-ND are displayed in *Fig. 67*, for CQD in *Fig. 68*.

Image of SAOS-2 cells incubated with Si-NCs, A-ND, CQD with various concentration incubated for 48 hours. a) control sample, b) Si-NCs concentration 0.75 μg/ml, c) Si-NCs concentration 7.5 μg/ml, d) Si-NCs concentration 75 μg/ml, e) A-ND concentration 0.75 μg/ml, f) A-ND concentration 7.5 μg/ml, g) A-ND concentration 75 μg/ml, h) CQD concentration 0.05 μg/ml, i) CQD concentration 0.5 μg/ml, j) CQD concentration 5 μg/ml.

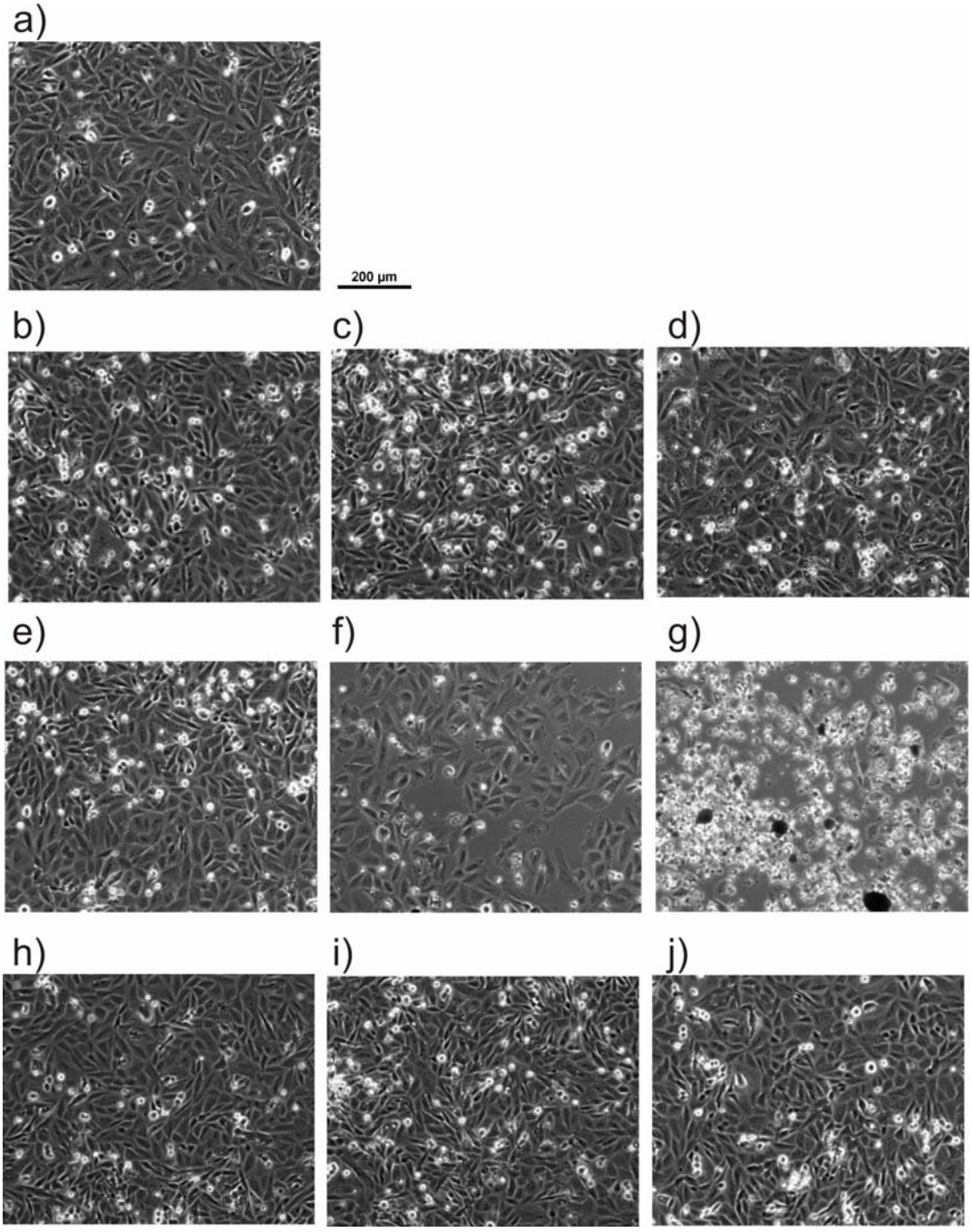

Ap4. **Illustration images of cells in Chapter 4.5**

Illustrative images (to *Fig. 70*) of HeLa cell cultures incubated for 60 hours with A-ND, CQD, or ND and a control sample. A – control sample, B – CQD, C – A-ND, D – ND. (Scale is 100 μm).

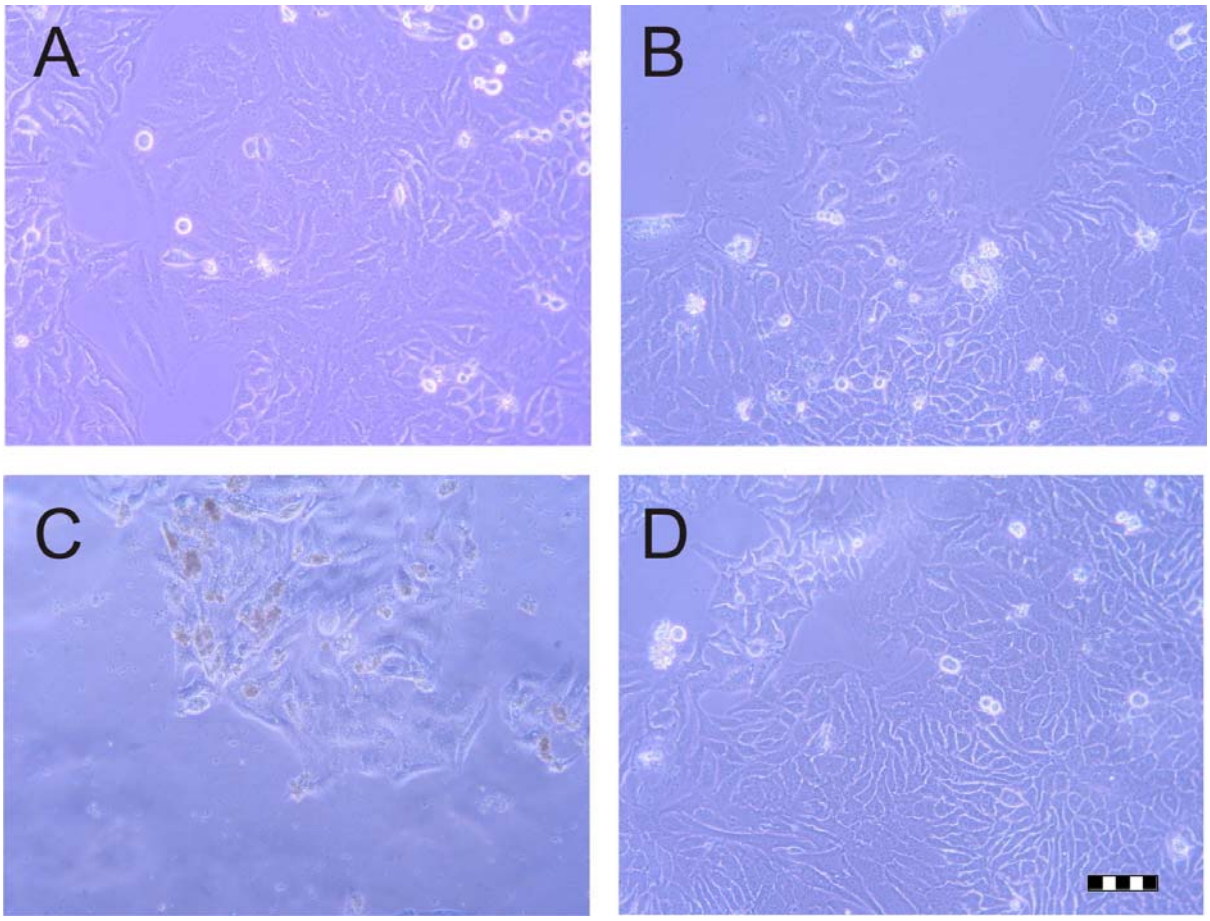

Ap5. **Transfection of live cells with pEYFP-N1/Actin plasmid**

By transfecting cells with pEYFP-N1/actin plasmid we obtain a modified cell line with fluorescent actin in living cells. pEYFP-N1/actin is a plasmid coding gene for actin under a strong CMV (cytomegalovirus) promoter in fusion with luminescent EYFP (Enhanced Yellow Fluorescent Protein). It also makes the cells resistant to Neomycin antibiotics for possible selection. The plasmid and transfection agents (Lipofectamin - Invitrogen) were mixed in nutrition medium without fetal bovine serum and antibiotics. The mixture was then left for 45 minutes at room temperature to form complexes of Lipofectamin and plasmids. This solution was added to cells and they were cultivated in cell incubator at 37° C with 5 % CO_2 enriched atmosphere for about 5 up to 72 hours (fetal bovine serum had to be added after few hours to keep the cells alive). The cells were incubated in standard nutrient medium after transfection. We can froze transfected cells in this step to store them for future use, or select the luminescent cells with Neomycin treatment (the non-luminescent cells are killed) – stably transfected cells.

Ap6. **Participating departments**

Majority of the work, including optical characterization (Chapter 3) and some biological experiments, was carried by myself at Department of Chemical Physics and Optics, Faculty of Mathematics and Physics, Charles University in Prague under supervision *of Doc. RNDr. Jan Valenta, Ph.D* and in case of use of FluoroMax®-3 under supervision of *Doc. RNDr. Dana Gašková, CSc.*

Preparation of Si-NCs and ND, organic capping of Si-NCs with xylene, DLS and FTIR measurements were carried out in the Institute of Physics, Academy of Sciences of the Czech Republic, v.v.i., Prague under supervision of *Prof. RNDr. Ivan Pelant, DrSc.* in case of Si-NCs, ND were prepared by *RNDr. B. Rezek, Ph.D.* and *Ing. A. Kromka, Ph.D* and in case of FTIR under supervision of *Prof. P. Matějka*.

The AFM of Si-NCs was measured at Institute for Biophysics, University of Linz, Austria under supervision of *Dr. G. Kada*.

PL blinking measurement of silicon nanocrystals was done in cooperation with J. Heyrovsky Institute of Physical Chemistry, Academy of Sciences of the Czech Republic, v.v.i., Prague under supervision *of Dr. M. Hof*.

Time-lapse microscopy, transmission optical microscopy and coloring of cells were carried out in cooperation with Centre of biological technologies, Institute of Systems Biology and Ecology, Academy of Sciences of the Czech Republic, v.v.i., Nove Hrady under supervison of *Ing. I. Březina*.

Confocal microscopy of nanomaterials interacting with SAOS-2 cells and LDH cytotoxicity test were carried out in cooperation with Institute of Inherited Metabolic Disorders, First Faculty of Medicine, Charles University in Prague under supervision of *RNDr. M. Kalbáčová, PhD.*

SEM images of cells were taken in Laboratory of Electron Microscopy, Biology Centre of Academy of Sciences of the Czech Republic, v.v.i - Institute of Parasitology, Ceske Budejovice, Czech Republic under supervision of *Ing. J. Nebesářová, CSc.*.

7. Acknowledgment

Publications by the author:

[1A] A. Fucikova, J. Valenta, I. Pelant, V. Brezina. *Novel use of silicon nanocrystals and nanodiamonds in biology*, Chemical Papers **63** (6), 704–708, (2009)

[2A] A. Fučíková, Diploma thesis: *Studies of nanocrystalline silicon colloidal suspensions*, Charles University in Prague, (2007)

[3A] A. Fucikova, J. Valenta, I. Pelant, K. Kusova, V. Brezina, *Nanocrystalline silicon in biological studies*, Physica Status Solidi (c) **8**,1093–1096, (2011)

[4A] K. Kusova, O. Cibulka, K. Dohnalova, I. Pelant, J. Valenta, A. Fucikova, K. Zidek, J. Lang, P. Stepanek, S. Bakardjieva, *Brightly Luminescent organically capped silicon nanocrystals fabricated at room temperature and atmospheric pressure,* ACS Nano **4** (8), pp 4495–4504, (2010)

[5A] K. Kůsová, O. Cibulka, K. Dohnalová, I. Pelant, A. Fucikova, J. Valenta, *Yellow-emitting colloidal suspensions of silicon nanocrystals: Fabrication technology, luminescence performance and application prospects,* Physica E **41** (6), 982-985, (2009)

[6A] J. Valenta, A. Fucikova, I. Pelant, K. Kůsová, K. Dohnalová, A. Aleknavičus, O. Cibulka, A. Fojtík, G. Kada, *On the origin of the fast photoluminescence band in small silicon nanoparticles*, New Journal of Physics **10**, 073022, (2008)

[7A] J. Valenta, A. Fucikova, F. Vacha, F. Adamec, J. Humpolickova, M. Hof, I. Pelant, K. Kusova, K. Dohnalova, J. Linros, *Light-Emission Performance of Silicon Nanocrystals Deduced from Single Quantum Dot Spectroscopy*, Adv. Funct. Mater. **18**, 1-7, (2008)

[8A] A. Fucikova, J. Valenta, I. Pelant, V. Brezina. *Nontoxic silicon nanocrystals and nanodiamonds as substitution for harmful quantum dots.* Mater. Res. Soc. Symp. Proc. Vol. 1241 (c) Materials Research 1241-XX03-11, (2010)

[9A] A. Fučíková, J. Valenta, I. Pelant, V. Březina. Studies of nanocrystalline silicon colloidal suspensions and their interaction with a biological system. Acta Metallurgica Slovaca, 13, 88–92, (2007)

Cited publications:

[1] R. Walters, H. Atwater, G. Bourianoff, Nature Mater. **4**, 143, (2005)

[2] M. Sailor, E. Lee, Adv. Materials **9**, 783, (1997)

[3] Z. Li, E. Ruckenstein, Nano Letters **4**, 1463, (2004)

[4] B. Geloz, A. Kojima, N. Koshida, Appl. Phys. Lett. **87**, 031107, (2005)

[5] D. Kovale, M. Fujii. Adv. Mater. **17**(21), 2531-2544 (2005)

[6] I. Pelant, J. Valenta, *Luminiscenční spektroskopie II*., Praha, Academia, 2010.

[7] A. G. Cullis, L. T. Canham, P. D. J. Calcott, J. Appl. Phys**. 82**, 909-965, (1997)

[8] F. Hua, M. T. Swihart, E. Ruckenstein, Langmuir**, 21** (13), 6054-6062, (2005)

[9] L. T. Canham, Applied Physics Letters, **57**, 1046–1048, (1990)

[10] K. Žídek, Diploma thesis: *Ultrafast processes in silicon nanocrystals*, Charles University in Prague, (2005)

[11] L. Pavesi, D. J. Lockwood (eds.), *Silicon Photonics, Topic in Applied Physics*, vol. **94**, Springer, Berlin, (2004)

[12] L. Khriachtchev (ed.), *Silicon nanophotonics*, World Scientific, Singapore, (2008)

[13] M. S. Hybertsen, Phys. Rev. Lett. **72**(10), 1514-1517 (1994).

[14] M. V. Wolkin, J. Jorne, G. Allan, C. Delerue and P. M. Fauchet, Phys. Rev. Lett. **82**(1), 197-200, (1999)
[15] A. Sa'ar, Y. Reichman, M. Dovrat, D. Krapf, J. Jedrzejewski, I. Balberg, Nano Lett. **5**, 2443, (2005)
[16] A. Fojtik, A. Henglein, J. Phys. Chem. B **110**, 1994-1998, (2006)
[17] M. Luppi, and S. Ossicini, J. Appl. Phys. **94**, 2130, (2003)
[18] A.Y. Vul, A.E. Aleksenskii, M. V. Baidakova, V. Y. Davydov, Y. A. Pevtsova, Physics Of The Solid State **39** (6), 1007, (1997)
[19] E. Osawa, Ch. 17, *Synthesis, properties and applications of ultracrystalline diamond*, (Eds: D. M. Gruen, O. A. Shenderova, A Ya. Vul'), Springer, Dordrecht, The Nederlands, (2005)
[20] S. Vial, C. Mansuy, S. Sagan, T. Irinopoulou, F. Burlina, J. P. Boudou, G. Chassaing, S. Lavielle, ChemBioChem **9**, 2113 (2008)
[21] L. Jarup, M. Berglund, C. G. Elinder, G. Nordberg, M. Vahter. Scandinavian Journal of Work, Environment & Health **24**, 3, 240-240, (1998)
[22] C. Kirchner, T. Liedl, S. Kudera, T. Pellegrino, A. M. Javier, H. E. Gaub, S. Stolzle, N. Fertig, W. J. Parak, Nano Letters **5**, 2, 331-338, (2005)
[23] B. Gelloz, Ch. 14, *Silicon Nanocrystals* (Eds. L. Pavesi, R. Turan), Wiley, Weinheim, (2010)
[24] H. A. Santos, J. Riikonen, J. Salonen, E. Mäkilä, T. Heikkilä, T. Laaksonen, L. Peltonen, V. P. Lehto, and J. Hirvonen, Acta Biomater. **7**, 2721-2731 (2010)
[25] R. R. K. Reddy, A. Chadha, and E Bhattachary, Biosens. Bioelectron. **16**(4-5), 313-317 (2001)
[26] F. Bessueille, V. Dugas, V. Vikulov, J. P. Cloarec, E. Souteyrand, and J. R. Martin, Biosens. Bioelectron. **21**, 908-916, (2005).
[27] H. Jang, L. E. Pell, B. A. Korgel, and D. S. English, J. Photochem. Photobiol. A, Chem. **158**, 111-117, (2003)
[28] J. D. Holmes, K. J. Zeigler, R. C. Doty, L. E. Pell, K. P. Johnston, B. A. Korgel, J. Chem. Soc. **123**, 3743-3748, (2001)
[29] J. R. Heath, Science **258**, 1131-1133, (1992)
[30] L. Mangolini, E. Thimsen, and U. Kortshagen, Nano Lett. **5**(4), 655-659, (2005)
[31] D. Jurbergs, E. Rogojina, L. Mangolini, U. Kortshagen, Appl. Phys. Lett. **88**, 233116, (2006)
[32] J. M. Buriak, Chem. Rev. **102** (5), 1271-1308, (2002)
[33] J. Valenta, R. Juhasz, J. Linnros, Appl. Phys. Lett**, 80** (6), 1070-1072, (2002)
[34] A. Fojtík, A. Henglein, J. Phys. Chem. B **110**, 1994-1998, (2006)
[35] A. Fojtik, J. Valenta, I. Pelant, M. Kalal, P. Fiala, Journal of Materials Processing Technology **181**, 88–92, (2007)
[36] E.D. Eidelman, V.I. Siklitsky, L.V. Sharonova, M.A. Yagovkina, A. Ya Vul', M. Takahashi, M. Inakuma, M. Ozawa, E. Ōsawa, Diamond and Related Materials **14**, 1765–1769, (2005)
[37] B. Rezek, L. Michalíková, E. Ukraintsev, A. Kromka, M. Kalbacova Michal, SENSORS **9** (5), 3549-3562, (2009)
[38] P. Bajaj, D. Akin, A. Gupta, D. Sherman, B. Shi, O. Auciello, R. Bashir, Biomed. Devices **9**, 787–794, (2007)
[39] T. Y. Didenko, K. S. Suslick, Am. Chem. Soc., **127** (35), pp (2005)
[40] T. Ohtsuka, J. Kawamata, Z. Zhu, T. Yao, Applied Physics Letters **65**, 466, (1994)
[41] http://www.ebioscience.com/knowledge-center/product-line/efluor/efluor-nanocrystals/nanocrystal-technology.htm

[42] K. Dohnalová, I. Pelant, K. Kůsová, P. Gilliot, M. Gallart, O. Crégut, J. L. Rehspringer, B. Honerlage, T. Ostatnický, S. Bakardjeva, New Journal of Physics **10**, 063014, (2008)
[43] L. Mangolini, U. Kortshagen, Ch. 13, *Silicon Nanocrystals Fundamentals, Synthesis and Applications* (Eds: L. Pavesi, R. Turan), Wiley-VCH, Weinheim, (2010)
[44] R. J. Walters, P. G. Kik, J. D. Cadperson, H. A. Atwater, R. Lindstedt, M. Giorgi, G. Bourianoff, Appl. Phys. Lett., **85** (13), 2622-2624, (2004)
[45] L. Mangolini, D. Jurbergs, E. Rogojina, U. Kortshagen, J. Luminescence **121**, 327-334, (2006)
[46] L. Pavesi, L. D. Negro, L. Mazzoleni, G. Franzò, F. Priolo, Nature **408**, 440, (2000)
[47] X. Li, Y. He, M. T. Swihart, Langmuir **20**, 4720-4727, (2004)
[48] M. Linford, C. Chidsey, J. Am. Chem. Soc. **115**, 12631, (1993)
[49] G. Sereda, V. Rajapara, Tetrahedron Lett. **48**, 3417, (2007)
[50] D. Kovalev, H. Heckler, G. Polisski, F. Koch, Phys. Status Solidi B **215**, 871, (1999)
[51] K. Dohnalová, K. Kusová, I. Pelant, Appl. Phys. Lett. **94**, 211903, (2009)
[52] P. M. Fauchet, Phys. Status Solidi b **190**, 53, (1995)
[53] S. Komuro, T. Kato, T. Morikawa, P. O'Keeffe, Y. Aoyagi, J. Appl. Phys. **80** , 1749, (1996)
[54] G. Amato, M. Rosenbauer, *Structural and Optical Properties of Porous Silicon Nanostructures* (Eds. G. Amato, C. Delerue and H-J. von Bardeleben), Gordon and Breach, London (1997)
[55] P. M. Fauchet Ch. 6, *Light Emission in Silicon: From Physics to Devices, Semiconductors and Semimetals vol. 49*, (Ed. D. J. Lockwood), CA: Academic, San Diego, (1998)
[56] G. Belomoin, J. Therrien, M Nayfeh, Appl. Phys. Lett. **77**, 779, (2000)
[57] V. Švrček, T. Sasaki, Y. Shimizu, N. Koshizaki, Appl. Phys. Lett. **89**, 213113, (2006)
[58] K. Dohnalová, L. Ondic, K. Kusová, I. Pelant, J. L. Rehspringer, R. R. Mafouana, J. Appl. Phys. **107**, 053102, (2010)
[59] V. I. Klimov, Ch. J. Schwarz, D. W. McBranch C. W. White, Appl. Phys Lett. **73**, 2603-2605, (1998)
[60] H. Song, X. Bao, Phys. Rev. B**, 55**, 6988-6993, (1997)
[61] C. Delerue, M. Lannoo, G Allan, E. Martin, I. Mihalcescu, J. C. Vial, R. Romestain, F. Muller, A. Bsiesy, Phys. Rev. Lett. **75**, 2228-2231, (1995)
[62] M. Zacharias, Ch. 8, *Silicon nanocrystals – Fundamentals, Synthesis and applications*, (Eds. L. Pavesi, R. Turan), Wiley-VCH Verlag GmbH & Co. KGaA, Weinheim, (2010)
[63] J. M. Buriak, M. P. Stewart, T. W. Geders, M. J. Allen, D. Raftery, L. T. Canham, J. Am. Chem. Soc. **121**, 11491-11502, (1999)
[64] K. Lutterova, I. Pelant, I. Mikulskas, R. Tomasiunas, D. Muler, J.-J. Grob, J.-L. Rehspringer, B. Hönerlage J. Appl. Phys. **91**, 2896-2900, (2002)
[65] A. D. Yoffe, Adv. Phys. **50**, 1-208, (2001)
[66] P. Reiss, J. Bleuse, A. Pron, Nano Lett. **2**, 781-784, (2002)
[67] P.P. Ingole, R. M. Abhyankar, B. L. V. Prasad, S. K. Haram, Materials Science and Engineering B **168**, 60-65, (2010)
[68] C.-C. Fu, H.-Y. Lee, K. Chen, T.-S. Lim, H.-Y. Wu, P.-K. Lin, P.-K. Wei, P.-H. Tsao, H.-Ch. Chang, W. Fann, PNAS **104**, 727-732, (2007)
[69] T. Plakhotnik, R. Chapman, New Journal of Physics **13**, 045001 (7pp), (2011)
[70] P. Achatz, J. A. Garrido, M. Stutzmann, O. A. Williams, D. M. Gruen, A. Kromka, D. Steinmüller, App. Phys. Lett. **88**, 101908, (2006)
[71] I. Pelant, J. Valenta, *Luminiscenční spektroskopie I.*, Praha, Academia, 2006.

[72] X. Wang, R. Q. Zhang, S. T. Lee, T. A. Niehaus, Th. Frauenheim, Appl. Phys. Lett. **90** 123116, (2007)
[73] J. Martin, F. Cichos, F. Huisken, Ch. von Borczyskowski, Nano Lett. **8**, 656, (2008)
[74] M. D. Mason, G. M. Credo, K. D. Weston, S. K. Buratto, Phys. Rev. Lett. **80**, 5405, (1998)
[75] D. Timmerman, J. Valenta, K. Dohnalova, W. D. A. M. de Boer, T. Gregorkiewicz, Nature Nanotechnology **6**, 710–713, (2011)
[76] S. P. Low, K. A. Williams, L. T. Canham, N. H. Voelcker, Biomater. **27**(26), 4538-4546, (2006)
[77] B. Gelloz, A. Bsiesy, R. Herino, Journal Of Luminescence **82**, 3, 205-211, (1999)
[78] M. Ibrahim, M. Alaam, H. El-Haes, A. F. Jalbout, A. de Leon., Eclet. Quím. **31**, 3, (2006)
[79] G. Ledoux, J. Gong, F. Huisken, O. Guillois, C. Reynaud, Appl. Phys. Lett. **80** (25), 1834-4836, (2002)
[80] G. Ledoux, O. Guillois, D. Porterat, C. Reynaud, F. Huisken, B. Kohn, V. Paillard, Phys. Rev. B. **62** (23), 15942-15951, (2000)
[81] I. Izeddin, D. Timmerman, T Gregorkiewicz, A. S. Moskalenko, M. Fuji, Phys. Rev. B, **78**, 035327, (2008)
[82] G. M. Credo, M. D. Mason, S. K. Buratto, Appl. Phys. Lett. **74**, 1978, (1999)
[83] F. Cichos, J. Martin, Ch. von Borczyskowski, Phys. Rev. B **70**, 115314, (2004)
[84] M. D. Mason, D. J. Sirbuly, P. J. Carson, S. K. Buratto, J. Chem. Phys. **114**, 8119, (2001)
[85] I. Sychugov, R. Juhasz, J. Linnros, J. Valenta, Phys. Rev. B **71**, 115331, (2005)
[86] A. L. Efros, M. Rosen, Phys. Rev. Lett. 78, 1110, (1997)
[87] P. Pellegrino, B. Garrido, C. García, R. Ferré , J. A. Moreno, J. R. Morante, Phys. E **16**, 424, (2003)
[88] X. Wang, X. Ren, K. Kahen, M. A. Hahn, M. Rajeswaran, S. Maccagnano-Zacher, J. Silcox, G. E. Cragg, A. L. Efros, T. D. Krauss, Nature **459**, 686-689, (2009)
[89] J. Park, L. Gu, G. Maltzahn, E. Ruoslahti, S. N. Bhatia, and M. J. Sailor, Nature Mater. **8**, 331-336, (2009)
[90] M. Stutzmann, J. A. Garrido, M. Eickhoff, and M. S. Brandt, Phys. Status Solidi A **203** (14), 3424-3437, (2006)
[91] C. S. S. R. Kumar (Ed.), *Biofunctionalization of nanomaterials*, Weinheim, Germany, Wiley–VCH, (2005)
[92] L. P. McGuinness, Y. Yan, A. Stacey, D. A. Simpson, L. T. Hall, D. Maclaurin, S. Prawer, P. Mulvaney, J. Wrachtrup, F. Caruso, R. E. Scholten, L. C. L. Hollenberg, Nature Nanotechnology **6**, 358-363, (2011)
[93] Y.-R. Chang, H.-Y. Lee, K. Chen, Ch.-Ch. Chang, D.-S. Tsa, Ch.-Ch. Fu, T.-S. Lim, Y.-K. Tzeng, Ch.-Y. Fang, Ch.-Ch. Han, H.-CH. Chang, W. Fann, Nature nanotechnology **3**, 284-288, (2008)
[94] F. Neugart, A. Zappe, F. Jelezko, C. Tietz, J. P. Boudou, A. Krueger, J. Wrachtrup, Nano Lett. **7** (12), pp 3588–359, (2007)
[95] L. M. Bimbo, M. Sarparanta, H. A. Santos, A. J. Airaksinen, E. Mkil, T. Laaksonen, L. Peltonen, V. Lehto, J. Hirvonen, and J. Salonen, ACS Nano **4** (6), 3023–3032, (2010)
[96] F. Erogbogbo, K. Yong, I. Roy, G. Xu, P. N. Prasad, and M. T. Swihart, ACS Nano **2**(5), 873-878, (2008)
[97] L. Wang, V. Reipa, J. Blasic, Bioconjugate Chem. **15**(2), 409-412, (2004)
[98] S. P. Low, N. H. Voelcker, L. T. Canham, K. A. Williams, Biomater. **30** (15), 2873-2880 (2009)
[99] I. L. Medintz, H. T. Uyeda, E. R., Goldman, H. Mattoussi, H., Nature Materials, **4**, 435–446, (2005)

[100] M. J. Murcia, C. A. Neumann (pp. 1–40). (Ed. C. S. S. R. Kumar), *Biofunctionalization of nanomaterials,* Weinheim, Germany, Wiley–VCH (2005)
[101] E. Borsella, M. Falconieri, N. Herlin, V. Loschenov, G. Miserocchi, Y. Nie, I. Rivolta, A. Rybanova, D. Wang. , Ch. 18, (Eds. L. Pavesi and R. Turan), *Silicon Nanocrystals* Wiley, Weinheim, (2010)
[102] R.Veselská, R. Janisch. Scripta Medica **73**, 393–408, (2000)
[103] Eds. Dr. S. C. Sahu, D. A. Casciano, *Nanotoxicity: From In Vivo and In Vitro Models to Health Risks*, Willey Wiltshire, England, (2009)
[104] K. Fujioka, M. Hiruoka, K. Sato, N, Manabe, R. Myasaka, S. Hanada, A. Hoshimo, R. D. Tilley, Y. Manome, K. Hirakuri, K. Yamamoto, Nanotechnology, **19**, 1-7, (2008)
[105] Y. Jin, S. Kannan, M. Wu, J. X. Zhao, Chem. Res. Toxicol. **20**, 1126-1133, (2007)
[106] Y. Xing, W. Xiong, L. Zhu, E. Osawa, S. Hussin, L. Dai, ACS Nano **5**, 3, 2376-84, (2011)
[107] L. Wang, D. K. Nagesha, S. Selvarasah, M. R. Dokmeci, R. L. Carrier, Journal of Nanobiotechnology **6**, 11, (2008)
[108] T. Schwerdtle, F. Ebert, Ch. Thuy, C. Richter, L. H. F. Mullenders, A. Hartwig, Chem. Res. Toxicol. **23** ,2, 432–442, (2010)
[109] S. P. Low, K. A. Williams, L. T. Canham, and N. H. Voelcker, J. Biomed. Mater. Res. A **93**(3), 1124-1131, (2010)
[110] M. Fujii, N. Nishimura, H. Fumon, S. Hayashi, D. Kovalev, B. Goller, and J. Diener, J. Appl. Phys. **100**(12), 124302-124302-5, (2006).
[111] P. Alivisatos, Nature Biotechnology **22** (1), 47-52, (2004)
[112] O. Faklaris , V. Joshi, T. Irinopoulou , P. Tauc, H. Girard, C. Gesset, M. Senour, A. Thorel, J.-Ch. Arnault, J.-P. Boudou, P. A. Curmi, F. Treussart., ACS Nano **3** (12), 3955–3962, (2009)